Water Balance Investigations of Groundwater Depletion in Asia: Information Needs and Uncertainty Analysis

by

Julie E. Kiang

Submitted to the Department of Civil and Environmental Engineering
in partial fulfillment of the requirements for the degree of

Doctor of Philosophy

at the

MASSACHUSETTS INSTITUTE OF TECHNOLOGY

February 2002

Author .....
Department of Civil and Environmental Engineering
January 28, 2002

Certified by .....
Dennis McLaughlin
Professor of Civil and Environmental Engineering
Thesis Supervisor

Accepted by .....
Oral Buyukozturk
Chairman, Departmental Committee on Graduate Studies

Water Balance Investigations of Groundwater Depletion in Asia: Information Needs and Uncertainty Analysis

by

Julie E. Kiang

Submitted to the Department of Civil and Environmental Engineering
on January 28, 2002, in partial fulfillment of the
requirements for the degree of
Doctor of Philosophy

Abstract

Irrigated agriculture is an essential component of global food production. In many regions of the world, and Asia in particular, groundwater is a major source of irrigation water. Overpumping of groundwater aquifers has depleted storage in some areas. Quantification of the degree to which groundwater is being used unsustainably is critical to our understanding of the stability of irrigated agriculture. In this study, we investigate the feasibility of estimating groundwater storage changes using the water balance equation and currently available sources of global data. We employ multiple measurements of each water balance component and a constrained least squares estimation method in order to reduce uncertainties.

Global datasets of precipitation, evapotranspiration, and runoff were obtained and evaluated for suitability for use in the water balance. In order to fill gaps in the existing data, we developed a new estimate of evapotranspiration based on NDVI measurements and land use information. Results are presented for the continental U.S. and for our study region in Asia. We also show that multiple regression of runoff against basin characteristics can provide additional runoff information in ungaged basins.

The water balance can be used as a screening tool for poor quality data, and we are able to identify problematic basins in Asia. In addition, the least squares water balance estimator can be used to reduce the uncertainty in estimates of each component of the water balance. However, the uncertainty which remains in estimates of groundwater depletion precludes definitive statements about the sustainability of resource use in Asia for the time being. Groundwater depletion may be easier to detect using the water balance technique in drier climates, and forthcoming data products from advances in remote sensing may help to alleviate problems with the current data. However, we are unable to effectively evaluate the sustainability of groundwater use in many parts of Asia using the currently available data. This has implications for our ability to evaluate water and food security throughout the region.

Thesis Supervisor: Dennis McLaughlin
Title: Professor of Civil and Environmental Engineering

Acknowledgments

This research was funded in part by a grant from the Alliance for Global Sustainability. In addition, I was fortunate to have additional support through a National Science Foundation Fellowship and a Martin Family Fellowship for Sustainability.

Numerous organizations and individuals provided data for this study or assisted in locating and processing appropriate data. Without their assistance, this work would not have been possible.

Data used by the authors in this study include data produced through funding from the Earth Observing System Pathfinder Program of NASA's Mission to Planet Earth in cooperation with National Oceanic and Atmospheric Administration. The data were provided by the Earth Observing System Data and Information System (EOSDIS), Distributed Active Archive Center at Goddard Space Flight Center which archives, managed, and distributes this dataset. Eric Senter of the California Department of Water Resources and Howard Franklin of Monterey County were particularly helpful in securing data on California's groundwater resources. Petra Döll and Stefan Siebert provided access to their irrigation dataset. Many others who are not specifically mentioned above are listed in the text and in the references. Having obtained the data, assistance from Daniel Sheehan, MIT's GIS guru, was invaluable in processing and analyzing the data.

My thesis advisor, Dennis McLaughlin, has been supportive throughout this process and I am grateful that the opportunity to study sustainability issues with him emerged. He has given me room to explore new ideas, and useful advice when needed. Warm gratitude is also due my committee: David Marks, Dara Entekhabi, and Charles Harvey. I always walked out of each committee meeting with added enthusiasm for my research.

Parsons lab is filled with people who have made my life here more enjoyable. In particular, some PhD's who went before me - Karen, Kirsten, and Freddi, whose friendship and example convinced me that I too could complete the degree. Thanks also to those who are still here at Parsons - Sutapa, Rachel, Steve, Megan, Neda, ... Outside of research, special thanks are due to Karina, Sue, Susan, Jon, Mort, Shannon, and many others, who have made my years here fuller by running many miles with me, both literally and figuratively. Finally, there are the friends and family who knew me before I ever set foot at MIT. Thanks for being there to remind me that the ability to calculate water balances is not the only measure of a woman.

Contents

List of Figures

List of Tables

Chapter 1

Introduction

Water and food are essential and intertwined resources. Agricultural production requires a significant input of water, whether in the form of natural rainfall or applied irrigation water. Irrigation is the largest user of the world's limited supplies of fresh water, accounting for 67% of all withdrawals (Postel 1999, Shiklomanov 1998). Further, irrigation is a consumptive water use, meaning that once water is applied to crops a significant fraction is consumed by evapotranspiration and cannot be reclaimed for further use. About 86% of the world's water consumption can be attributed to irrigation (Shiklomanov 1998). Thus, sound management of water resources is needed for successful and sustainable irrigated agriculture. Poor management of water can lead to depleted supplies, degraded water quality, or water logging and salinization of soils. In fact, such problems have already arisen in numerous locations and the sustainability of agriculture and water resources in many regions of the world has been called into question by a number of recent publications. For example, Gleick (1993), Postel (1996,1999), and Brown(1999,2000) present data which suggest that in many regions of the world water scarcity and degradation of water quality threaten food production, human health, and economic security. Developing countries are considered to be especially at risk. Hall et al. (1999) categorize such views as those of "Water Pessimists". In contrast, "Water Optimists" have proposed that technological advances and increases in water use efficiency will allow nations to meet the water and food requirements of future generations (Hall et al. 1999, Rockstrom 1999).

Assessing the actual situation is difficult as data are incomplete, particularly at the regional level. Estimates of the total renewable fresh water supply of the globe suggest that in an absolute sense, there is plenty of water to go around. Globally, only 8.4% of renewable surface waters are withdrawn annually (Shiklomanov 1998). Most nations withdraw less than 40 percent of their total renewable supplies (FAO 2000). Unfortunately, the uneven spatial and temporal nature of these supplies means that not all of the available water can be utilized and that some regions do experience serious water shortages (Shiklomanov 1993). Temporal variation in rainfall and water availability can be especially acute in arid and semi-arid tropical regions, where monsoonal climates create significant seasonal variability, and fickle weather patterns can result in large interannual variability. As suggested by Savenije (2000), "a cubic meter of water in Europe is a much more reliable resource than a cubic metre in Africa." The situation is further complicated by the fact that water which has historically been used by agriculture is under increased competition from urban and industrial water users. Increasing water transfers between regions may be possible, but the effects on hydrology and crop yields of these alterations to the natural system have not been

well documented in many regions (Postel 1996).

According to the UNEP, nations face high water stress when they withdraw more than 40% of their total renewable supplies, medium to high water stress when utilizing 20%-40% of supply, moderate water stress when utilizing 10%-20% of supply, and low water stress when utilizing less than 10% of supply. Figure 1-1 shows the level of water stress as determined using this scale, estimated by the United Nations Environment Program (UNEP 1999).

Another common measure for categorizing the degree of water scarcity in a region is a region's per capita availability of renewable water, sometimes called the water stress index. Falkenmark (1992) introduced this concept with the additional supposition that about 1700 m^3/year/person are needed to grow sufficient grains to meet basic caloric requirements and to provide for household use, drinking water, and adequate sanitation. When per capita water availability falls below this mark, the population begins to experience water stress. When water availability falls below a still lower threshold of 1000 m^3/year/person, the region is said to experience chronic water scarcity that may impede development and be detrimental to human health (WRI 1996). This 1000 m^3/year/person level of water availability has been used in many publications as a benchmark for assessing water scarcity. For example, the World Resources Institute has published data indicating that 20 nations with a population of about 132 million already face water scarcity using this benchmark. Using population projections, the global population facing water scarcity will rise to between 653-904 million by 2025, and to 1.06-2.43 billion by 2050. Tropical and subtropical Asia and Africa appear to be especially vulnerable to water scarcity due to rising population.

Both water stress indices described above show a high potential for water stress in Asia and Africa, suggesting that these regions may merit additional study to evaluate the sustainability of their water resources. Asia, in particular, is heavily dependent on irrigation for its food production and this important link between water and food makes water scarcity a particular concern in parts of Asia. Rapid population growth and widespread irrigation are most prevalent in southern Asia, southeast Asia, and parts of east Asia. For this reason, we will focus on river basins in the portion of Asia highlighted in Figure 1-2. This study region includes river basins which do not drain northwards into the Arctic Ocean.

While the Falkenmark water stress index and the percentage of renewable resources currently utilized can provide a rough idea of where water scarcity has the potential to be problematic, neither measure can reliably predict whether or not water scarcity is currently a problem. As has been pointed out, some nations do perfectly well on smaller amounts of water by importing grains and other food staples and focusing instead on exports of less water intensive cash crops and manufactured goods (Shuval 2001, Allan 1999). Savenije (2000) lists a number of other limitations to the water stress index, including the masking of differences in perceived water scarcity due to differences in potential evapotranspiration and temporal variablility of water availability in disparate climates. Finally, the water stress index does not necessarily indicate whether or not a nation is currently meeting food needs by utilizing water unsustainably. For example, a nation with large surface water resources might nevertheless be pumping groundwater unsustainably because the groundwater provides a more accessible and stable water supply.

Groundwater is an especially important resource for irrigation and water supply in many arid and semi-arid regions of the world (Moench 2000). It is generally a more reliable source of fresh water than surface water because it responds less dramatically to interannual variability in meteorologic conditions. While surface water supplies may experience wide fluctuations, groundwater reacts more slowly, and can thus provide a critical buffer against

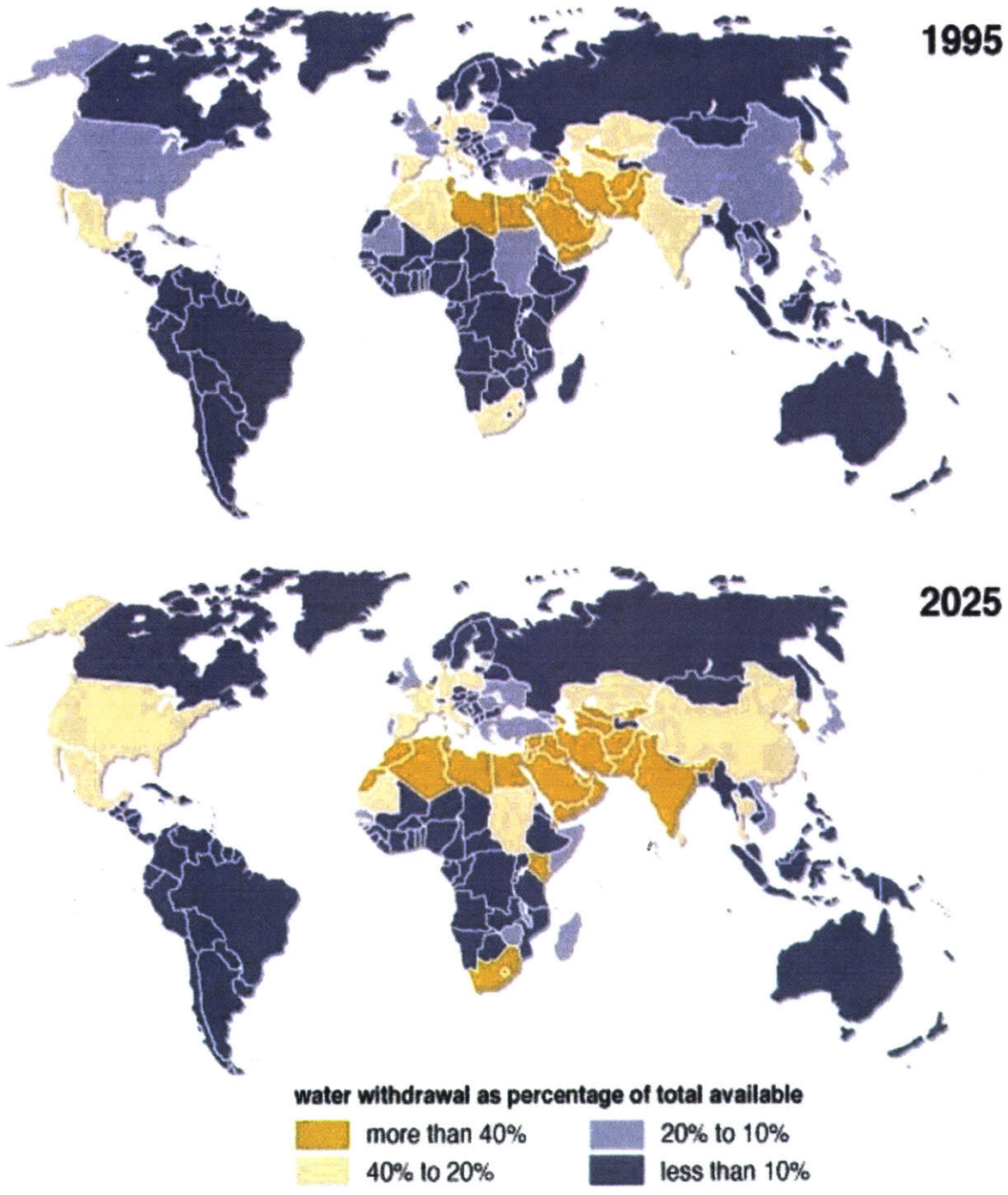

Figure 1-1: UNEP's mapping of global water stress. Water stress is considered low when less than 10% of renewable resources are being utilized, moderate when 10-20% are being utilized, medium-high when 20-40% are being utilized, and high when greater than 40% are being utilized. Source: UNEP (1999)

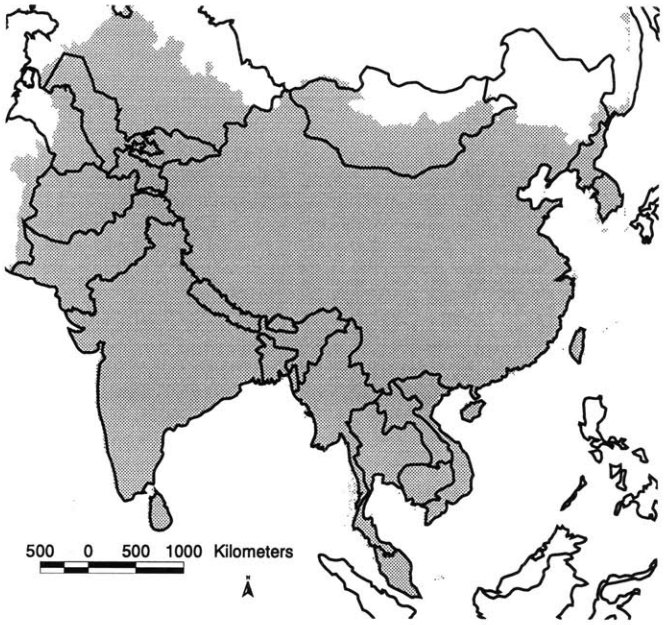

Figure 1-2: Our study region in Asia includes river basins which do not drain northwards into the Arctic Ocean.

drought (Shah et al. 2000). Unfortunately, this characteristic also means that if overexploited, groundwater supplies may take many years or decades to replenish themselves. In some cases, groundwater is being drawn from ancient aquifers which were filled during wetter climatic periods and cannot be replenished in the current climate. A recent report published by the World Water Council estimates that 10% of the world's food production relies on mined groundwater (WWC 2000).

A complication in the assessment of groundwater resources stems from the fact that the total amount of water stored in an aquifer is often not the important quantity. Rather, the amount readily accessible to the local population is the quantity that needs to be considered. For example, in the Gangetic Basin in India, the aquifer extends to a depth of many thousands of meters. However, this fact matters little to the rural households whose only access to the water is through shallow, hand-dug wells which extend only a few meters into the ground (Moench 2000). Even in more developed regions, deep groundwater stores can only be extracted by incurring large energy costs.

Groundwater overdrafts are not the only threats related to expanded irrigation. Shah et al. (2000) also note that waterlogging and salinization of soils can result from poor drainage of irrigated fields and that groundwater pollution due to agricultural chemicals is increasing.

1.1 Objectives

In this study, we would like to evaluate the sustainability of water resources and food production in critical areas of Asia. According to a United Nations paper, the "main

principle for the sustainable development of water resources is that the rate of extraction both from ground and surface water sources should not exceed the rate at which the resource is renewed and its extraction must not jeopardize the biodiversity of the ecosystem." (United Nations, 1997)

As a first step towards evaluation of water and food security in Asia, we will focus on just one aspect of sustainability - the question of whether or not groundwater extraction exceeds groundwater recharge, or renewal. Persistent groundwater extraction in excess of recharge will result in depletion of groundwater storage over the long term. With sufficiently accurate data, this change in storage can be calculated using simple water balance techniques.

Recent efforts to create global databases of surface measurements and remote sensing data have made a great deal of global data available. These can be used to construct water balances for much of the world, hopefully with the required accuracy.

The primary objectives of this research are to:

1. **Develop a methodology for estimating groundwater depletion using the long term water balance in large regions.** This approach will make use of all available data and include minimization of uncertainty as an important part of the analysis. Data from California basins will be used to validate the method.

2. **Assess the adequacy of current data in estimating groundwater depletion in Asia.** Can this estimation approach provide meaningful estimates of persistent storage changes in Asia, if they exist?

3. **How much can we expect to further reduce uncertainty in our estimates by incorporating the data expected to be available in the next 5-10 years?**

Chapter 2 provides a detailed discussion of the rationale behind our estimation methodology as well as the mechanics behind it. Chapter 3 describes global data which are currently available for large scale water balance estimates. The chapter also outlines the development of additional estimates of some components of the water balance, specifically for use in this study. Evapotranspiration data are discussed separately in Chapter 4. In Chapter 5, watersheds with known levels of groundwater depletion are used to test the methodology. The results of application of the methodology to watersheds in Asia are discussed in Chapter 6. Chapter 7 gives some perspectives on where the methodology is likely to be most successful and what improvements can be expected with additional information from upcoming data campaigns. Finally, Chapter 8 presents the conclusions of our research and suggests areas for further study.

Chapter 2

Estimation Technique

A number of different techniques have been used to study large scale hydrologic systems, from the simple water balance to complex numerical models. In recent years, numerical modeling of the hydrologic system has taken the forefront in many research circles. These models are especially useful in studying "what if" scenarios. (What if land use changes? What if the climate changes? etc.) These models range from simple bucket models of the land surface to conceptual representations of the actual processes which take place in the soil and vegetation. Such representations, while based on physical processes, often introduce complex algorithms and rely on (sometimes shaky) estimates of many parameters.

Instead of relying on models, we focus on extracting as much information as possible from available data, although some modeling and parameterization is unavoidable in developing usable data.

The most straightforward way to estimate rates of groundwater depletion is with observations of groundwater level. Unfortunately, while direct observations of groundwater are sometimes available locally, comprehensive, long term datasets over large scales are unavailable. While groundwater monitoring networks exist in many regions of the world and farmers are certainly aware if groundwater levels in their wells are declining, there has been no systematic colection of groundwater data worldwide. Historically, some nations have been reluctant to share groundwater data, as water is sometimes considered a strategic resource. For example, water resources data in the Ganges river basin in India has been considered classified information, and even data for other regions of India are not generally available outside of government circles (Moench 1992). Further, some groundwater monitoring networks are relatively new, so that long term data are not always available (Moench 2001). To effectively monitor groundwater, the monitoring network must also be fairly dense, so that localized conditions are not misinterpreted as representative of large areas. This is especially true for highly non-uniform aquifers. Care must also be taken to obtain measurements only after groundwater levels have had a chance to equilibrate after pumping.

The principle advantage of well level measurements is that it provides a means of directly monitoring groundwater. The quantity measured is also the quantity most relevant to evaluating the sustainability of groundwater use, as the feasibility and cost of pumping are both highly dependent on the depth to water.

The current lack of a global database of groundwater levels means that direct monitoring of groundwater use at large scales has thus far been impossible. However, if existing data were made available, we could quickly develop a more comprehensive picture of groundwater

resource use.

2.1 Water balance techniques.

An alternative means of calculating groundwater depletion by relying primarily on available data is through application of the principle of mass balance. According to this basic principle,

$$Inputs - Outputs = \Delta Storage \tag{2.1}$$

The equation can be applied to hydrological problems at any spatial or temporal scale. Depending on how the control volume is drawn, it can be applied to the groundwater aquifer itself or to the entire land surface.

Application of the principle of mass balance to the groundwater aquifer itself results in the following inputs and outputs:

$$Recharge - Discharge - Pumping = \Delta Storage \tag{2.2}$$

While this method can be used to estimate changes in groundwater storage, it can be difficult to apply, as recharge and discharge are both difficult to estimate accurately, and records of pumping are not readily available in many areas.

An alternative is to apply the water balance to the entire land surface system, including the groundwater aquifer, unsaturated soils, and surface vegetation, lakes, and rivers. Depending on the selected scale, accounting for all of the inputs and outputs can become quite difficult, as groundwater flow and lateral surface flows must be considered. However, the problem is simplified when applied to a watershed, as the very definition of a watershed allows us to assume that lateral movements of water are zero except at the watershed outlet point. In some cases, the surface water basin and the groundwater basin do not coincide, so care must be taken to ensure that significant lateral flows are not neglected. In the remainder of this work we will assume that the groundwater and surface water basins share the same boundaries.

The water balance for a watershed is diagrammed in Figure 2-1. With the control volume drawn as shown, the water balance equation can be expressed in the same manner as was first introduced by Thornthwaite (1944):

$$P - ET - R = dS/dt \tag{2.3}$$

where P is precipitation, ET is evapotranspiration, and R is runoff, or streamflow. S is the storage of water in lakes and river channels, snow, vegetation, unsaturated soils, and groundwater.

A common simplifying assumption is that at sufficiently long time scales any change in storage is negligible. (e.g., Baumgartner and Reichel, 1975; Korzoun, 1974; Oki, 1995) This leaves just three variables in the water balance equation:

$$P - ET - R = 0 \tag{2.4}$$

This equation is useful for estimating either P, ET, or R when the other two quantities are known. Indeed, Thornthwaite used the water balance as a means of estimating ET.

Early examples of water balance work can be found in a number of "water atlases"

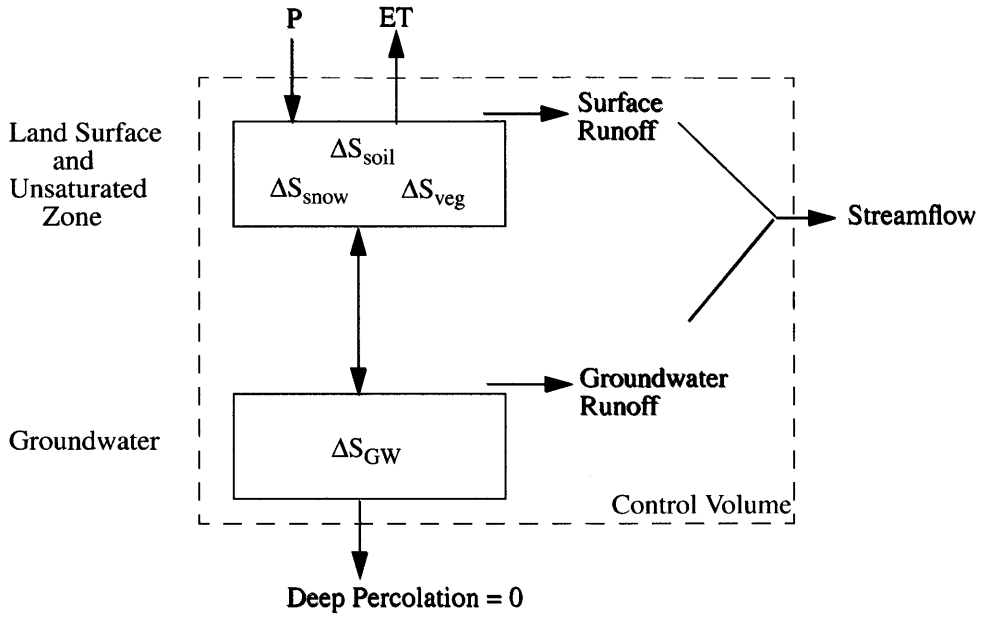

Figure 2-1: Elements of the land surface water balance.

which have been developed for the globe (e.g. Baumgartner and Reichel (1975) and Korzoun (1974)). Similar atlases, with more extensive regional data, have been developed for the United States and Canada (Miller, Geraghty and Collins 1962, den Hartog and Ferguson 1978) and other regions of the world. These water atlases generally present surface observations of precipitation and runoff (interpolated from streamflow) at an annual timestep. Evapotranspiration is often calculated using the water balance equation. In other cases, it is calculated with empirical equations or measurements of pan evaporation, adjusted for observed land cover. The water balance equation is then brought in to check for discrepancies in the data. den Hartog and Ferguson (1978), for example, assumed that runoff measurements were generally unbiased, whereas precipitation was consistently underestimated due to undercatch of rain gauges and biased placement of gauges in valleys with lower rainfall than nearby mountains. The components of the water balance were adjusted according to these principles. However, since these studies make the assumption that the storage change is equal to zero, they give no information about changes in groundwater storage.

In many situations the assumption of negligible storage change is reasonable. At the long term mean, most watersheds experience little change in snowpack, unsaturated soil water storage, lake storage, or river storage. Each of these quantities may change from season to season, and may even fluctuate somewhat from year to year. However, averaged over many years, these quantities tend to be stable. There are some notable exceptions, such as the markedly diminished storage of the Aral Sea or Lake Victoria over recent decades. In addition, climate change may be influencing the stability of glaciers and permanent snowpack. In most cases, however, long term changes in watershed storage can be attributed to changes in groundwater storage.

In this study, we take an updated approach to the catchment water balance to study regional hydrology and estimate groundwater depletion. Previous work assumed that over the long term, there is no change in land surface water storage. In this study, we continue

to work with the basic water balance equation, but relax the assumption that changes in storage are zero for the long term annual mean. Here, we do not assume that the storage change, ΔS, is zero, but instead take advantage of its presence in the water balance equation to calculate it from more readily available data on precipitation, evapotranspiration, and runoff. Throughout this study, ΔS refers to the total change in water storage at the surface and in the subsurface. However, unless otherwise stated, we assume that groundwater change is the only significant source of changes in storage at the mean annual timescale.

The very simple water balance equation can be an effective tool for the study of large scale hydrologic systems, because of its suitability for incorporating multiple data sources and because of the relative ease with which estimates of uncertainty can be made.

Caution must be taken when calculating the storage change as the residual of the water balance equation. In most cases, storage change is small when compared to precipitation, evapotranspiration, and runoff, and the uncertainty of an estimate obtained by differencing large numbers can be significant. Throughout this study, we make an effort to both quantify and reduce that uncertainty.

The quantification of uncertainty allows us to assess whether or not estimated storage changes are statistically significant. The problem can be framed as a hypothesis test. Our null hypothesis, H_o, is that $\Delta S = 0$. The null hypothesis will be rejected only when there is strong evidence that the alternate hypothesis, $H_a : \Delta S < 0$, has more validity. As shown in Figure 2-2, the same ΔS estimate, used as the test statistic, can lead to acceptance or rejection of the null hypothesis, depending on the standard deviation of the estimate. In Figure 2-2a, the test statistic, ΔS, lies in the rejection region. The test statistic is different enough from zero that we reject the null hypothesis in favor of the alternate hypothesis, that $\Delta S < 0$ and there is ongoing groundwater depletion in the basin. In Figure 2-2b, the same test statistic now lies within the acceptance region because the standard deviation is so large. In this case, there is not enough contradictory evidence to reject the null hypothesis.

As drawn in Figure 2-2, it is unlikely that we will mistakenly reject the null hypothesis when it is actually true. There is a higher chance that we will mistakenly accept the null hypothesis even though it is actually false. Consequently, even if we accept the null hypothesis, we cannot rule out the possibility that groundwater depletion is a problem in a basin. Even if we must accept the null hypothesis based on the available data, the water balance can sometimes give us additional information about the quality of our input data. If the absolute value of the storage change estimate is unrealistically large and yet we accept the null hypothesis, this may be an indication that the quality of the measurements is poor.

2.2 Reduction of uncertainty: Multiple measurements and the water balance estimator

As one step towards reducing uncertainty, we have collected and/or synthesized multiple estimates of many of the elements of the water balance. By using multiple measurements, the uncertainty of the resulting estimate can be reduced considerably, as demonstrated in the following section. The global data sources we have utilized are described in detail in Chapter 3.

In addition to the use of multiple measurements, we have attempted to reduce uncertainty through application of a least squares water balance estimator. This estimation method allows us to utilize all of the available data, assigning weights to each data source according to its uncertainty. Applying the water balance equation as a constraint ensures

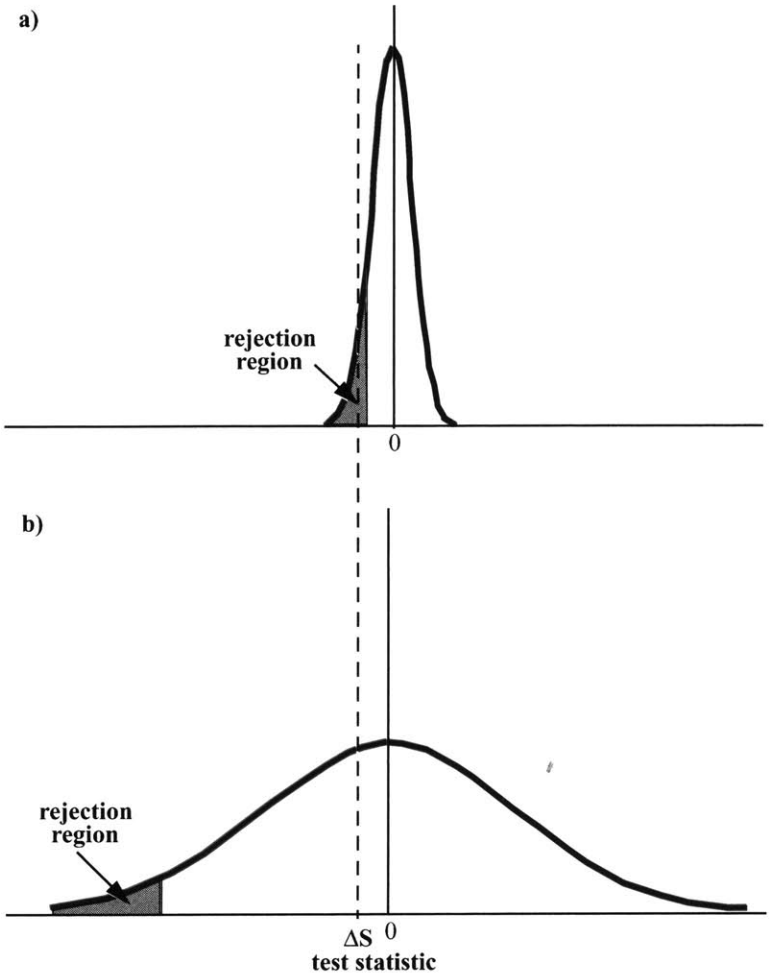

Figure 2-2: Our ability to reject the null hypothesis, $H_o : \Delta S = 0$ in favor of the alternate hypothesis, $H_a : \Delta S < 0$ depends on the uncertainty in our estimation. In (a), a small standard deviation in the estimate puts our test statistic in the rejection region while in (b), a large standard deviation places our test statistic well within the acceptance region.

that mass is conserved in the estimation. In essence, the water balance estimator creates best fit estimates of each component of the water balance equation, adjusting the estimates based on uncertainty in the measurements. Prior information (e.g., that $R \leq P$ on an annual basis) can also be incorporated into the estimation process to further refine the estimate. However, we have not incorporated this option in the estimator used in this study.

Because of imperfections in measurement equipment and techniques, any measurement can be expected to deviate from the true value, such that:

$$z = x + v \tag{2.5}$$

where z is the measured value, x is the true value, and v is measurement noise. The true value, x, is the quantity we would like to estimate from the available measurements. If we have multiple measurements of multiple variables, the measurement equation can be expressed in matrix form:

$$z = Ax + v \tag{2.6}$$

In this case, z is an array containing the available measurements, A is the measurement matrix (showing which variables each measurement provides information for), x is an array containing the true values of the variables (to be estimated), and v is an array of the noise in each measurement.

The water balance constraint can be expressed as:

$$Bx = 0 \tag{2.7}$$

where B is an array specifying the constraint.

According to the least squares approach, we want to minimize the square of the difference between the measured and true values of each variable ($[z - Ax]^2$). (We are estimating the 'true' value, x.) We add terms to the minimization problem in order to weight each measurement according to its uncertainty, and to constrain it with the water balance equation.

$$MIN \quad \underbrace{[z - Ax]^T C_v^{-1} [z - Ax]}_{\textit{weighted least squares}} + \underbrace{\lambda Bx}_{\textit{water balance constraint}} \tag{2.8}$$

Here C_v is the covariance matrix for uncertainty in the measurements. It is used to weight the measurements according to their uncertainty. λ is a Lagrange multiplier used to include the constraint in the minimization.

By choosing values for x and λ which minimize the above equation, we obtain an estimate for x that satisfies the water balance constraint and combines all available estimates in an optimal manner. The standard deviation of each estimate can easily be calculated if we know the standard deviation of the inputs.

As an example, suppose that at one location we have two measurements of precipitation, P, one measurement of evapotranspiration, E, two measurements of runoff, R, and zero measurements of the storage change, ΔS. (In some cases these "measurements" are not direct observations but are derived from other types of data.) Then the elements of the measurement equation and the minimization take on the following values.

$$z = \begin{bmatrix} P_1 \\ P_2 \\ E_1 \\ R_1 \\ R_2 \end{bmatrix} \tag{2.9}$$

$$A = \begin{bmatrix} 1 & 0 & 0 & 0 \\ 1 & 0 & 0 & 0 \\ 0 & 1 & 0 & 0 \\ 0 & 0 & 1 & 0 \\ 0 & 0 & 1 & 0 \end{bmatrix} \tag{2.10}$$

$$x = \begin{bmatrix} P \\ E \\ R \\ \Delta S \end{bmatrix} \tag{2.11}$$

$$v = \begin{bmatrix} v_{P_1} \\ v_{P_2} \\ v_{E_1} \\ v_{R_1} \\ v_{R_2} \end{bmatrix} \tag{2.12}$$

$$C_v = \begin{bmatrix} \sigma^2_{P_1} & 0 & 0 & 0 & 0 \\ 0 & \sigma^2_{P_2} & 0 & 0 & 0 \\ 0 & 0 & \sigma^2_{E_1} & 0 & 0 \\ 0 & 0 & 0 & \sigma^2_{R_1} & 0 \\ 0 & 0 & 0 & 0 & \sigma^2_{R_2} \end{bmatrix} \tag{2.13}$$

$$B = \begin{bmatrix} 1 & -1 & -1 & -1 \end{bmatrix} \tag{2.14}$$

Throughout this study, we will denote *estimates* from the water balance estimator with a hat (for example, $\hat{P}$, $\hat{E}$, $\hat{R}$, and $\Delta\hat{S}$). *Measurements* used as inputs to the estimator will be denoted by omitting the hat (for example, P, E, R, ΔS).

2.3 Example with one measurement for each variable

Pared down to the minimum, this approach would involve just one measurement each of precipitation, runoff, and evapotranspiration. In this case, it reduces to direct application of the water balance equation and storage change is calculated as the difference between precipitation and evapotranspiration and runoff. Our resulting estimates of P, E, and R are unchanged from the measurement, and retain the same uncertainty. The standard deviation of the error in the storage change estimate is equal to the standard deviation of the storage change estimate itself, because the estimate is unbiased. This gives:

$$\sigma_{\Delta\hat{S}} = \sqrt{\sigma_P{}^2 + \sigma_E{}^2 + \sigma_R{}^2} \tag{2.15}$$

If each measurement has the same standard deviation, σ_m, then the standard deviation of the storage change estimate is 1.73 σ_m, larger than the standard deviation of the individual measurements of P, E, and R.

If we also have a measurement of the storage change, then we could simply estimate $\Delta\hat{S}$ as the measured value. No further calculations are required. However, we can employ the water balance estimator to reduce uncertainty in estimates of $\Delta\hat{S}$ as well as $\hat{P}$, $\hat{E}$, and $\hat{R}$. When measurements of all four components of the water balance are available, the water balance constraint forces an adjustment to each component of the water balance so that the constraint is satisfied. Each element is estimated as a weighted combination of all available measurements. If all the measurements have the same uncertainty, the values of the water balance components are estimated as:

$$\hat{P} = \frac{3}{4}P + \frac{1}{4}E + \frac{1}{4}R + \frac{1}{4}S \tag{2.16}$$

$$\hat{E} = \frac{1}{4}P + \frac{3}{4}E - \frac{1}{4}R - \frac{1}{4}S \tag{2.17}$$

$$\hat{R} = \frac{1}{4}P - \frac{1}{4}E + \frac{3}{4}R - \frac{1}{4}S \tag{2.18}$$

$$\Delta\hat{S} = \frac{1}{4}P - \frac{1}{4}E - \frac{1}{4}R + \frac{3}{4}S \tag{2.19}$$

and the standard deviation of any of the resulting estimates is:

$$\sigma_{\hat{x}} = 0.87\sigma_m \tag{2.20}$$

Thus, we see that application of the water balance constraint is able to reduce the uncertainty of the estimates below the original uncertainty of the measurements. In particular, the standard deviation of the $\Delta\hat{S}$ estimate is reduced from 1.87 σ_m when no measurement of ΔS is used, to 1.0 σ_m when an estimate is available but the water balance estimator is not used, to $0.87\sigma_m$ when the estimator is used.

If each measurement has a different uncertainty, the measurements are weighted according to their uncertainty. At the extreme, if one measurement has a much higher uncertainty than the others, the least squares solution again reduces to simple application of the water balance equation.

2.4 Example with a hypothetical climate

A similar reduction in uncertainty can be seen when applying the water balance estimator to a hypothetical climate. By assuming the hypothetical "true" climate described by the variables in Table 2.1, we can show the reduction in uncertainty which is achieved by applying the water balance estimator when multiple measurements are available. The hypothetical climate is similar to that found in California.

In a traditional water balance, only one measurement of each water balance element is used (no storage change measurement). $\Delta\hat{S}$ is then calculated by direct application of the water balance equation and the standard deviation of the $\Delta\hat{S}$ estimate is 150 mm/year.

Even if no ΔS measurement is available, we can improve our estimate by using multiple measurements of precipitation and evapotranspiration. Using the standard deviations listed

Table 2.1: Hypothetical climate used in Monte Carlo simulations

Variable	True value [mm]	Standard Deviation [mm]	Number of measurements
Precipitation	600	100	up to 2
Evapotranspiration	425	100	up to 2
Runoff	200	50	1
ΔS	-25	50	up to 1

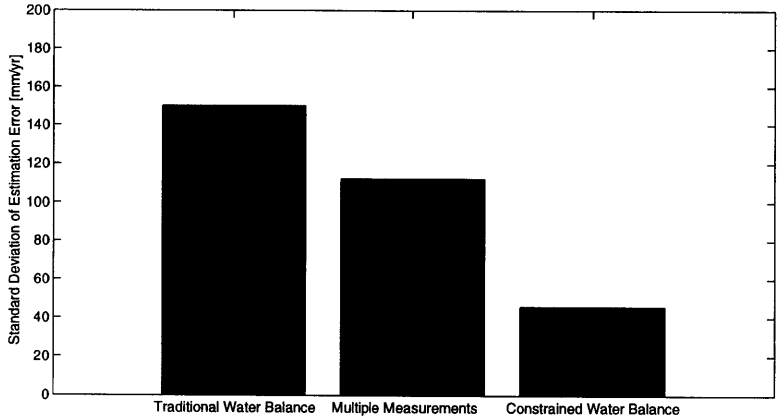

Figure 2-3: The standard deviation of the estimation error is reduced by using multiple measurements and the water balance estimator.

in Table 2.1 to weight the measurements, $\Delta\hat{S}$ is calculated as:

$$\Delta\hat{S} = \frac{1}{2}P_1 + \frac{1}{2}P_2 - \frac{1}{2}E_1 - \frac{1}{2}E_2 - R_1 \tag{2.21}$$

and the standard deviation, $\sigma_{\Delta\hat{S}}$, is reduced to 112 mm/yr.

If we are also able to incorporate a ΔS measurement, then $\Delta\hat{S}$ is calculated as:

$$\Delta\hat{S} = \frac{1}{12}P_1 + \frac{1}{12}P_2 - \frac{1}{12}E_1 - \frac{1}{12}E_2 - \frac{1}{6}R_1 + \frac{5}{6}S1 \tag{2.22}$$

and the standard deviation is further reduced to 45.6 mm/yr. The reduction in the standard deviation of the estimation error by incorporating multiple data sources and a measurement of ΔS is shown in Figure 2.4. Additional measurements of any component of the water balance can be expected to further decrease the uncertainty.

2.5 Application of surrogate measurement of ΔS

As long as our measurements are unbiased, then the least squares solution is also unbiased. Appendix A contains a mathematical proof of the unbiasedness of the estimator.

In most cases, we do not have measurements of ΔS based on observed data for our

watersheds. We can improve our estimate by using multiple measurements of the inputs, but greater gains can be made by the water balance estimator when a ΔS measurement is available. While we do now know exactly what the storage change in any watershed is, we do know that it is relatively small. Barring additional information, we make the initial guess that the storage change is equal to zero. This surrogate measurement is included in the measurement array, z, and the measurement matrix, A. The use of a surrogate measurement of ΔS is equivalent to incorporating prior information to the estimation in a Bayesian approach. While inclusion of a surrogate storage change measurement of zero introduces some bias to the estimation, there is also a large reduction in uncertainty. If the true storage change is negative, then using a surrogate measurement of zero storage will make our estimate more optimistic. That is, we are unlikely to predict large groundwater depletion in areas where it is not in fact occurring.

This can be demonstrated using Monte Carlo simulations. Assuming a "true" climate with the chracteristics listed in Table 2.1, we used Monte Carlo simulations to assess the bias introduced by using a surrogate measurement of $\Delta S = 0$. We generate "measurements" around the true climate by assuming that errors are random and normally distributed with specified standard deviations. Instead of using just one fixed value for the standard deviation in measurement errors, we assigned the standard deviation as a percentage of the true value of the variable. Figure 2.5 shows the results for measurement errors from 1 to 25 percent.

The simulations show that in this climate scenario, the surrogate measurement of zero storage change leads to a small upwards bias in the storage change estimate. To a lesser degree, precipitation is also biased upwards, and evapotranspiration and runoff are biased downwards. As seen in Figure 2.5, this bias increases as the uncertainty of our measurements increases. However, the bias tends to make our estimates of groundwater depletion less severe than the true state. This makes it unlikely that our surrogate measurement of zero storage change will lead us to predict significant groundwater depletion where it does not exist. For this reason, we include a surrogate measurement of zero storage change in basins where we have no other data on storage change as a means of reducing uncertainty.

The standard deviation, $\sigma_{\Delta S}$, assigned to the surrogate measurement can have a significant effect on the $\Delta\hat{S}$ estimate and its uncertainty. Using the same hypothetical climate, we use the fixed standard deviations in measurements listed in Table 2.1 and vary the standard deviation of the ΔS surrogate measurement. Figure 2.5 shows the tradeoff between low bias and low standard deviation in $\Delta\hat{S}$. A smaller $\sigma_{\Delta S}$ causes the water balance estimator to weight the zero storage change "measurement" more heavily, keeping the estimated $\Delta\hat{S}$ closer to zero and increasing the bias. Larger $\sigma_{\Delta S}$ gives the water balance estimator more leeway to shift $\Delta\hat{S}$ away from zero, as the ΔS measurement is deemed less reliable and given less weight. This results in smaller bias but more uncertainty. At the extreme, a very large $\sigma_{\Delta S}$ will cause the estimator to ignore the ΔS measurement and calculate $\Delta\hat{S}$ by direct application of the water balance equation to estimated values of $\hat{P}$, $\hat{E}$, and $\hat{R}$.

An actual storage change may be masked by the introduction of bias, so the use of a surrogate measurement of ΔS is most useful not to detect groundwater storage change, but to reduce uncertainty in estimates of P, E, and R.

Throughout most of this work we present results both when no measurement of ΔS is used, and when a surrogate measurement of zero is used. The standard deviation of the surrogate measurement, $\sigma_{\Delta S}$, is set at 50 mm on the assumption that storage changes over large watersheds that include both natural and irrigated lands are unlikely to greater than 50 mm.

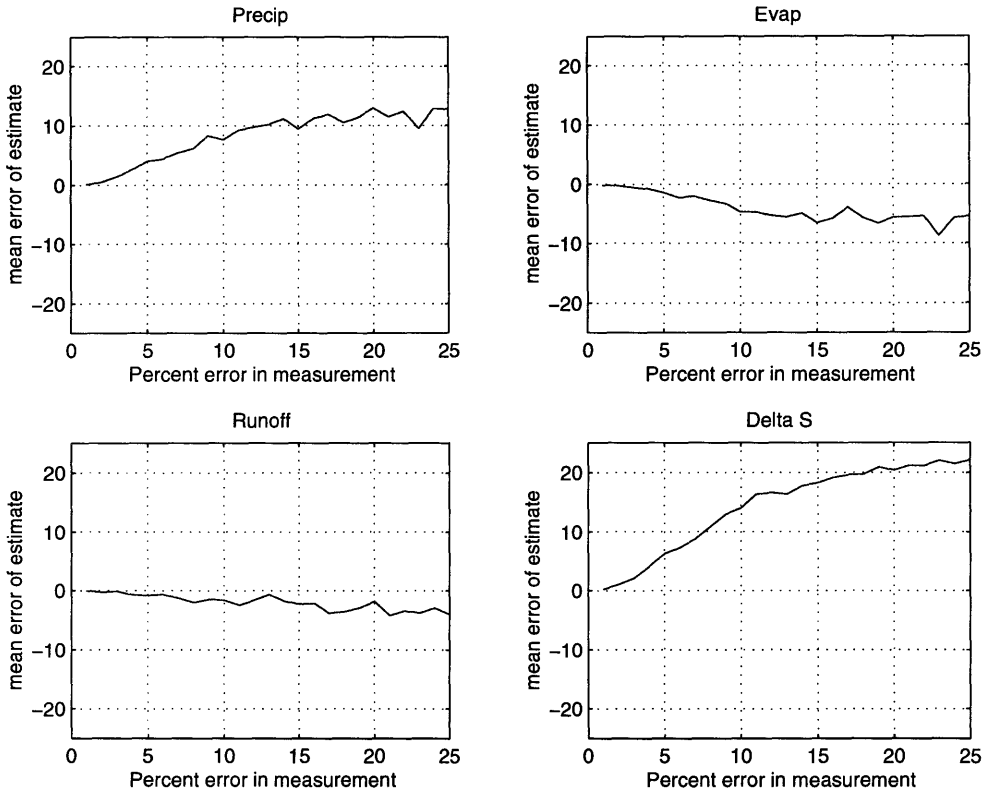

Figure 2-4: Mean error (bias) introduced in the water balance estimator by using a surrogate measurement of storage change of zero. The x-axis shows standard deviation of the measurement error, as a percentage of the true value of the variable.

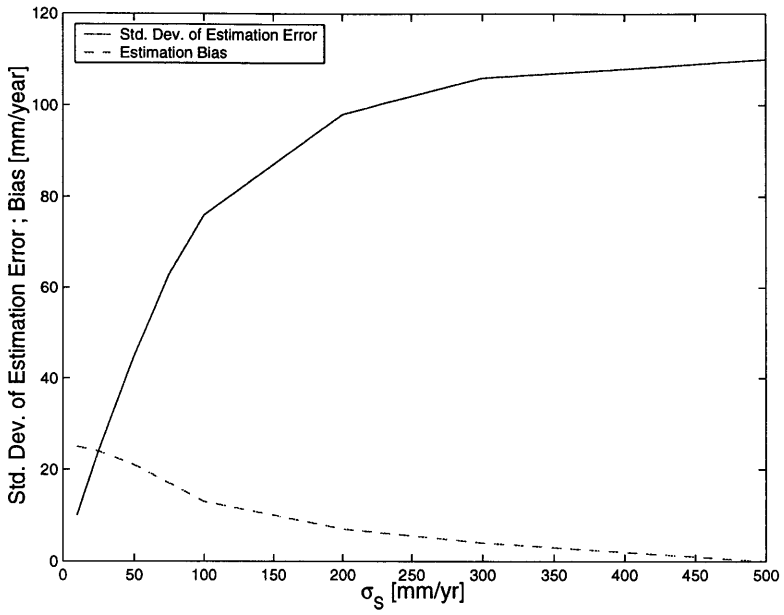

Figure 2-5: There is a tradeoff between low bias and high uncertainty, reflected in the standard deviation of the estimation error.

2.6 Limits to the water balance estimator

The water balance estimator includes a number of assumptions which restrict its applicability to some basins.

One underlying assumption of our methodology is that the surface water and the groundwater basins coincide. This presents difficulty in basins where the groundwater basin is distinct from the surface water basin. For example, the Ogallala aquifer in the great plains area of the United States crosses several surface water divides. In basins such as in the Sacramento/San Joaquin of California, where the principal groundwater basin is contained within, but is significantly smaller than the surface water basin, even relatively high rates of groundwater overdraft cannot be detected because results are averaged over the entire surface water basin, and not just the portion overlying the groundwater aquifer.

Both of these examples point out the limitations imposed by using the watershed as the control volume. It is also possible to draw the control volume around only the land surface area containing the groundwater aquifer. The drawback is that we now have to account for lateral flows into and out of the control volume, adding additional uncertainty to the estimation. However, this increase in uncertainty may be warranted if it allows us to study important groundwater regions which cross surface divides. It is also possible that a stronger storage change signal will emerge when it is not diluted over a larger surface area.

In constructing our water balances, we have also assumed that over the long term, changes in water storage in soils, snow and ice, and lakes and reservoirs is minimal. Particularly in light of possible climate change induced snowmelt and glacial retreat, this assumption may not be strictly valid in some basins. Using the long term mean may also cover up the effects of interannual variability in climate on water storage. If the same amount of water is needed every year for crops, wet years and dry years may not even out in terms of

groundwater usage because flood waters during wet years are not necessarily captured and may not completely restore depleted groundwater reserves.

Finally, it is important to note that this analysis does not attempt to consider other sustainability issues which may arise from groundwater extraction for irrigation use. For example, saltwater intrusion in coastal areas, salinization from poor management of irrigation waters, and groundwater pollution may all jeopardize groundwater aquifers used for irrigation.

Chapter 3

Components of the Water Balance: Global Data

The following data are required to carry out our water balance estimates:

- Watershed boundaries and catchment area (static)
- Precipitation (mean annual)
- Evaporation (mean annual)
- Streamflow/Runoff (mean annual)

In addition, groundwater data are needed for validation in our test basins, and information on interbasin transfers of water is required, where applicable.

Remote sensing has allowed significant expansion in the availability of spatially distributed datasets in recent years. In particular, sparsely populated areas removed from scientific centers are now being monitored for the first time. In this study we make use of both remote sensing data and surface based station data collected at point locations. Because of the large spatial scales which we wish to study, we focus only on readily available global datasets. The data sources we have identified are by no means the only sources of data available for specific regions. More detailed local data are often available from local and regional governments and other sources. However, the difficulty in obtaining such data make its use impractical for the large scales we are considering.

The following sections describe available global datasets and also the alternative estimation techniques that we have employed for some types of data. Evapotranspiration "measurements" in particular required significant development beyond what is readily available and are discussed separately in Chapter 4.

3.1 Watershed boundaries and catchment area

Watershed boundaries are needed to define the control volume for our mass balance. Once the watershed boundaries are identified, they are used to calculate the contributing drainage area and basin average precipitation, evapotranspiration and runoff. Surface water divides can be determined based on topographic features. Unless specific information to the contrary is available, we will assume that the surface water basins and the groundwater basins have the same boundaries.

3.1.1 Hydro1k

Hydro1K is a hydrologic dataset based on GTOPO30, an elevation database for the entire globe developed by the USGS (2001a). Data are available at 30 arc-second horizontal resolution (approximately 1 km) and 1 meter vertical resolution. Globally, the GTOPO30 data was developed from 8 different sources. In Asia, the predominant source is the Digital Terrain Elevation Data (DTED), a raster topographic database produced by the National Imagery and Mapping Agency (NIMA). DTED are available at 3-arc second resolution. Elevation in some regions of Asia are obtained from the Digital Chart of the World, a vector cartographic dataset which includes elevation contours and information on the drainage system. Data in the U.S. are digitized from USGS topographic maps.

The Hydro1K database was created by processing the GTOPO30 data into several derivative datasets (USGS 2001b). Separate files are available for each continent. The datasets include the following variables at a 1 km resolution:

Elevation. The GTOPO30 data was processed to remove spurious sinks while preserving natural sinks such as closed inland basins, thus producing a hydrologically correct digital elevation model (DEM).

Flow direction. The flow direction is defined as the direction of steepest descent from each grid cell to any of its eight neighboring cells.

Flow accumulation. The area draining through each cell was calculated from the flow direction grid. It can be used as a measure of the upstream catchment area from any point in the dataset domain.

Basins. Basins were delineated based upon the flow direction and flow accumulation grids and checked against existing digital and non-digital data.

Streams. Streams were outlined based upon the flow direction and flow accumulation grids and checked against existing digital and non-digital data.

The actual creation of the DEM and its associated grids was done iteratively. Sinks were removed, and the resulting flow direction, flow accumulation, and basins/streams were computed. Basins and streams were checked against existing maps, and the DEM was adjusted as necessary. Figure 3-1 shows the Hydro1K derived topography for Asia, and Figure 3-2 shows the Hydro1K derived streams.

Slope, aspect, and the compound topographic index (CTI) are also distributed with the Hydro1K datasets.

3.1.2 GIS Hydro '99

Topographic data are also available on GIS Hydro '99, a CDROM produced by the University of Texas (Asante et al. 1999). Available data include elevation, basin boundaries, and streams. This data was used as a secondary source of topography and watershed configuration.

3.1.3 Basin delineation

The basins delineated and distributed with the Hydro1K and GIS Hydro '99 datasets do not necessarily correspond to locations where streamflow records are available. Consequently, we also delineated our own basins at stream locations of interest. Basins were drawn at the streamgage locations used in our water balance analysis using the USGS Hydro1K data and ArcInfo's function for watershed delineation. The routine calculates the contributing area to a stream location using flow direction and flow accumulation data derived from

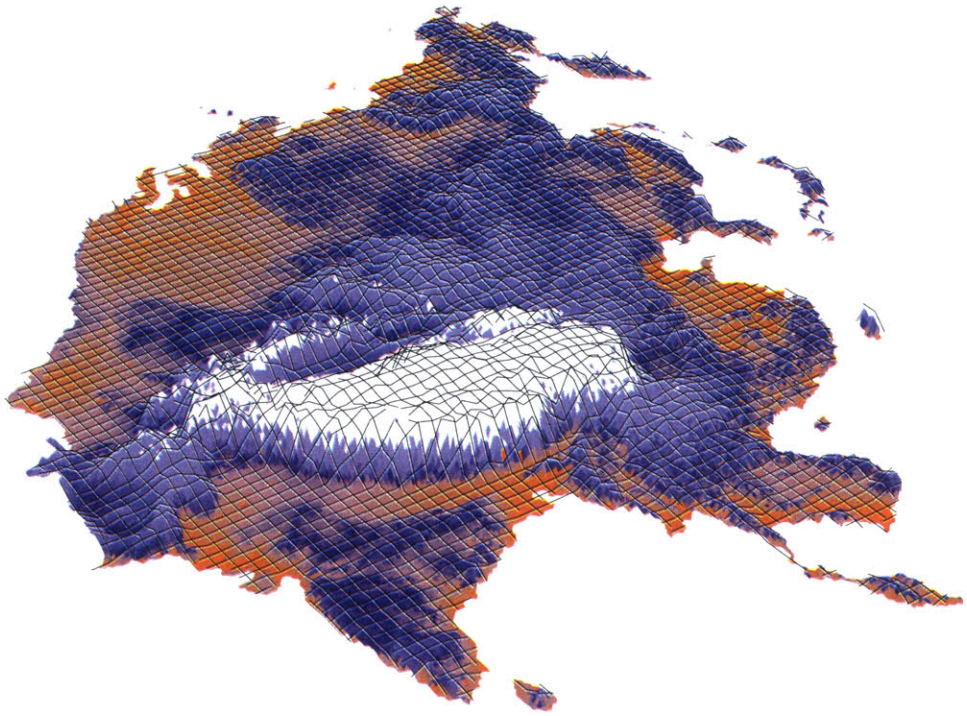

Figure 3-1: USGS Hydro1K topographic data for Asia.

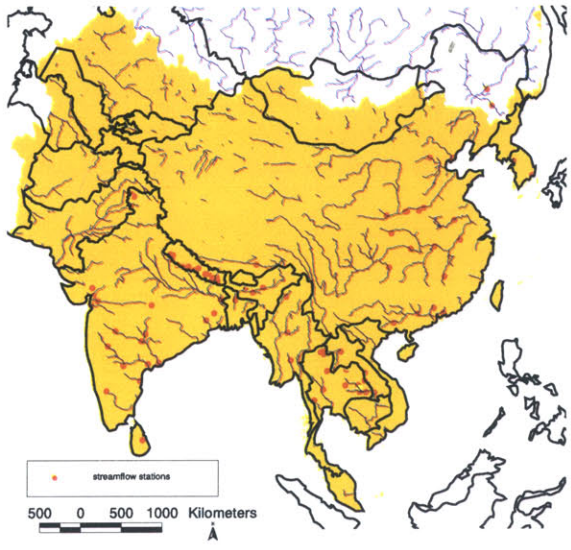

Figure 3-2: Streams in Asia, as defined by Hydro1K data, and streamflow gaging stations with long term data available.

Table 3.1: Summary of Precipitation Data used in this Study

Source	Resolution	Years
Willmott et al. (1998)	0.5° x 0.5°	1920-1980
Cramer (1996)	0.5° x 0.5°	1931-1960
GPCP, Huffman et al. (1997)	2.5° x 2.5°	1988-1998

the elevation data. The routine yields the same basin boundaries as those distributed with Hydro1K, except that the outlet point corresponds to a streamgage location. Watershed areas were checked against existing maps and reported values for the contributing area.

3.2 Precipitation

Precipitation makes up the largest component of the water balance and good estimates are essential to an accurate analysis. Spatially distributed estimates of precipitation can be obtained through remote sensing (satellite, airplanes, land-based radar) while point measurements are available from surface gauges at many fixed station locations. Table 3.1 summarizes the precipitation data used in this study. Each is described briefly in the following sections. Table 3.1 is not a comprehensive list of all available global or large scale precipitation datasets. A number are excluded because of coarse resolution or short periods of record.

3.2.1 Willmott et al. Regridded Climatology Version 2.01

Willmott, Matsuura and Legates (1998) reinterpolated Legates and Willmott's (1990) station records of monthly precipitation to produce a regridded climatology. The precipitation estimates were based on 26,858 stations with records spanning the period 1920-1980. Stronger emphasis was placed on data from latter years. The data are available on a 0.5° x 0.5° grid for monthly and annual means.

Precipitation data were first corrected for gage error before performing the interpolation. Estimates of the cross-validation error (errors due to interpolation) are distributed along with the precipitation climatology. For most land areas in Asia, these errors are on the order of 200 mm or less. However, in some areas, particularly mountainous areas, they can be much higher, even exceeding 1000 mm in some places.

Figure 3-3a shows the Willmott et al. precipitation climatology for our study region in Asia.

3.2.2 Cramer Precipitation Climatology

Leemans and Cramer (1991) developed a climatological dataset of long term monthly precipitation. This dataset was updated in 1996 and is available as part of the IIASA Climate database Version 2.1 (W. Cramer, Potsdam, personal communication). Precipitation gage data for the period 1931-1960 are interpolated onto a 0.5° x 0.5° grid. The updated dataset has been used by many groups for large scale studies, including the IGBP NPP model intercomparison.

Figure 3-3b shows the Cramer precipitation climatology for our study region in Asia.

3.2.3 GPCP

The Global Precipitation Climatology Project (GPCP) provides global precipitation data at a spatial resolution of 2.5° by 2.5° degrees (Huffman et al. 1997). Satellite estimates of precipitation from multiple sensors are combined with surface gage data. Satellite estimates are obtained from Special Sensor Microwave/Imager (SSM/I) emmission estimates and scattering estimates, and infrared images obtained from several geostationary satellites. Surface gauge data from about 6700 stations around the globe are corrected for systematic gaging errors (e.g., wind effects) and interpolated onto a global grid. The combination dataset provides data at a monthly timestep for July 1987 - present. In this analysis, we utilize data from January 1988 to December 1998.

Figure 3-3c shows the GPCP precipitation climatology for our study region in Asia. Estimated errors for the combined dataset are large in some regions, on the order of 300 mm/year.

In Version 2 Combination, TOVS estimates of precipitation are included to extend the temporal length of the dataset. This data may be included in our analysis if a longer time series becomes necessary. There is also a daily 1°x1° dataset available for the area between 40N and 40S. Data are currently available for a shorter time period, from January 1997 to December 1999.

3.2.4 Measurement uncertainty

While the Willmott et al. and the GPCP datasets include information on the uncertainty of the measurements, the Cramer dataset does not. When using these data in the water balance estimator, we will use the error estimates distributed with the datasets along with the rough guideline that precipitation estimates are commonly within about 25% of actual values. In addition, the range in precipitation values reported among the three datasets can help to give a sense of the uncertainty.

3.3 Runoff/Streamflow

Streamflow consists of both surface runoff and groundwater baseflow discharging into streams. Aside from known interbasin transfers of water, streamflow is the only lateral outflow from a watershed that is considered in this study. Additional groundwater outflow directly to the oceans or parallel to the stream is possible.

In our water balance approach we rely primarily on streamflow gage data from the sources described below. Mean annual streamflow is divided by the basin area to obtain mean annual runoff. Other sources of runoff data which could be incorporated into the estimation in the future are also described here. However, because the uncertainty of these runoff estimates for ungaged areas remains high we did not use them in our analysis.

3.3.1 Streamflow gage data

GRDC

The Global Runoff Data Center (GRDC) in Koblenz, Germany has a large database of river discharge. The complete dataset includes monthly and some daily data. The GRDC has also released a database containing the long term mean monthly and annual flows in selected rivers. Included in this database are 1352 stations from around the world, selected on the

a) Willmott et al (1998) Regridded Precipitation Climatology

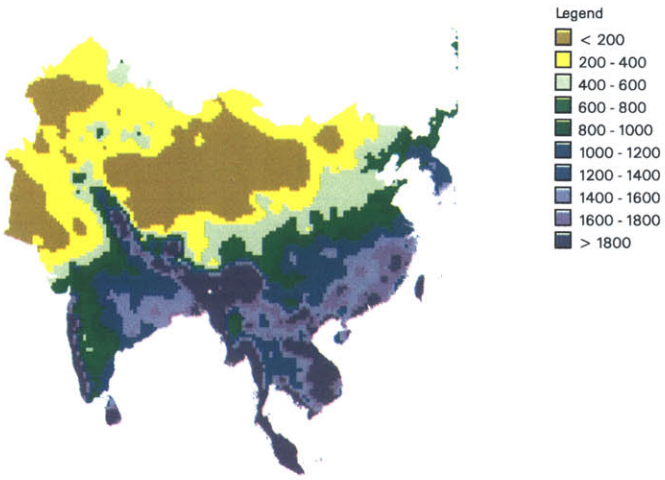

b) Cramer Update of Leemans and Cramer (1991) Precipitation Climatology

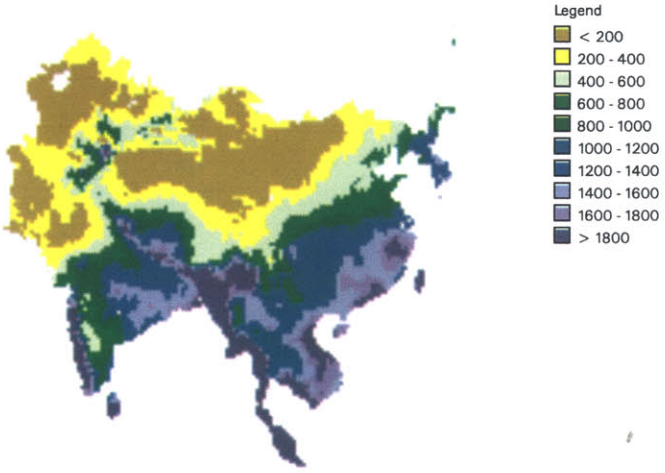

c) GPCP Precipitation Climatology

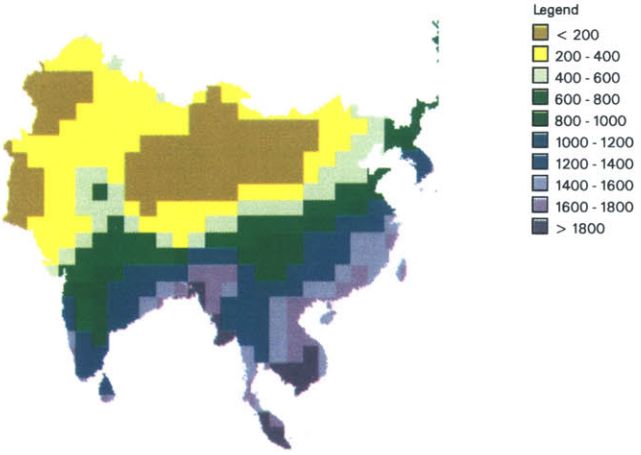

Figure 3-3: Precipitation climatologies for Asia from available global datasets.

basis of length of record (at least 10 years without missing values) and size of drainage area (at least 2500 km^2). Mean, mininum, and maximum monthly flows are provided, along with station information. There are 200 stations available in Asia, of which approximately 89 are within our study area. A number of the 89 stations report river flow at different points along the same river.

RivDIS

Vorosmarty and others at the University of New Hampshire have established a clearinghouse for river discharge data. Most of their data are obtained from UNESCO. The database, titled RivDIS (version 1.0), contains 949 stations, of which 215 are in Asia. RivDIS includes many of the same stations available from the GRDC.

Other sources of streamflow gage data

Streamflow data has also been tabulated in various publications. We have made use of such data to supplement the digital data described in the above sections. Sources of tabulated data include: van der Leeden (1975) and Gleick (1993).

Figure 3-2 shows the gage locations available in Asia, and the stream network defined in the Hydro1K dataset.

3.3.2 Gridded streamflow/runoff data

Streamflow gages do not cover all land areas. Shiklomanov (1998) estimates that 15% - 20% of the global land surface is not covered by regular observations of streamflow. Because streamflow gages do not cover all river reaches, there have been various efforts to extend runoff datasets beyond the areas covered by gages through modeling, spatial interpolation, and regression techniques. While these datasets were not incorporated into our study, some large scale efforts are described briefly below.

GCRD

In collaboration, the GRDC and UNH have developed the Global Composite Runoff Database (GCRD) also known as the UNH-GRDC Composite Runoff Fields V1.0 (Fekete et al. 2000). This database combines river discharge data from the GRDC with output from a simple monthly runoff model. Output is routed through a simulated topological network (STN-30p) developed by UNH. Total runoff in gaged basins is scaled to match the observed runoff at the gage, preserving the spatial distribution of runoff predicted by the model. In ungaged areas, model output alone is used to estimate runoff. The gridded runoff data are available globally at 0.5° x 0.5° resolution.

Prior to scaling, the modelled runoff showed significant scatter when compared to streamflow measurements. Consequently, we chose not to use this dataset in our water balance estimation.

ISLSCP

ISLSCP has included on its Initiative I CD-ROM a gridded runoff dataset. The runoff data was derived from a number of different maps, of which Korzoun's Atlas of the World Water Balance was cited as the most important. Korzoun estimated runoff by interpolating data

from streamflow gages. The ISLSCP data are available at 2° x 2° resolution. As will be seen in the following section, runoff amounts do not always conform to observations available from the GRDC gages. As a result, we have not used this data in our analysis.

3.3.3 Watershed-scale runoff regression

Vogel et al. (1999) used multiple regression techniques to show that streamflow correlated well with various more readily available basin characteristics. Their analysis was conducted for 18 hydrologic regions in the U.S. Following this approach, we explored the feasibility of using easily measured basin characteristics to predict runoff in ungaged areas of Asia. Using multiple regression, we relate streamflow to more easily obtainable statistics for the watershed. Our watershed statistics differ from those used by Vogel et al. and include:

- mean annual precipitation
- mean annual potential evapotranspiration
- dryness index (PET/Preciptation)
- compound topographic index, $CTI = ln\left[\frac{flow\ accumulation}{tan(slope)}\right]$
- cropping intensity
- precipitation ratio July:Jan
- precipitation difference July - Jan

Runoff was hypothesized to be calculable as an empirical function of several variables:

$$R = e^k A^a B^b C^c \tag{3.1}$$

Where R is runoff, A, B, and C are the basin characteristics, and k, a, b, and c are regression constants. By taking the logarithm of this equation, we can transform it into a linear function:

$$\ln R = k + a \ln A + b \ln B + c \ln C \tag{3.2}$$

Multiple linear regression can be easily performed on this equation, to estimate values for the regression constants. Once these constants are determined, lnR can be calculated using this function and then transformed back to runoff, R.

Using the long term annual records from GRDC, we identified 39 basins with a drainage area larger than 25,000 km^2 and whose reported drainage area matched the Arc-delineated drainage area within 15% (Figure 3-4a). Where possible, larger basins were divided into upstream and downstream areas with additional streamflow stations.

Our results show that the combination of several basin characteristics can provide information about runoff in the basin. When used in conjunction, the mean annual precipitation, dryness index, CTI, and the July - Jan precipitation had the highest correlation with runoff. When all of these variables were used in the regression, the R^2 between watershed characteristics and runoff was 0.71 and the RMS error was 270 mm/yr. A split sample test gave slightly lower R^2 for the second sample at 0.60, but the RMS error was about the same at 280 mm/yr.

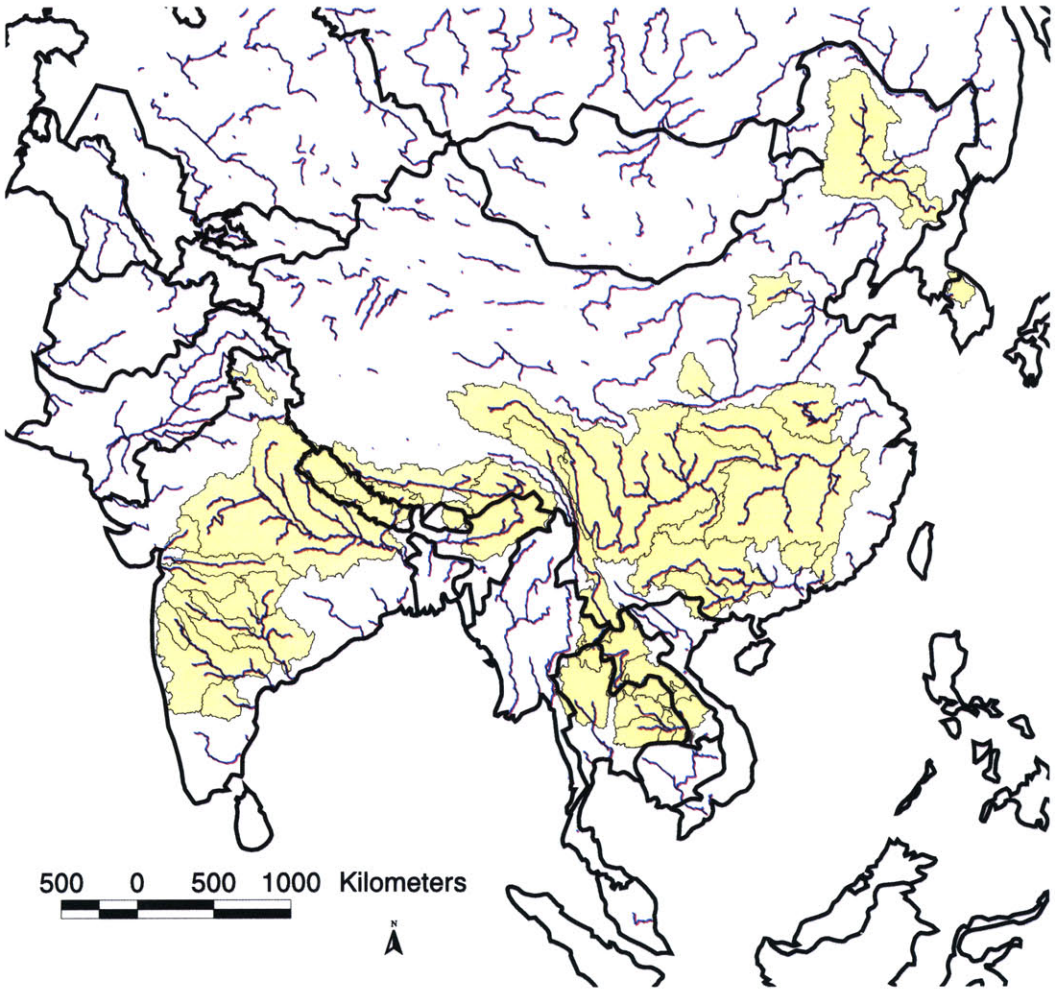

Figure 3-4: River basins used in the multiple regression of runoff against watershed characteristics.

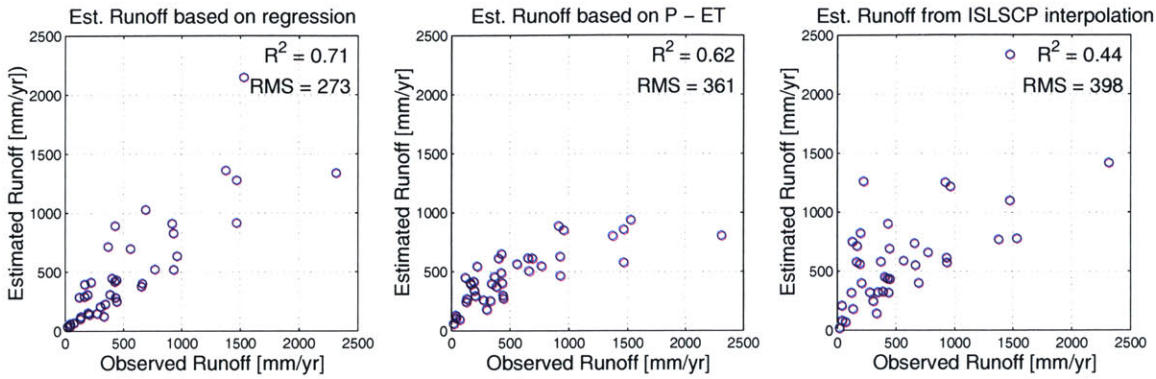

Figure 3-5: Observed vs. estimated runoff a) using multiple regression of regional runoff and basin characteristics b) using the water balance equation and c) from ISLSCP interpolation

.

While an RMS error of 270 mm/yr may sound substantial, it is actually smaller than the RMS error (360 mm/yr) for runoff estimated using the basic water balance equation, P-ET. Figure 3-5b compares the estimated and observed runoff using the multiple regression and the water balance. For the water balance, precipitation was taken as the average of the 3 global sources, and the selective average AET estimate was used for the ET estimate. When observed runoff is regressed against ISLSCP's gridded runoff estimates for these Asian basins, we again see a smaller R^2 (0.44) and a larger RMS error (400 mm/yr) as compared to results from the multiple regression. Thus, the multiple regression is a useful means of obtaining additional information on runoff in ungaged basins.

3.3.4 Measurement uncertainty

According to Fekete et al. (2000), streamflow records are usually accurate to about 10-20%. We use this as a rough guideline for uncertainty in streamflow measurements when no other information is available. We also consider the length of the streamflow record, assigning higher uncertainty for short periods of record.

3.4 Projection

Throughout this work, we utilize the Lambert Azimuthal Equal Area Projection, optimized for either Asia or North America, depending on the area with which we are working. The parameters are shown in Table 3.2. As an equal area projection, the Lambert Azimuthal projection facilitates computations requiring measurements of distance or area. Many of the datasets described in this chapter were distributed in latitude-longitude or other coordinates and were converted to the appropriate Lambert Azimuthal projection for use in this study. These transformations are all completed using the ArcView/ArcInfo Geographic Information System (GIS).

Table 3.2: Lambert Azimuthal Equal Area Projection Parameters

Parameter	Asia	North America
Radius of Sphere of Reference	6,370,997 meters	6,370,997 meters
Longitude of Center of Projection	100° 0' 0"E	100° 0' 0" W
Latitude of Center of Projection	45° 0' 0"N	45° 0' 0"N
False Easting	0.0	0.0
False Northing	0.0	0.0

Chapter 4

Evapotranspiration Estimation

Evapotranspiration (ET) is the sum of two processes: evaporation and transpiration. Both processes convert liquid water on the land surface into water vapor in the atmosphere. Evaporation takes place from water surfaces (e.g., lakes, rivers, puddles, intercepted water), soil, snow, and ice. Transpiration takes place when liquid water in plant tissues is transformed into water vapor and released to the atmosphere. The two processes occur simultaneously and are difficult to distinguish (Allen et al. 1998).

ET has been conceptualized as two distinct quantities - potential evapotranspiration (PET) and actual evapotranspiration (AET). PET is the climatically controlled rate at which water would evaporate and transpire into the atmosphere under dense vegetative conditions if water were not limiting. AET is the rate at which water is actually transferred from the land surface to the atmosphere depending on moisture availability (Bras 1990). AET is always less than or equal to PET, depending on the degree of water scarcity.

The quantity needed for our water balance is AET. Unfortunately, AET is difficult to measure directly and is also difficult to estimate from other data. Various approaches for AET estimation range from empirical formulas to numerical models to the use of remote sensing data. The remainder of this chapter deals mainly with the methods we selected to estimate AET. However, we first discuss estimation of PET, as PET is often used as an input in the estimation of AET.

4.1 Potential Evapotranspiration (PET)

We are interested in PET because it is often used as an input when estimating AET. One common approach to estimating AET involves first calculating PET, and then determining the fraction of PET which is likely to be met given soil moisture and vegetative conditions. This method has been especially popular in agricultural applications, and in this context, PET is sometimes called the reference crop evapotranspiration. The standard "reference crop" is an idealized grass of specified height and roughness and with access to a plentiful supply of water (Doorenbos and Pruitt 1977, Smith, Allen and Pereira 2000).

4.1.1 Measurements

Pan evaporation measurements are the most common source of observed PET data. Evaporation rates from a shallow container filled with water are measured by tracking changes in the volume of water. Because these measurements deal exclusively with evaporation from

a water surface, they are more precisely a measure of potential evaporation. The lip of the pan creates different wind patterns than those experienced by open water surfaces such as lakes. In addition, the thermal characteristics of an evaporation pan are not the same as those of larger bodies of water. Consequently, pan evaporation measurements must be adjusted in order to reflect true potential evaporation levels. This is generally done by multiplying the measured pan evaporation by a pan coefficient. Typical pan coefficients range from about 0.6 - 0.8, with 0.7 being the most commonly used coefficient (Singh 1992). The appropriate coefficient depends on the pan design and local meteorologic conditions. Less well-documented is an appropriate coefficient to relate pan evaporation to reference crop ET.

While pan data is collected at many locations around the world, the data are often difficult to obtain outside of the region in which they are measured. In addition, inconsistencies between measurement apparatus and measurement techniques at different stations can make regional comparisons of PET based on pan data difficult. Studies of pan evaporation measurements indicate that the "methods are susceptible to the microclimatic conditions under which the pans are operating and the rigour of station maintenance. Their performance proves erratic." (FAO 1998, Chapter 2)

Plants are sometimes grown in lysimeters in order to measure PET. The lysimeter is essentially a container with a permeable bottom. By keeping track of the amount of applied water, the amount of water draining from the lysimeter bottom, and any changes in moisture storage, PET can be calculated using a mass balance. Measurements are scattered, and rarely provide the long term data needed for this study.

Because of limitations in the accuracy and availability of measured PET data, we did not use any such data in this study. Instead, we relied on PET estimated as a function of other more readily measured quantities.

4.1.2 Estimation methods

Significant inputs of energy are required to overcome the latent heat of vaporization and convert liquid water into water vapor. In addition, water vapor can only be added to the atmosphere if the atmosphere is not already saturated. These two requirements result in two important paths by which potential evapotranspiration is restricted: either by the available energy or by the available mechanisms for transport of water vapor. PET estimation methods focus on either one or both of these limits to the PET rate.

The simplist techniques for PET estimation are empirical formulas which were developed many years ago. These methods typically calculate PET as a function of more easily measured quantities like temperature and number of daylight hours, both of which can be considered indicators of the available energy. More complicated, physically based methods consider both energy and mass transport constraints. Although many more methods exist, the following discussion describes only the two PET estimation methods used in this study.

Thornthwaite Equation

Thornthwaite (1948) developed one of the most commonly used empirical equations for PET estimation. It has been widely used in many global and regional studies because it requires only temperature data as input (Choudhury 1997). However, some have noted that the Thornthwaite method tends to underestimate PET, especially in arid regions (Choudhury

1997, UNEP/GRID n.d.). Mintz and Walker (1993), on the other hand, showed good agreement between Thornthwaite PET and PET derived from several radiation based equations.

Two sources of global PET data calculated using the Thornthwaite method are available. The first was developed by Willmott et al. (1985), as part of their terrestrial water budget. An updated version (1.02) was released in 2001 (Willmott and Matsuura 2001). It uses over 24,000 temperature stations with data over the period 1950-1999 as input.

A second Thornthwaite PET dataset is distributed by UNEP/GRID. This dataset uses the Thornthwaite method, but attempts to correct for low bias by calibrating the Thornthwaite estimates against PET calculated by the Penman method at locations in Europe and Sudan (Deichmann and Eklundh 1991). The Penman estimates are assumed to be unbiased. Precipitation is used as an additional variable in the calibration. Temperature data are taken from 1,834 stations and interpolated onto a grid using a nearest neighbor approach. The climatology is based on the period 1951-1980. The distributed data do not include the actual calculated PET values, but only classifications into 400mm bins, limiting their usefulness for our analysis.

Penman-Monteith Equation

Of the more physically based techniques for PET estimation, the Penman-Monteith equation is perhaps the best known. It is often regarded as the most accurate method of estimating PET (Shuttleworth, 1993; Allen, 1998). However, other formulations have been shown to be just as successful or better, when calibrated to local conditions (Garatuza-Payan et al. 1998). For global estimates that do not benefit from local calibration, the Penman-Monteith equation is likely to produce better results.

The Penman Monteith equation combines the energy balance equation with the aerodynamic equation for vapor transfer. It makes specific provision for plant transpiration by use of a canopy resistence term. While the equation gives good results, it has significant data requirements, making it more difficult to apply at large scales than empirical methods.

Choudhury (1997) estimated global values of potential evapotranspiration using the Penman-Monteith equation for the period January 1987 - December 1988. Data are available at a monthly timestep at a 0.25° x 0.25° resolution, but incorporate input data at up to 2.5° x 2.5° resolution. These inputs include satellite estimates of solar radiation, fractional cloud cover, air temperature and vapor pressure along with aerodynamic resistance calculated from assimilated data. The estimated potential evaporation values are compared to lysimeter observations at 35 well-watered grassland sites in different regions of the world.

While the period of record for this dataset is short, we chose to use this dataset as one representation of the long term mean PET because of the acknowledged accuracy of the Penman-Monteith method and because the interannual variability in PET is generally small. For example, Jackson (1989) gives the coefficient of variation for PET at just 5% on an annual basis.

4.1.3 Estimation Uncertainty

Vorosmarty, Federer and Schloss (1998) conclude that the choice of PET estimate can make a large difference in the subsequent calculation of AET. Differences between estimates based on different techniques can be as high as several hundred millimeters. We attempt to account for the uncertainty by using two different PET estimates - the Choudhury dataset based on the Penman-Monteith equation and the Willmott et al. dataset based on the Thornthwaite

equation. The adjusted PET dataset from UNEP/GRID could not be used directly because of the large bin size used in reporting the data. However, this dataset was visually compared to PET data from Willmott et al. and Choudhury. In the U.S., the adjusted Thornthwaite dataset tended to to show values intermediate to the other two datasets. In Asia, the differences between the 3 datasets tended to be less pronounced and less systematic.

Incorporation of additional PET estimates in the future can further reduce uncertainties.

4.2 Actual Evapotranspiration (AET)

Actual evapotranspiration (AET) data will be used directly in our water balance. Sources of AET data are described below.

4.2.1 Measurements

Very few measurements of actual evapotranspiration are available, and usually only at scattered point locations around the world with records of short duration. The FluxNet program has a small repository of ET measurements at scattered locations around the globe. Measurement stations were developed to study carbon dioxide fluxes, and often include ET measurements as part of the data.

The scarcity of AET measurements, as well as the scale difference between point measurements and the regional scales used in modeling work has made it difficult to validate ET estimates intended to be used on regional or global scales. Annual AET estimates are sometimes validated against the difference between precipitation and runoff in a catchment (e.g., Choudhury and DiGirolamo 1998; Szilagyi 2000). In doing so, care must be taken to choose basins in which the assumption of zero storage change is appropriate. AET estimates at shorter time scales are also sometimes compared to other estimates of AET, on the assumption that common trends should be evident if both estimates are reasonable. These may include estimates based on empirical equations (e.g., Szilagyi et al. 1998; Seevers and Ottmann 1994) or numerical modeling (e.g., Szilagyi and Parlange 1999; Cihlar et al. 1991; Kerr et al. 1989).

4.2.2 Estimation methods

For our work, we require only annual mean values of the actual evapotranspiration. Estimates of AET at the annual timescale can be made using a variety of techniques, but all carry with them considerable uncertainty. As with the other water balance variables, we use multiple estimates of AET to reduce this uncertainty, selecting from existing models and datasets and developing our own estimate based on remote sensing data. The following sections describe the various estimation techniques available and discuss the reasons we choose to include or exclude particular estimates in our water balance study.

Empirical relations

Empirical approaches to AET estimation try to relate AET to more readily measured quantities. The following equation has been variously attributed to Turc (1954) and Pike (1964)

$$AET = \frac{P}{(1 + (P/PET)^2)^{0.5}} \tag{4.1}$$

where P is precipitation and PET is the potential evapotranspiration (Choudhury and DiGirolamo, 1998; Vogel et al., 1999). The equation has been validated using basins from all over the world (Vogel et al. 1999).

The dependence of AET on soil and vegetation characteristics is not directly considered by this equation, although precipitation and PET can influence the soils and vegetation present at a location. However, changes to natural AET due to changes in land use cannot be accounted for by this method.

We chose to use an estimate of AET using Turc's equation because of its ease of application at large scales and its previous use at locations around the world. As noted previously, we have two PET datasets and three precipitation datasets. AET is calculated separately for each combination of precipitation and PET and all of the resulting estimates are then averaged to obtain the empirical AET used in subsequent analysis. Calculations are made on an annual basis at a 0.5° x 0.5° resolution. The results of the calculations are shown in Figure 4-2a and Figure 4-3a for the continental U.S. and Asia, respectively.

Annual Water Balance

A number of global maps of AET were produced in the 1970's based on the water balance technique (Baumgartner and Reichel 1975, Korzoun 1974). As discussed more fully in Chapter 2, these studies assume that there is no long term change in water storage in soils or groundwater. Because these AET estimates also rely on the water balance equation but use assumptions incompatible with ours, we exclude these estimates from our study.

Atmospheric Water Balance

The atmospheric water balance, expressed in equation form, is:

$$ET - P = \nabla \cdot Q$$

where ET is evapotranspiration, P is precipitation, and $\nabla \cdot Q$ is the water vapor divergence. This is easily rearranged to provide an estimate of ET, provided P is well known:

$$ET = P + \nabla \cdot Q \tag{4.2}$$

Yeh, Irizarry and Eltahir (1998) applied the atmospheric water balance to estimate AET over Illinois, with good success. Their estimate of mean annual AET from the atmospheric water balance was within 5% of that calculated using a soil water balance. Atmospheric convergence estimates were based on NCEP reanalysis data at coarse 2.5° x 2.5° resolution. NCEP reanalysis data merges data from observed radiosonde data and predictions from an atmospheric general circulation model (AGCM). The soil water balance was based on 19 soil moisture monitoring stations and 19 groundwater monitoring wells scattered throughout Illinois.

Oki (1993,1995) employed the atmospheric water balance in a study of 70 large river basins around the world. He used ECMWF Reanalysis data to estimate the atmospheric vapor convergence for each basin. Oki made the assumption that $\Delta S = 0$ in order to use atmospheric convergence as an estimate for land surface runoff. While the storage change may not have been zero in all of his basins, the errors in runoff estimates using this method are instructive. Runoff estimated by the atmospheric balance differed from observed discharge by more than 50% at over 65% of Oki's basins, and by more than 100%

at nearly half of the basins. In part, these discrepancies may be attributed to mismatch in the timescales used. Four years of ECMWF data were used to construct the atmospheric water balance, while mean annual streamflow was calculated over periods ranging from 4 to 126 years.

Oki's very modest success at predicting runoff and our own preliminary analysis of atmospheric data indicated that errors in estimating atmospheric vapor convergence can be quite large. An absence of significant topography in the Illinois region may have contributed to the success of Yeh et al. (1998) in using coarse atmospheric data to estimate the water balance. However, because of the large overall errors encountered with the atmospheric water balance we chose not to use this estimation method for our study.

Numerical Models

Numerical models have also been used to estimate AET. These can range from simple bucket models of rainfall-runoff processes (with AET as a by-product) to complex models which attempt to simulate physical processes. While many models are available, global output are not readily available from most. We chose to use the output from Choudhury and DGirolamo's (1998) model. The advantages and limitations of this data are discussed below.

Choudhury and DiGirolamo (1998) use a biophysical processed based model to estimate global AET for the peiod 1987-1988. Results are available at a monthly timestep (although the model is run on a daily timestep) and at 0.5° x 0.5° resolution. The model includes simple parameterizations of interception, runoff, and groundwater runoff. Soil evaporation proceeds at an energy limited rate for 1 day following rainfall, and then at an exfiltration limited rate in subsequent periods. Unstressed transpiration is calculated based on meteorological conditions and fractional vegetation cover estimated from satellite data. Actual transpiration is reduced due to soil water stress and due to suppression of transpiration while foliage is wet. Precipitation falls as rain when the air temperature exceeds 273.2K, and falls as snow otherwise. Snow melt is calculated based on air temperature, and snow evaporation is set at a daily average rate of 0.15 mm/day. Precipitation, one of the most important inputs to any model of land surface hydrology, was taken from GPCP data.

AET results were validated against field observations at Cabauw, Netherlands and at Manaus, Brazil. Results were also compared to AET estimates from atmospheric water budgets for the Arkansas-Red River basin and the Volga River basin. Finally, results were compared to AET estimates calculated using a catchment water balance for 132 basins. The basin sizes ranged from 1-1000 km^2, included 2-30 years of data, and the mass balances assumed no change in storage. In a followup paper, Choudhury et al. (1998) compared their AET estimates with other data on AET for different latitude bands.

While results from this model are available for only two years, we chose to include them in this study because it is one of the few modeling studies which focus primarily on AET simulation. Although the data from 1987 - 1988 may not be entirely consistent with long term data, the data agreed favorably with estimates of long term mean evapotranspiration in Choudhury et al's validation work. The authors estimate uncertainties of about 15% for their annual AET estimates and 20% for their monthly AET estimates.

The National Centers for Environmental Prediction (NCEP) use an atmospheric general circulation model (AGCM) to simulate global meteorology. Observations of the atmospheric state are assimilated into the model at regular intervals to constrain the simulation. The reanalysis project produced data for 1982 - 1996 using consistent model code and assimila-

tion procedures. We explored the use of output from this model. However, inconsistencies in the large scale patterns seen in this dataset as compared to our other AET estimates led to exclusion of this dataset. ECMWF reanalysis data were not explored and may have better results. Incorporation of ECMWF or other modeling results can be further explored in the future.

4.2.3 Previous work on remote sensing for the estimation of AET

Satellite measurements of vegetation have the potential to provide additional estimates of AET. Satellite based estimates of AET have utility for reducing uncertainty because they are based on different types of data than estimates based on empirical or numerical models. For example, empirical and model based estimates are heavily dependent not only on the parameterization, but also on the precipitation data used as input. In contrast, AET estimates from satellite-based land cover data do not require precipitation as an input. Instead, estimates are based on the idea that AET is related to the amount of vegetation present, a quantity that can be observed with remote sensing data.

Higher rates of AET are associated with increased LAI and fractional cover. The leaf area index is the area of (multiple) layers of leaves which overlie a unit area of the ground. Due to the placement and orientation of leaves, light can often penetrate below multiple layers of leaves, allowing even lower layers to be active in photosynthesis and transpiration. The fractional cover of vegetation is the fraction of a given area which is completely covered by vegetation. Since greater LAI and fractional cover imply more vegetation which is able to transpire, it is expected that areas of high LAI and fractional cover also have high transpiration rates. Transpiration makes up a large percentage of ET from vegetated surfaces (Szilagyi and Parlange 1999). The remaining ET comes from interception loss (which also increases with higher LAI and fractional cover) and soil evaporation, which is generally low except immediately after a storm event.

If AET rates are related to LAI and fractional cover, then observations of LAI and fractional cover can give us information about AET. Satellite observations have been used to create vegetation indices which can give us the necessary information. Previous work relating AET to satellite vegetation indices is described below.

NDVI

Definition

The Normalized Difference Vegetation Index (NDVI) is the most commonly used satellite based measure of vegetation. It is calculated as the ratio between measured reflectivity in the red and near infrared portions of the electromagnetic spectrum. More precisely, it is defined as,

$$NDVI = \frac{NIR - RED}{NIR + RED} \tag{4.3}$$

where NIR is the reflectance in the near infrared band, and RED is the reflectance in the visible red portion of the spectrum. These two spectral bands are chosen because they yield a measure of the "greenness" of the land surface. NDVI ranges between -1 and 1, with higher numbers associated with increased "greenness". Negative numbers are associated with non vegetated surfaces such as water, snow, or ice or with cloud interference.

Other vegetation indices have been defined by using different algebraic formulas to combine data on reflectances in the near infrared and red bands. However, the bulk of the

existing literature on the use of satellite reflectances for AET estimation deals with NDVI, and we confine the following review to studies using this index.

The existence of a relationship between NDVI and transpiration or evapotranspiration has been well-established in the literature, as discussed below. Since both NDVI and AET can be expected to increase as LAI and fractional cover increase, a larger NDVI value implies greater AET. This relationship rests on the additional assumption that at different locations, and at different times of the year, vegetation retains only as much leaf area as it can utilize for photosynthesis given the availability of water. Note that in their dormant stages, deciduous trees lose their leaves and grasses turn brown, decreasing their greenness and NDVI. Evergreen trees, however, remain green even during their dormant stages, and NDVI measurements may be less effective for estimating ET from evergreen vegetation. In irrigated areas, NDVI can provide an indicator for when crops are actively transpiring, without the need to obtain detailed data on local agricultural practices.

The relationship between NDVI and AET is not uniform across different vegetation types (Cihlar et al. 1991; Szilagyi 2000; Choudhury et al. 1994). However, the feasibility of using NDVI to predict AET has been shown in many papers, as discussed below.

Previous studies

Choudhury et al. (1994) used modelled transpiration to test the relationship between the transpiration coefficient and NDVI. The transpiration coefficient was defined as the ratio of unstressed transpiration and reference crop evaporation. Using simulation results, he showed R^2 of 0.81 between NDVI and the transpiration coefficient.

Szilagyi et al. (1998) correlated NDVI calculated from Landsat-MSS images with estimates of monthly evapotranspiration in a prairie environment. NDVI data were calculated for the growing seasons between 1979 - 1983 for the Crescent Lake National Wildlife Refuge in Nebraska, an area of undisturbed natural mixed-grass prairie. The study area covered approximately 130 km^2. Monthly evapotranspiration estimates were obtained using an empirical algorithm based on monthly precipitation and potential evaporation. Results showed good correlation between NDVI and AET ($R^2 = 0.64$)

Szilagyi and Parlange (1999) used NDVI data derived from NOAA AVHRR data to estimate evaporation at 5 U.S. watersheds (Nebraska, Pennsylvania, Maryland, and Georgia) using a linear model. The NDVI evaporation estimates correlated well with estimates from a semi-distributed hydrologic model run at an hourly timestep ($R^2 = 0.77$). The NDVI estimated evaporation was used in a classical water balance model (at monthly timestep) to estimate runoff. The two derived runoffs (one from the water balance constructed with the NDVI-based ET and one from the hydrologic model) were compared to observed runoff. Each did about as well as the other, with a mean R^2 of about 0.7 in the verification period.

Cihlar, St.-Laurent and Dyer (1991) used NDVI data in pixels surrounding about 300 meteorological stations in Canada to examine the relationship between NDVI and AET for the 1986 growing season. AET was estimated using the Versatile Soil Moisture Budget Model, Version 3. Working with 15-day periods, Cihlar et al. found a fairly high correlation between AET and same period NDVI ($R^2 = 0.58$). The correlation increased when NDVI was correlated to AET during the preceding 15-day period ($R^2 = 0.76$). In other words, increases or decreases in AET are not immediately reflected in the measured NDVI. A period of time is required before vegetation grows or withers in response to changing conditions. Szilagyi et al. (1998) also obtained the highest correlation between NDVI and AET ($R^2 = 0.64$) when AET was lagged by one month. This finding is also consistent with the results

of Kerr et al. (1989) showing a time lag between AET and NDVI.

While many studies have related NDVI measurements to AET, good results have also been found by correlating NDVI to the AET/PET ratio. Smith and Choudhury (1990) tested the correlation between NDVI and AET calculated using a soil water balance model. Using data from May 1986 - April 1987 over Australia, they showed improved correlation when the AET/PET ratio, rather than AET itself, was used. Gutman and Rukhovetz (1996) used NDVI data to estimate AET globally with the equation AET = β PET. Mean July NDVI data aggregated to a 1° x 1° grid and results from hydrologic balance calculations on a 4° x 5° grid were used to define the relationship between β and NDVI. These data showed a correlation coefficient of 0.83. The resulting equation was then used to used to estimate β globally and to calculate AET on a finer grid.

Szilagyi and Parlange (1999) derived basin-specific linear models of the NDVI-AET relationship. They assumed that there was zero AET at an NDVI value of 0.1, a little higher than the theoretical value for zero AET of 0. With this intercept set, the slope of the line was found for each watershed by optimizing the runoff predicted when the AET values were fed into the catchment water balance model. The authors suggest that a good fit can be found by simply using NDVI values during wet months (P > PET), when AET is presumably at the potential rate, to set the slope of the line. Thus, linear models could be developed even for basins without runoff data.

Seevers and Ottmann (1994) used several days of Thematic Mapper and AVHRR data to investigate the relationship between NDVI and AET. 2-week average AET was estimated using the Blaney-Criddle empirical formula. All fields were irrigated and water availability was assumed to be unrestricted. They showed good spatial correlation between NDVI and AET at different field locations. The authors were able to define a linear relationship between NDVI and the crop coefficient with just two points - one defining zero AET and one defining maximal AET. Like Szilagyi and Parlange (1999), they set AET equal to zero at an NDVI slightly higher than zero (0.05-0.10). The second point was defined by assigning the maximum crop coefficient for a particular crop to the highest observed NDVI for that crop.

SSM/I

Polarization differences from microwave meaurements of brightness temperature have also been shown to correlate well with vegetation (Choudhury, 1989; Smith and Choudhury, 1990). In particular, the 37 GHz polarization differences and the 19 GHz polarization differences have been suggested as alternative vegetation indices. Smith and Choudhury (1990) showed that the 37GHz polarization difference from the Nimbus-7 Scanning Multichannel Microwave Radiometer had value in predicting AET in Australia. Choudhury (1989) showed that globally, polarization differences correlated well to empirical estimates of AET. Future work can explore the feasibility of adding information from polarization differences to our satellite-based AET estimate.

4.2.4 A new AET estimate based on NDVI measurements

The normalized difference vegetation index (NDVI) has been shown to be a good measure of the amount of vegetation present in a landscape. NDVI has also been used to estimate transpiration and AET in various locations around the world (e.g., Seevers and Ottmann, 1994, Szilagyi and Parlange, 1999, and Szilagyi, 2000). However, a given NDVI level does

not imply the same ET level everywhere, as different vegetation in different climatic settings will respond differently. Building on previous work, we have developed an algorithm for estimating AET based on land use, the seasonality of NDVI measurements, and potential evapotranspiration.

As discussed, numerous studies have shown a linear relationship between NDVI and AET. Our monthly NDVI-based AET estimation algorithm is based on that basic finding and a few additional points made in previous work. Following work by Seevers and Ottmann (1994) and Smith and Choudhury (1990) indicating that the correlation was improved when the AET/PET ratio, rather than AET itself was used as the dependent variable, we used NDVI to provide an estimate of the coefficient K_c in the following equation:

$$AET = K_c \cdot PET \tag{4.4}$$

In essense, then, we are using NDVI to estimate an appropriate monthly crop coefficient. In addition, we used a one-month lag between AET and NDVI, in accordance with work by Cihlar et al. (1991), Szilagyi et al. (1998), and Kerr et al. (1989). Finally, as proposed by Szilagyi and Parlange (1999) and Seevers and Ottmann (1994), we defined a linear relationship between AET and NDVI by defining two points: one at which zero AET takes place (AET/PET ratio = 0), and one at which AET is maximized. The NDVI value at which zero AET takes place was found to be approximately 0.05 - 0.1 by Szilagyi and Parlange (1999) and Seevers and Ottmann (1994). We used a value of 0.1. This locks in the x-intercept of Figure 4-1. For our work, we assume that the AET/PET ratio reaches unity when the fractional vegetation cover is at 100%, as illustrated in Figure 4-1. The plateauing of the coefficient, K_c, at full vegetative cover is consistent with results discussed by Seevers and Ottmann (1994) showing that the crop coefficient no longer increases after LAI has achieved a threshold level. The algorithm is applied to all land use classifications. However, the NDVI value associated with full cover varies with vegetation type, as listed in Table 4.1. Values are taken from Zeng et al. (2000), based on expert estimation of fractional cover in aerial photos for regions in which NDVI is known and land use is specified by the GLCC dataset. Although the NDVI values are similar for most vegetation types, differences in the frequency at which vegetation is observed with full cover also influences evapotranspiration rates. For example, forest landscapes have 100% fractional cover at a far greater frequency than open shrubland or barren, desert landscapes. Consequently, evapotranspiration from forest cover can generally be expected to be higher than that from areas with sparse vegetative cover.

Snow and Ice

The total storage of water in snow and ice varies with snow accumulation and ice formation, melting, and direct evaporation. We have assumed that the mean annual change in this storage is zero in this analysis. This may not be strictly true, especially in light of rising global temperatures. In any case, because snowfall is included in precipitation data, and snowmelt leaving the watershed is accounted for in streamflow data, evaporation from snow and ice surfaces must be accounted for.

Evaporation from snow and ice is generally small, as potential evaporation in cold climates is small. Further, the latent heat of sublimation is larger than the latent heat of vaporization. Choudhury and DiGirolamo (1998), based on work by Gray and Prowse (1993) estimate daily evaporation of 0.15 mm - 0.45 mm from snow. Condensation reduces

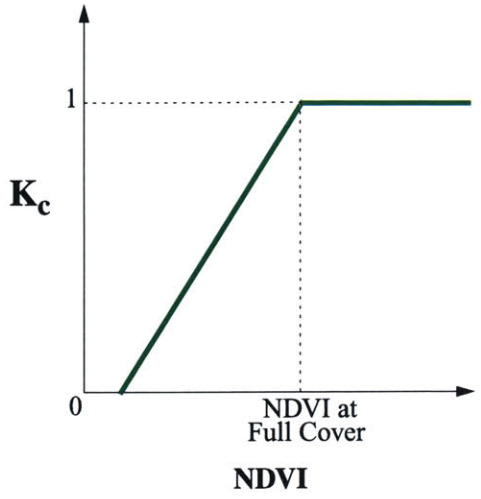

Figure 4-1: NDVI algorithm.

Table 4.1: NDVI value at full canopy cover for different land use categories. (Data from: Zeng et al., 2000)

	Land Cover Description	NDVI at full cover
1	Evergreen needleleaf forest	0.63
2	Evergreen broadleaf forest	0.69
3	Deciduous needleleaf forest	0.63
4	Deciduous broadleaf forest	0.70
5	Mixed forest	0.68
6	Closed shrublands	0.60
7	Open shrublands	0.60
8	Woody savannas	0.62
9	Savannas	0.58
10	Grasslands	0.49
11	Permanent wetlands	0.56
12	Croplands	0.61
13	Urban and built-up lands	0.62
14	Cropland/natural vegetation	0.65
15	Snow and ice	n/a
16	Barren	0.60
17	Water bodies	n/a

that quantity by 20-30%. These estimates are based on limited snow evaporation and condensation data. In developing their own evaporation dataset, Choudhury and DiGirolamo assumed a daily net evaporation of 0.15 mm from snow covered surfaces. We also used this value.

The presence of snow for any pixel is determined based on the frequency at which snow cover is reported in the National Snow and Ice Data Center's (NSIDC) Northern Hemisphere Snow Cover Dataset. When snow is present more than 50% of the time, AET for that month is set at the rate of 0.15 mm/day rather than using the NDVI algorithm.

Data

PET

As was demonstrated by Vorosmarty et al. (1998), PET estimates can vary widely depending on the estimation method used. We attempt to minimize the uncertainty in our AET estimate stemming from uncertainty in the PET estimate by using data from both the Penman-Monteith equation (Choudhury 1997) and the Thornthwaite equation (Willmott et al. 1985). The NDVI-based AET is calculated separately for each PET estimate and the results are then averaged.

NDVI

NDVI data were obtained from NASA, and were derived from AVHRR data from the Pathfinder mission. In order to limit the effects of cloud contamination, data are composited to 10 day periods, in which only the highest observed NDVI value in each pixel is included. NASA has further composited the data to monthly periods at 0.5° x 0.5° resolution. Data from the period August 1981 to July 1994 are used.

Land Use Data

USGS Global Land Cover Characterization (GLCC)
This high resolution dataset is derived primarily from Advanced Very High Resolution Radiometer (AVHRR) data from April 1992 - March 1993. The seasonal pattern of NDVI is used with ancillary data to derive land cover types at 1km resolution. Calibration of the land cover classifications are specific to each continent. Several different classification systems are used to report land use, ranging from very detailed breakdowns into as many as 200 different land cover types, to more general classifications of 10-20 cover types. For consistency with the categories used by Zeng et al. (2000) for relating fractional vegetation cover to NDVI values, we use the International Geosphere Biosphere Program (IGBP) classification system.

Croplands
Using the USGS global land characterization data and national and regional agricultural inventory data, Ramankutty and Foley (1998) developed a cropland dataset by estimating the fraction of each pixel that is used as permanent cropland. The data reflect conditions in the early 1990's, as much of the information is derived from the GLCC data for that time period.

Data are available at both 0.5° x 0.5° and 5' x 5 ' spatial resolution. We used the lower resolution data for consistency with the PET and NDVI data.

Irrigated Area

Döll and Siebert (1999) developed a digital global map of irrigated areas based on FAO data on total irrigated areas in each country and numerous maps showing the main irrigated areas in each country. The data are available at a 0.5° x 0.5° resolution and provide the percentage of each grid cell that was equipped for irrigation in 1995. It is likely that the area that was actually irrigated in many countries is smaller, but this information is largely unknown.

Summary of land use used for NDVI-based AET estimate

Land use is taken from the three sources described above. The GLCC data were used to create a base map of land use by calculating the dominant land use over 100 km^2 grid cells. Ramankutty and Foley's croplands dataset and Döll and Siebert's irrigated area dataset were used as supplemental sources of agricultural land use information. The GLCC land use was overridden if these datasets indicated that more than 50% of the land was used as cropland or was equipped for irrigation.

Estimation Results

Regional trends

Figure 4-2 shows the ET ratio for the continental U.S. The ET ratio is defined as the ratio of mean annual AET to mean annual PET. AET is estimated using three different methods: the Turc empirical formula, the Choudhury and DiGirolamo model, and with our NDVI-based method. PET is calculated as the average of Choudhury's Penman Monteith estimate and Willmott's Thornthwaite estimate. Use of this PET average results in ET ratios greater than one in some areas. Figure 4-3 shows the corresponding maps for our study domain in Asia. As seen in the figures, the NDVI-based ET ratio shows a similar pattern of variability as the ET ratios based on the other two AET estimates. The ET ratio in the humid eastern U.S. is generally higher than the ET ratio in the western U.S., except along the Pacific Coast. The ET ratio is especially low in the arid southwest, where there is little moisture to meet a high evaporative demand. In Asia, the highest ET ratios are found in eastern Asia. The ET ratio is smallest along the western edge of our domain, and in northwestern China.

Figure 4-4 and Figure 4-5 show the difference between the 3 estimates of AET for the U.S. and Asia, respectively. In the U.S., the NDVI-based AET is generally the highest and the Choudhury estimate is generally the lowest. Conversely, in Asia, the NDVI-based estimate is generally the lowest of the three.

A notable regional difference between the NDVI-based estimate and the other two estimates can be seen in the Central Valley region of California. The NDVI-based AET estimate is notably higher here than the other two AET estimates. In part, this may be attributed to the NDVI-based method's high estimates of ET along most of the U.S. west coast. However, a band of even higher ET can be seen along the irrigated Central Valley. This difference can also be seen in Figure 4-2, where a band of high ET ratio is seen in the Central Valley area. Burt, Howes and Mutziger (2001) estimate the rate of evaporation from irrigated lands in California under normal conditions at about 820 mm/year. Their estimate is based on application of crop coefficients to a reference ET. Crop coefficients are selected based on agricultural data which show crop selection and growing season. AET estimates from our three global estimates were averaged for grid cells identified by the USGS classification as irrigated cropland. AET estimates by Choudhury and using Turc's empirical formula are significantly lower than Burt's, at approximately 260 mm/yr and 340 mm/year, respectively. The NDVI-based AET estimate of 700 mm/year is in closer agreement with Burt's

a) Turc Empirical Estimate

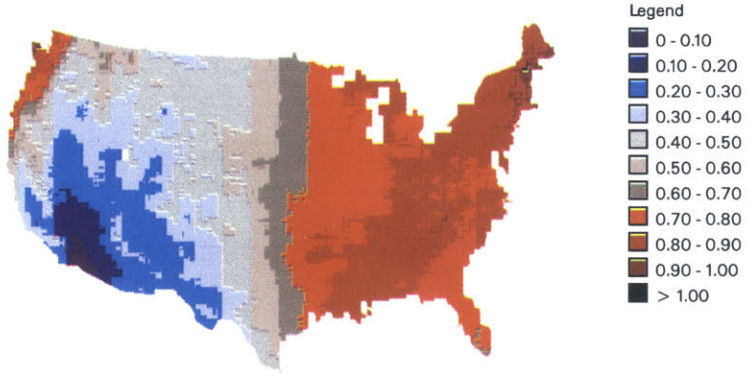

b) Choudhury Model Output

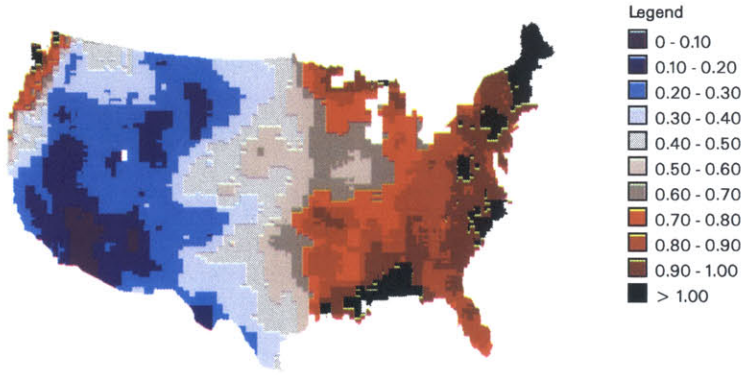

c) NDVI-based Estimate

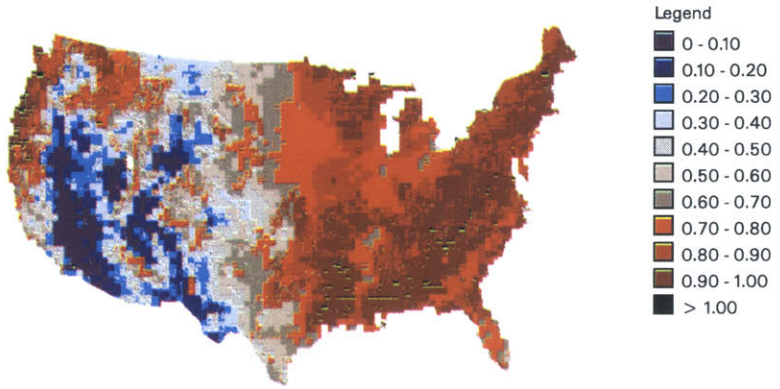

Figure 4-2: Ratio of AET/PET estimated by different methodologies over the continental U.S. Values greater than one for the Choudhury model output are the result of averaging PET from the Thornthwaite and Penman Monteith methods.

a) Turc Empirical Estimate

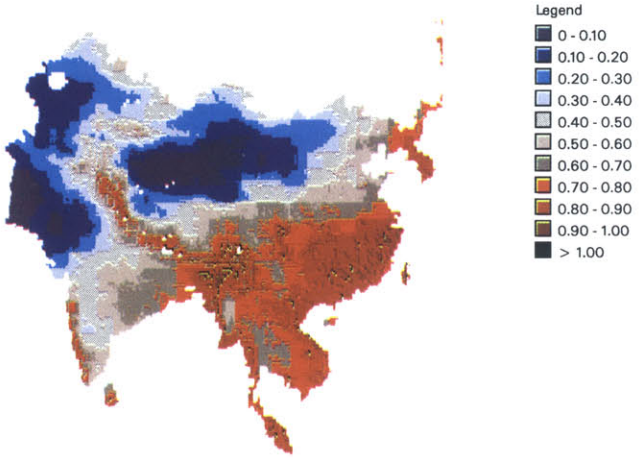

b) Choudhury Model Output

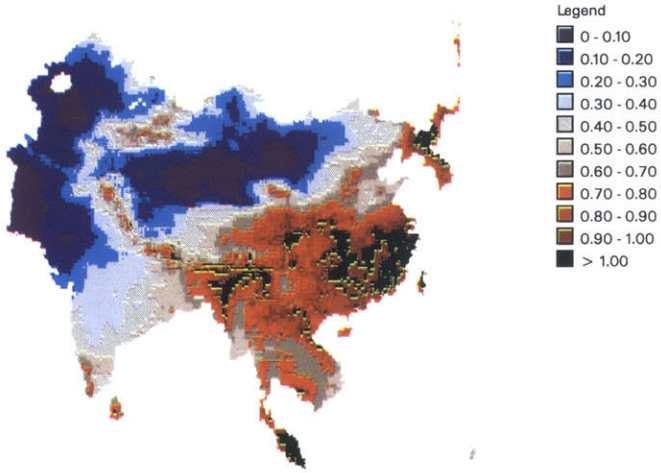

c) NDVI-based Estimate

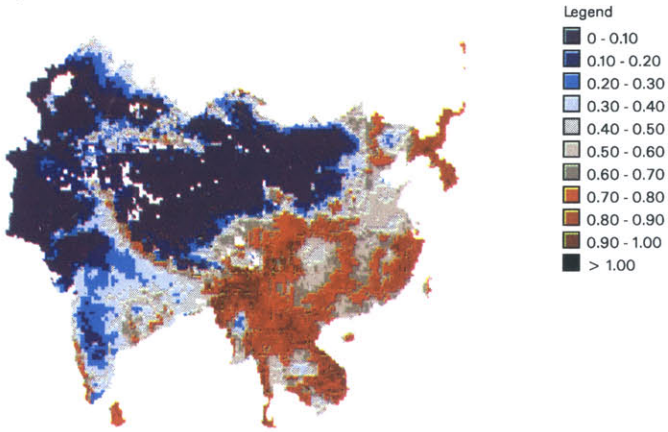

Figure 4-3: Ratio of AET/PET estimated by different methodologies over our study domain in Asia. Values greater than one for the Choudhury model output are the result of averaging PET from the Thornthwaite and Penman Monteith methods.

estimate.

Monthly AET estimated by Choudhury and our NDVI-based method are compared at two points in California in Figure 4-6. The first point contains natural savanna vegetation, and AET calculated by both methods generally follows the seasonal trend in precipitation. The NDVI-based estimate is somewhat higher than the Choudhury estimate. The second point is located in an irrigated section of the Central Valley. While the Choudhury AET estimate again follows the seasonal precipitation, AET calculated using our NDVI-based method has a higher overall magnitude year round and includes an early summer peak which can be attributed to irrigation.

In Asia, we can also see locally increased AET estimated by the NDVI-based method in locations with intense irrigation, notably the Indus River basin and the region just south of the Aral Sea. Differences are not as pronounced in other irrigated regions, perhaps due to the generally lower AET estimates from the NDVI-based method in parts of Asia.

The general agreement between the different AET estimates on a regional scale can also be demonstrated by calculating spatial correlations between two different estimates, as shown in Figure 4-7 and Figure 4-8. In each plot, AET estimated at each pixel with one estimation method is plotted against AET estimated for the same pixel with a different estimation method. There is a positive correlation between all estimates. While the strongest correlation is seen between the Choudhury and Turc estimates (U.S.: $R^2 = 0.88$, Asia: $R^2 = 0.88$), the correlation between our NDVI-based estimate and the Turc estimate (U.S.: $R^2 = 0.77$, Asia: $R^2 = 0.83$) and the Choudhury model output (U.S.: $R^2 = 0.66$, Asia: $R^2 = 0.83$) are also high, particulary over Asia.

The analysis can also be separated by land use, and results are summarized in Table 4.2. Using the IGBP land use classifications, we can see that the correlation between the NDVI-based AET estimates and Choudhury and Turc estimates are generally good except in shrubland and barren areas. Some of these land use based differences meet our expectations. Shrubs and barren areas typically do not show a great deal of seasonal variation in greenness and NDVI. Consequently, we do not expect our NDVI-based estimation method to do well in these regions. However, although we would expect the same limitations for evergreen vegetation, the correlation for evergreen vegetation is high. On average, however, NDVI-based estimates for evergreen areas are about 25% higher than estimates by Choudhury or Turc in the U.S. Savanna and grassland areas also tend to have higher NDVI-based AET estimates.

The cropland category in the IGBP classification includes both irrigated and non-irrigated cropland. Another classification system distributed with the GLCC data is based on USGS categorizations of land use and includes separate categories for irrigated agriculture, mixed dryland and irrigated agriculture, and various mixes of dryland agriculture with pasture or natural vegetation. When the spatial correlations are calculated using these categories, we see that irrigated agriculture has a noticeably smaller correlation than the other categories in the U.S. In addition, the NDVI-based AET estimate tends generally to be higher than the other two estimates of AET. This is consistent with the idea that NDVI is able to capture the longer growing season and enhanced AET in irrigated areas. Both the Choudhury model and the Turc empirical estimate assume that only natural precipitation is available for AET even in irrigated areas. The decreased correlation between NDVI-based AET and other AET estimates is not as evident for irrigated areas in Asia.

Catchment scale comparisons

a) NDVI-based Estimate - Turc Empirical Estimate

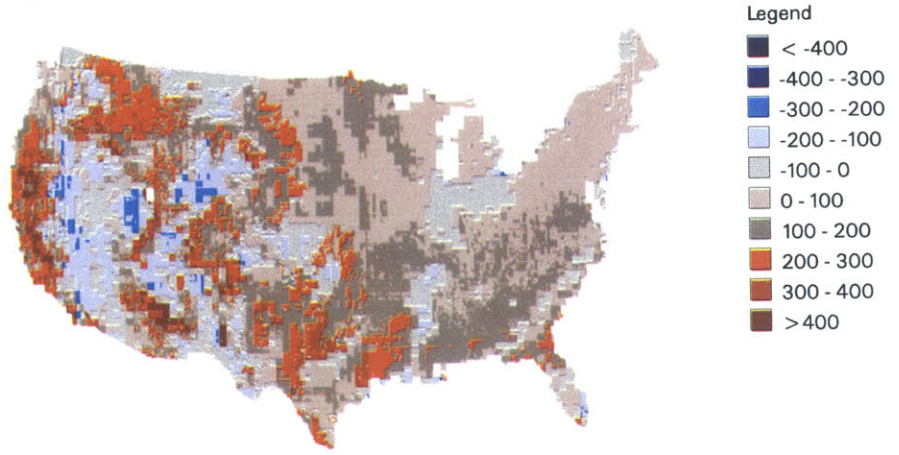

b) NDVI-based Estimate - Choudhury Model Output

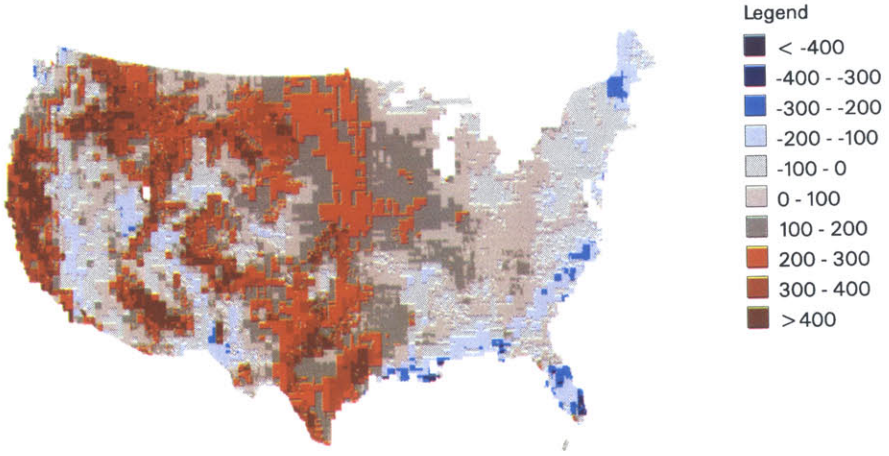

c) Turc Empirical Estimate - Choudhury Model Output

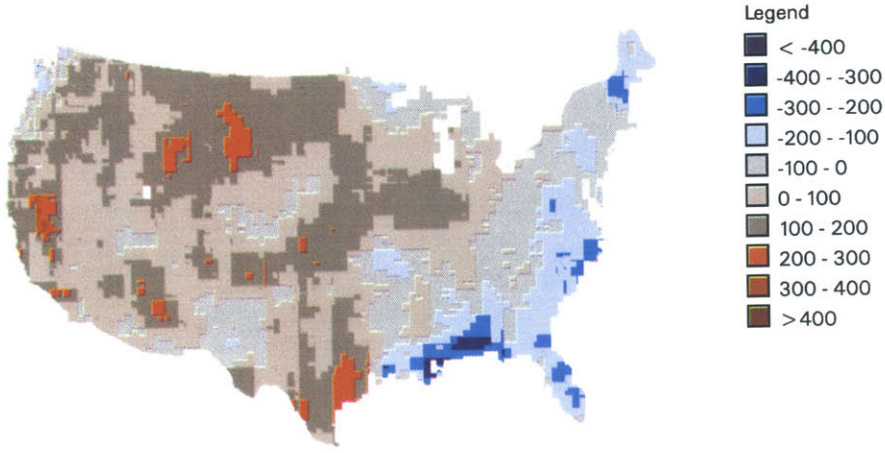

Figure 4-4: Difference between AET estimated by different methodologies over the continental U.S.

a) NDVI-based Estimate - Turc Empirical Estimate

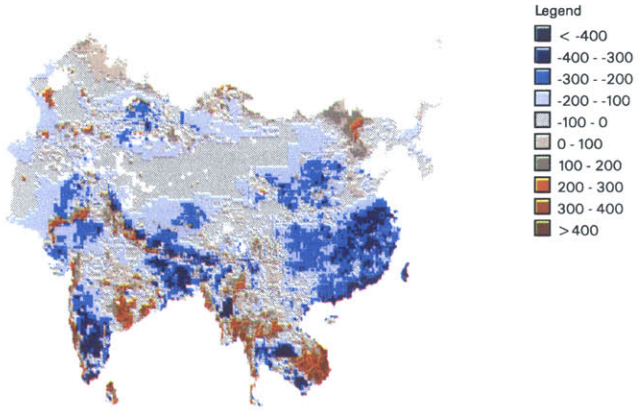

b) NDVI-based Estimate - Choudhury Model Output

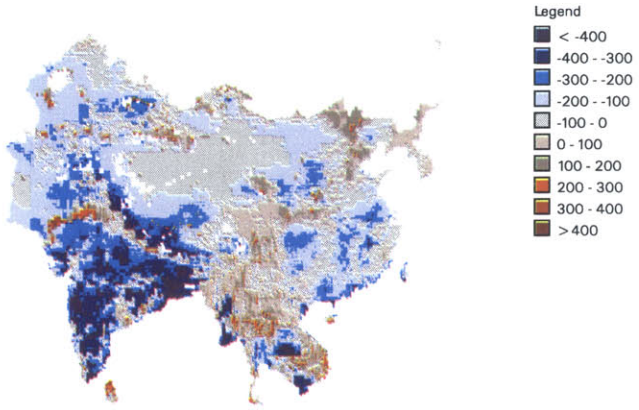

c) Turc Empirical Estimate - Choudhury Model Output

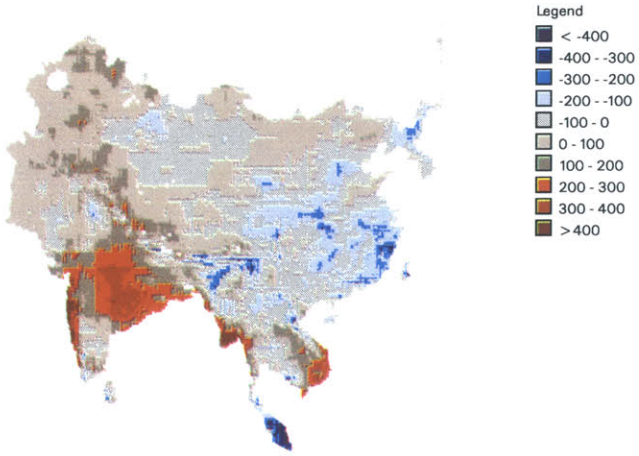

Figure 4-5: Differences between AET estimated by different methodologies over our study domain in Asia.

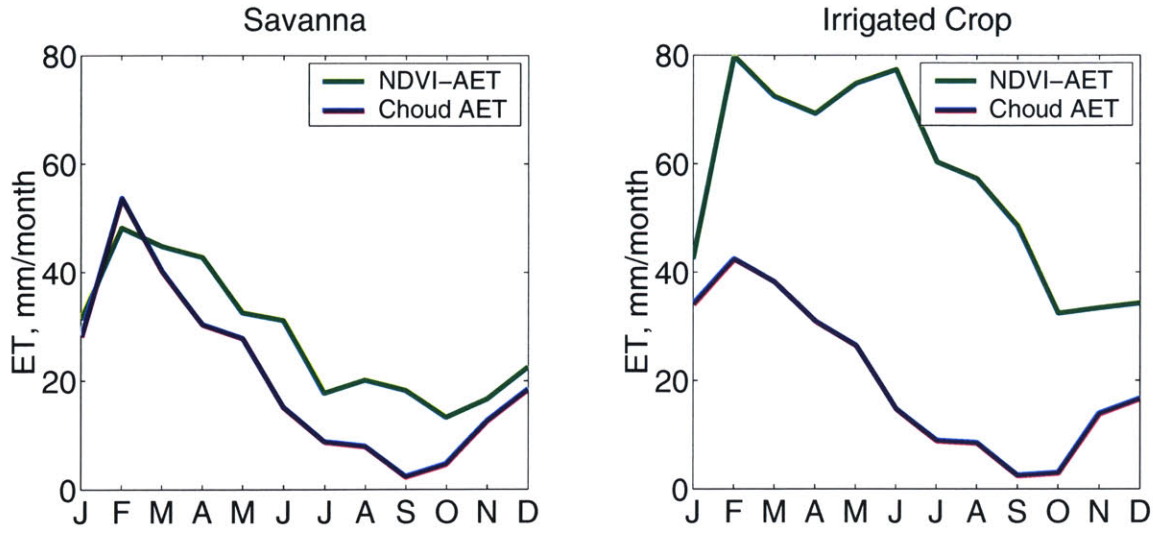

Figure 4-6: Comparison of AET estimated by different methodologies for two points in California. AET over savanna estimated by both Choudhury and our NDVI-based method follow the seasonality of precipitation. Over irrigated cropland, Choudhury's estimate again follows precipitation. Our NDVI-based estimate has a higher overall magnitude and shows an early summer peak which can be attributed to applied irrigation water.

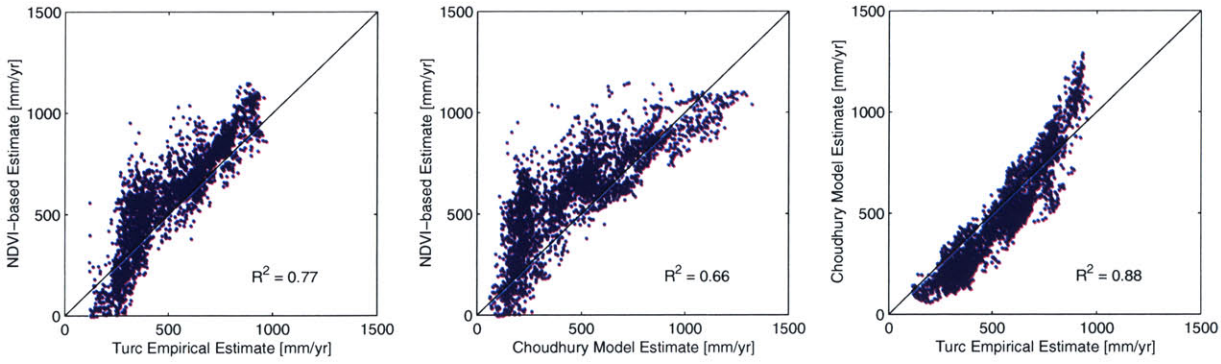

Figure 4-7: Correlation between different AET estimates over U.S.

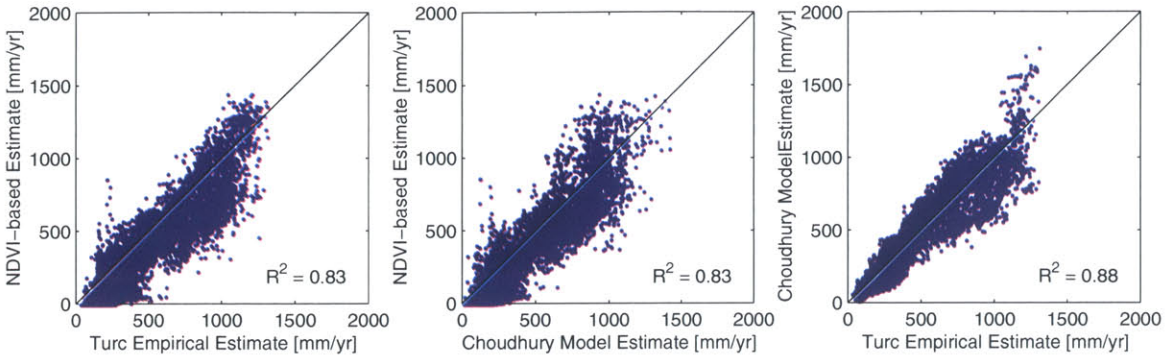

Figure 4-8: Correlation between different AET estimates over our study domain in Asia.

Table 4.2: Correlation between NDVI-based AET estimate, Choudhury model output, and Turc empirical estimate.

Land Use	R^2, NDVI-based v. Choudhury		R^2 NDVI-based v. Turc	
	U.S.	Asia	U.S.	Asia
IGBP CLASSIFICATION				
Evergreen Needleleaf Forest	0.72	0.79	0.80	0.85
Evergreen Broadleaf Forest	n/a	0.17	n/a	0.66
Deciduous Broadleaf Forest	0.42	0.50	0.70	0.84
Mixed Forest	0.72	0.60	0.93	0.82
Closed Shrubland	n/a	0.34	n/a	0.33
Open Shrubland	0.22	0.40	0.34	0.35
Woody Savanna	0.60	0.05	0.72	0.66
Savanna	0.55	0.22	0.83	0.57
Grassland	0.51	0.61	0.68	0.46
Cropland	0.48	0.56	0.69	0.60
Cropland/Natural	0.77	0.68	0.83	0.77
Barren	0.03	0.21	0.05	0.19
Overall	0.66	0.83	0.77	0.83
USGS CLASSIFICATION				
Irrigated Crop	0.12	0.51	0.05	0.61
Crop/Pasture	0.45	0.50	0.74	0.47
Crop/Grassland	0.65	0.64	0.75	0.62
Crop/Woodland	0.50	0.60	0.49	0.86

Figure 4-9: Location of watersheds used in the catchment scale comparisons of AET estimation methods.

The NDVI-based AET estimate was compared to water balance estimates of AET for 5 catchments in the continental U.S. (see Figure 4-9) where long term changes in watershed storage are expected to be minimal. In calculating the water balance, mean annual precipitation from our 3 global sources was averaged and the mean annual streamflow was used. As summarized in Table 4.3, the NDVI-based estimate does well in 4 of the 5 basins. For the Moreau River watershed in South Dakota, however, the NDVI-based estimate is almost one third higher than the water balance estimate. The Choudhury estimate underestimates AET while the Turc estimate is quite near the water balance estimate. This example points to the uncertainty in not only our NDVI-based estimate, but also in other estimates of AET. Incorporating multiple estimates of AET can help to reduce that uncertainty.

Illinois Additional validation of the NDVI-based AET estimates was carried out for Illinois. The NDVI-based estimates over the Illinois region were compared to AET estimates by Yeh et al. (1998). The region is defined by NCEP grid locations, and encompasses the area between 37.50 - 42.5 N latitude, and 87.50 -0 92.5 W longitude, an area of about 240,000 km^2. It includes Illinois and parts of Iowa and Missouri. Land use in this region is predominantly agricultural, with little to no irrigation. Yeh et al. used both an atmospheric water balance and a monthly soil water balance to estimate AET for the region for 1983-1994. The NDVI-based estimate of 701 mm/yr is just 3-6% higher than Yeh et al.'s two estimates. The NDVI-based estimate also clearly lies within the range estimated by Jones (1996) for AET from Illinois. The Turc estimate is also in this range, while the Choudhury estimate is somewhat lower.

Groundwater data described by Yeh et al. (1998) exhibit no significant trend over the period 1983-1994. Hence, we also used a basin-scale water balance over the Illinois River watershed to estimate AET as the difference between precipitation and runoff. Results for this smaller area are also tabulated in Table 4.4. Again, the NDVI-based estimate is similar

Table 4.3: Comparison of AET calculated by global estimation techniques for U.S. catchments.

Watershed	Catchment Area [km^2]	Water balance estimate [mm/yr]	NDVI-based estimate [mm/yr]	Choudhury estimate [mm/yr]	Turc empirical estimate [mm/yr]
Illinois River, IL	69,300	696	640	506	647
Little Washita, OK	584	765	816	622	673
Merrimack River, NH	8008	706	608	762	590
Potomac River, MD	24,950	663	704	775	615
Moreau River, SD	12,056	421	558	238	405

Table 4.4: Illinois region AET estimates from various sources.

Source	Annual AET [mm] Yeh and Eltahir region	Annual AET [mm] Illinois River basin
NDVI-based estimate	701	640
Yeh and Eltahir (1998) Soil Balance	660	n/a
Yeh and Eltahir (1998) Atmospheric Balance	682	n/a
Choudhury et al (19??) Biophysical Model	562	506
Turc empirical equation	667	647
Water balance, P-R	n/a	696
Jones (1966)	635-762	n/a

to estimates from the water balance and from the Turc empirical equation. The Choudhury estimate is lower.

Figure 4-10 plots monthly AET estimates calculated by different methods for the Illinois region. While the NDVI-based estimate follows the same seasonal trend as the Yeh et al. estimates, the Choudhury estimate displays strange seasonal behavior.

4.3 Selective Average AET

The previous sections have described some of the commonly used approaches for estimating AET. From this body of work, we selected two AET estimates for inclusion in our work. First, the simple empirical relation suggested by Turc (1954), and second, the results of numerical modeling by Choudhury and DiGirolamo (1998). In addition, we developed our own estimate based on monthly NDVI. Each estimate has its own strengths and limitations. For example, the empirical and model based estimates have been more extensively validated than our NDVI estimate, but do not make specific provisions for enhanced evaporation over irrigated areas and are generally representative of AET only over non-irrigated vegetation. Both also depend on the accuracy of precipitation data used as input. In contrast, the NDVI-based AET is based on observed seasonal changes in vegetation and is appropriate for

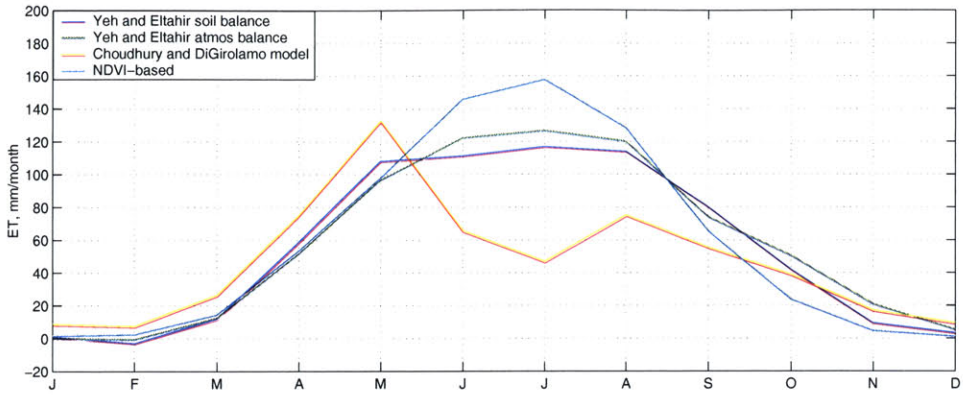

Figure 4-10: Comparison of monthly AET estimated by different methodologies for Illinois region. While Yeh and Eltahir and the NDVI-based estimate show a similar seasonal cycle, the Choudhury estimate shows inconsistent seasonal behavior.

irrigated cropland. However, it is not expected to be appropriate for evergreen vegetation, as dormant periods are not reflected by changing NDVI. This is a particular problem in regions where dry conditions, rather than cold conditions, induce dormancy. Under cold conditions, PET is low and snow cover can reduce NDVI. Thus, overestimation of AET is not as as severe. The NDVI-based estimates also seemed to have less consistency with other AET estimates for shrubland, barren landscapes, and grasslands.

Because of the limitations of each of the AET estimates, we have calculated a selective average, in which only those AET estimates which have been shown to give reasonable estimates for the land use that is present are included in an average value calculated for that grid cell. For non-evergreen forest and savanna vegetation and non-irrigated cropland, all 3 estimates are averaged. Only the NDVI-based estimate is used for irrigated cropland and only the Turc and the Choudhury and DiGirolamo estimates are used for remaining vegetation types. The results of the application of this selective averaging are shown in Figure 4-11. The selective average AET is used in our contrained water balance estimator.

a) Selective Average AET Estimate over U.S.

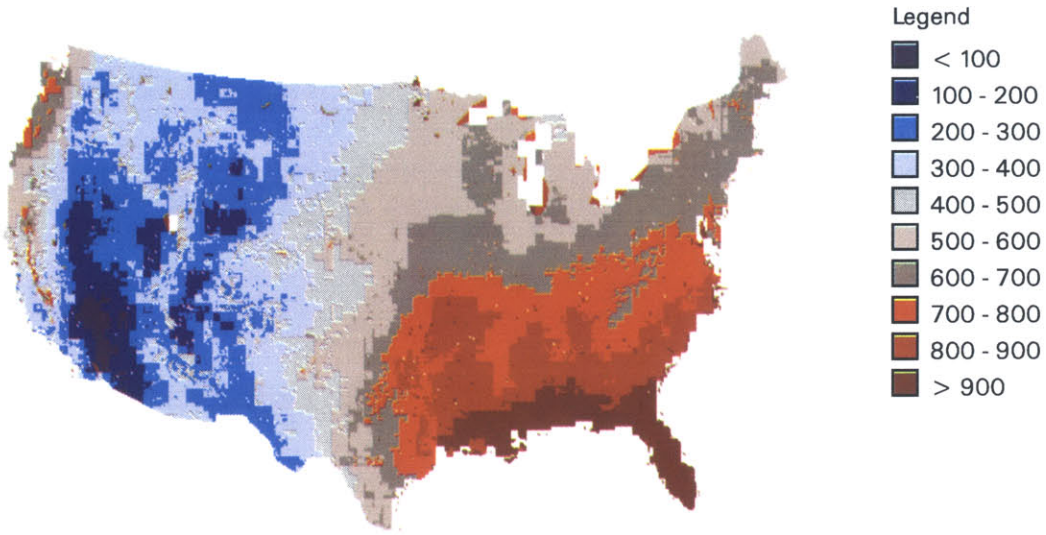

b) Selective Average AET Estimate over Asia

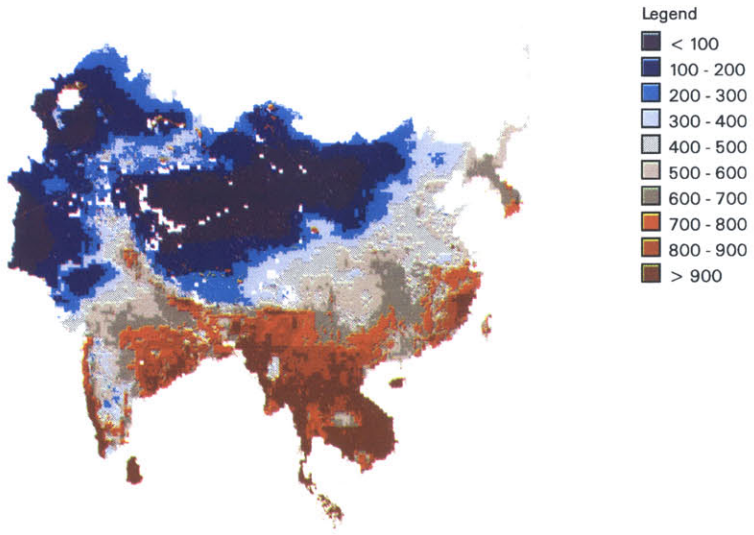

Figure 4-11: The selective average AET calculated using up to 3 estimates of AET.

Chapter 5

Case study of California

We tested our water balance estimator (described in Chapter 2) by applying it to test basins in the U.S. We focused on two watersheds in California - the Sacramento/San Joaquin River watershed and the Salinas River watershed. The location of these two watershed is shown in Figure 5-1. Both basins are good candidate regions for testing of our methodology because data on groundwater changes are readily available. Data for the other elements of the water balance are available from both global and local sources.

The two basins will be used to illustrate both the benefits and the limitations of the water balance estimator. In application of the water balance equation, a large storage change estimate can be interpreted as either an actual change in storage or a consequence of poor input data. If the data quality is poor, application of the water balance estimator can improve estimates of not only the storage change, but also of precipitation, evapotranspiration, and runoff.

5.1 Sacramento/San Joaquin Basin

The Sacramento/San Joaquin Basin is made up of 3 hydrologic regions. From north to south, they are: the Sacramento River watershed, the San Joaquin watershed, and the Tulare Lake watershed. California's Central Valley extends through all 3 watersheds and is underlain by both a confined and unconfined aquifer system which hydraulically connect the 3 watersheds.

The Sacramento River and the San Joaquin River converge to form an extensive delta near San Francisco Bay. The Tulare Lake hydrologic region is the southernmost section of the Sacramento/San Joaquin River basin. Streams from this catchment area once emptied into Tulare Lake, which is now a dry lakebed that has been converted to agriculture. Most publications from the DWR treat the Tulare Lake watershed as a separate hydrologic region from the San Joaquin watershed. In an average year, the Tulare basin is a closed basin with no natural outlet to the sea. However, in wet years, the Kings River carries excess flows to the San Joaquin River (DWR 1998). In addition, the groundwater flow system runs through the entire central valley, hydraulically connecting the Tulare Lake region to the San Joaquin and Sacramento basins. Because of these connections, we include the Tulare Lake region as part of the Sacramento/San Joaquin River basin.

As we have defined it, the total basin covers approximately 155,600 km^2 and includes the heavily irrigated farmlands of the Central Valley, as well as the mountains of the Sierra Nevada and the Coast Range. According to the DWR, about one-fifth (30,000 km^2) of

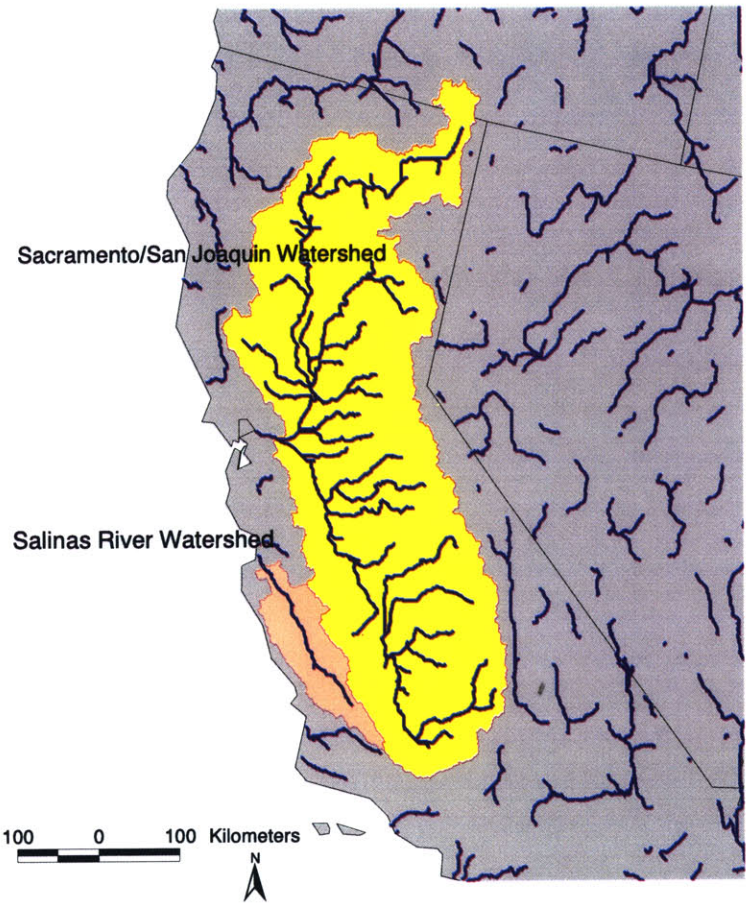

Figure 5-1: Location map of Sacramento/San Joaquin and Salinas River Watersheds in California.

the area is used as irrigated cropland (DWR 1998). The extent of the irrigated area, as determined by Döll and Siebert (1999), is shown in Figure 5-2. Its overall pattern is consistent with local information on irrigated acreage. Irrigation is present throughout the Central Valley, but is most widespread in the southern part of the watershed. Also shown in Figure 5-2 is the cropped area as estimated by Ramankutty and Foley (1998). This area is actually somewhat smaller than the area outlined by the Döll and Siebert dataset. This inconsistency points to the limitations of global data sources. Nevertheless, the agricultural areas defined by both datasets are similar.

Large groundwater withdrawals in irrigated areas have induced land subsidence of up to 10 meters in parts of the valley (Galloway et al. 2000). Precipitation amounts vary significantly throughout the watershed but are generally higher in the north and increase quickly with elevation.

Hydro1K elevation data from the USGS was used to delineate watersheds using ArcInfo. The drainage area of the Sacramento River watershed at Sacramento is 60,886 km^2, as reported by the USGS. The Arc delineated watershed at that location had an area of 66,942 km^2, a difference of just under 10%. Arc was somewhat less successful at delineating the San Joaquin River watershed. The USGS reports the drainage area of the San Joaquin River at Vernalis at 35,058 km^2. Arc's delination created a basin of 28,753 km^2, a difference of about 18%. This is largely due to the exclusion of the upper San Joaquin River, an area on the order of 5,000 km^2. Arc was also unable to capture the dynamic behavior of the Kings River, which as mentioned earlier remains in the Tulare basin during normal and dry years but overflows to the San Joaquin River during wet years. The watershed area was manually extended to include the Tulare Lake region for use in the subsequent GIS analysis. The basin was also extended downstream of the two streamflow gages mentioned above, to a point just below the confluence of the Sacramento and San Joaquin Rivers. This extension allows for continuity of the groundwater aquifer within our study region and creates a total watershed area of 155,600 km^2. Based on maps produced by the DWR, our watershed boundaries appear similar to the boundaries of the DWR hydrologic regions.

The deficiencies of automatic watershed delineation encountered in this example highlight the importance of manually checking watershed areas. In more data poor regions of the world where watershed maps are not as readily available, this may be more difficult to accomplish. At the least, the drainage areas reported at the stream gage location and used in the GIS analysis should be compared.

5.1.1 Interbasin transfers

While California has an extensive water transportation network, the transfers are generally well documented. Approximately 1 km^3/year (7 mm/year) is imported from the Trinity region of Northwest California to the Sacramento/San Joaquin basin. In addition, about 3 km^3/year (21 mm/year) are exported from the basin to regions further to the south and to metropolitan areas (DWR 1998, DWR 1993). In our water balance, the imports were added as additional "precipitation" water while the exports were added to "runoff" leaving the watershed.

5.1.2 Precipitation Data

Figure 5-2 lists the mean annual precipitation derived from five different sources. Precipitation data from the same global datasets described in Chapter 3 are also available in

California. They are the Global Precipitation Climatology Project (GPCP) dataset, the Willmott et al. (1998) climatology, and the Cramer (1996) climatology. Basin average precipitation amounts from each dataset are listed in Figure 5-2. It is noteworthy that the discrepancies between precipitation amounts in each of these datasets are large. One potential benefit of applying the water balance estimator, then, is to obtain an improved estimate of precipitation in the watershed.

Two additional sources of precipitation data were also available. The DWR published estimates of average annual precipitation in the Sacramento/San Joaquin watershed (DWR 1998). In addition, NOAA's National Climatic Data Center (NCDC) maintains a precipitation database titled NCDC Surface Airways Hourly Precipitation. An easily accessible version of the data is produced by EarthInfo, Inc., and was used in this study. Precipitation data from this product were imported into ArcInfo format. Data were available at nearly 100 stations inside the watershed, or just outside its boundaries. Using ArcInfo's kriging function, we interpolated the station data onto a grid and calculated the annual average rainfall over the watershed. Arguably, these two locally derived estimates of annual precipitation are more reliable than the three global estimates. GPCP uses a very coarse resolution, which may mask the enhanced preciptation at high elevation areas. The degree to which the Cramer dataset and the Willmott dataset accurately reflect precipitation in the Sacramento/San Joaquin watershed depends on the gage distribution. Whereas we know that our own estimate includes a substantial number of gages in mountainous areas, we do not know the exact distribution of gages in either the Cramer or the Willmott et al. datasets.

While each of the precipitation measurements are treated as if they are independent, the reality is that there is probably significant correlation between some of the measurements. In particular, the Willmott et al. climatology, the Cramer climatology, and the climatology based on NCDC data undoubtedly include many of the same precipitation stations. However, each estimate uses a different interpolation method. In addition, DWR's estimate almost certainly also utilizes some of the same station data. Even the GPCP dataset, as a combined satellite-gage product, is likely to include some of the stations used in the other datasets. Unfortunately, it is not possible to determine the degree of overlap in station usage. In the water balance estimation, we will treat the precipitation measurements as if they are independent because we are unable to quantify the correlation between them. Assuming that the actual correlation is positive, this may result in some underestimation of the uncertainty of our estimates.

In the Sacramento/San Joaquin watershed, the uncertainty of the precipitation data from GPCP (Huffman et al, 1997) and Willmott et al. (1998) were each estimated at about 150 mm/year. Because of the wide range of values across the different datasets, we assigned a slightly higher standard deviation of 200 mm/year for each of the three global precipitation datasets.

5.1.3 Evapotranspiration Data

The selective average AET, described in Chapter 4, was the only source of AET data used for the watershed. Based on AET estimated from 3 different methods, the basin average AET was estimated at 445 mm/yr. The standard deviation assigned to this estimate takes into account the incorporation of multiple estimates of AET. The differences between the AET estimated in regions where we expect all AET estimates to be valid was used as a guideline for assigning a standard deviation to the individual estimates. Based on the range

Table 5.1: California overdrafts by region as reported in the California Water Plan Update (DWR 1993; DWR 1998).

Region	1990 Overdraft taf (km^3)	1995 Overdraft taf (km^3)
Sacramento River	30 (0.04)	33 (0.04)
San Joaquin River	210 (0.26)	239 (0.29)
Tulare Lake	650 (0.80)	820 (1.0)
Total	890 (1.1)	1092 (1.3)

of values observed, each of the individual AET estimates used to calculate the selective average was assigned a standard deviation of 150 mm/year. Based on these numbers, the selective average was assigned a smaller standard deviation of 125 mm/year.

5.1.4 Runoff Data

Data from USGS streamflow discharge stations located on the Sacramento and San Joaquin Rivers are included in the RivDIS database. Data are available for the Sacramento River at Sacramento and for the San Joaquin River at Vernalis. Together, these gages cover 90% of the total basin area as we have defined it. The basin area extends below these gages to a point just below the confluence of the two rivers to include the entire Central Valley as one continuous unit. The runoff for the total basin was estimated by assuming that the runoff rate calculated for the basin area covered by the gages was the same as the runoff rate for the total basin. This yielded basin average runoff of 181 mm/year.

Additional estimates of runoff were available from the DWR. DWR Bulletin 160-98 estimates runoff in the Sacramento/San Joaquin basin at 240 mm/year. A DWR report on the Delta included an estimate of total inflow into the Delta (from the Sacramento/San Joaquin rivers) at 181 mm/year. Presumably because different sections of DWR produced these estimates, they are somewhat different. The two DWR estimates are undoubtedly also based largely on streamflow gage measurements and it is is unclear that they are any more reliable than our own estimate based on USGS gage data.

Each runoff measurement was assigned a standard deviation of 30 mm/year.

5.1.5 Groundwater data

The California DWR estimates groundwater overdraft in each of the major basins in California as part of its planning process. Estimates for the Sacramento, San Joaquin, and Tulare Lake Basins for 1990 and 1995 are shown in Table 5.1. Overdrafts are most severe in the southern part of the watershed. The total groundwater overdraft for the basin is between 1.1 - 1.3 km^3/yr. Averaged over the entire watershed, this translates to a relatively small groundwater overdraft of 7-9 mm/yr.

The DWR also publishes data from its extensive database of groundwater surface elevation in wells throughout the state. We used this data to make a second estimate of groundwater depletion in the basin. Groundwater aquifers in the Central Valley include both an unconfined aquifer and a semi-confined aquifer confined by a clay lens extending across part of the valley. The data for any particular well do not indicate whether it is

Sacramento/San Joaquin Watershed

Basin area: 155,600 km^2

a) Cropping Intensity (Ramankutty and Foley, 1998)

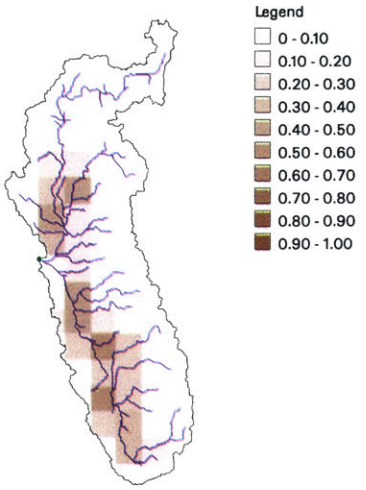

b) Irrigation Intensity (Döll and Siebert, 1999)

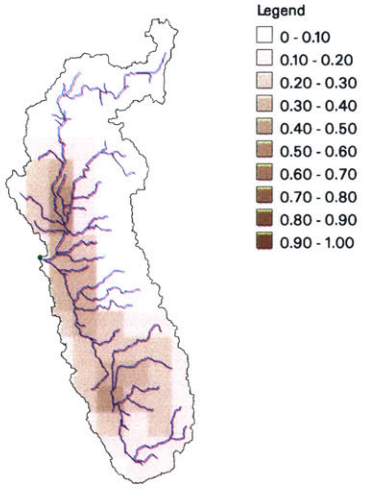

	Value [mm/yr]	Std Dev [mm/yr]
PRECIPITATION		
GPCP	404	200
Willmott et al.	638	200
Cramer and Leemans	321	200
EVAPOTRANSPIRATON		
Selective Average	445	125
RUNOFF		
Streamflow gage	181	30
GROUNDWATER CHANGE		
DWR Bulletin	- 7 - -9	-
Well data	- 5 - -15	-
INTERBASIN TRANSFERS		
Imports	7	-
Exports	21	-

Figure 5-2: Sacramento/San Joaquin Watershed. Fraction of each 0.5 degree grid cell a) used for agriculture and b) equipped for irrigation.

drawing water from the confined or unconfined aquifer, or both. A more detailed analysis of well logs or screening data could give some indication of this for some wells, but such an undertaking was beyond our available resources. Thus, we treated all well data as if they pertained to a single aquifer underlying the Central Valley. Groundwater levels for 1980 and 1995 were interpolated onto a regular grid using an inverse distance weighted interpolation scheme in ArcInfo. The data indicate an overall drop in water levels of approximately 0.5 ft/year over the period 1980-1995.

To estimate the actual volume of the groundwater overdraft, we also need estimates of the specific yield of the aquifer. DWR has published estimates of the specific yield for the aquifer in the Central Valley. Unfortunately, because the aquifer is actually made up of many different units, all with different specific yields, and because exact specific yield numbers are difficult to estimate even for a single unit, we cannot know the effective specific yield of the total aquifer exactly. Based on the data from DWR on the aquifers and their specific yields, a reasonable estimate of specific yield is probably in the range of 0.10 - 0.25. Additional uncertainty is created because we do not know the exact boundaries of the groundwater aquifer. Based on topography and the location of wells, we are able to make an estimate of the areal extent of the aquifer. Using these assumptions, the groundwater overdraft is estimated at 5 mm/yr - 15 mm/yr, consistent with the DWR estimates.

5.1.6 Application of the water balance estimator.

Figure 5-2 summarizes the global information available for the water balance for the Sacramento/San Joaquin basin.

A traditional water balance estimate of the storage change would use just one measurement for each element of the water balance. The value of the ΔS estimate would then be computed directly from the water balance equation. In this case, the standard deviation in the storage change estimate is about 250 mm/yr if we assume that errors/uncertainties in the individual flux estimates are independent.

Water balance with multiple measurements

We can significantly reduce this uncertainty by using multiple measurements. By using the global data only (3 measurements of precipitation, selective average AET, and 1 measurement of runoff) with no measurements of storage change, we obtain a storage change estimate, $\Delta\hat{S}$ = -186 mm/yr. The standard deviation of the estimate is reduced from 250 mm/yr (when using just one measurement of each variable) to 173 mm/yr, as shown in Figure 5-3. While this is a considerable reduction, the uncertainty remains quite high. Figure 5-4a shows that despite the large magnitude of the estimated storage change, we must accept the null hypothesis that the storage change is equal to zero at the 5% significance level because of large uncertainty in the estimate.

In previous sections, we have suggested that an estimate of a high rate of groundwater depletion using the water balance approach can be indicative of either actual groundwater depletion or poor quality data. In the absence of additional information, the proper interpretation may be subjective. In this case study, we have additional data that was withheld from the estimation that can suggest the actual state of affairs.

According to DWR's estimates and well level data, the actual rate of groundwater depletion in the Sacramento/San Joaquin basin is on the order of 10 mm/yr, well below our estimate. Since our estimate of 186 mm/yr of groundwater depletion does not match actual

groundwater depletion of that magnitude, this casts suspicion on the quality of our inputs to the water balance. As discussed previously, we have two additional estimates of precipitation in the watershed, which we believe to be more reliable than the three estimates based on global data. The two local sources estimate precipitation at 638mm/yr and 698 mm/yr, for an average of 668 mm/yr. In comparison, the average of our three global estimates is just 454 mm/yr, a difference of over 200 mm/yr. The low precipitation estimate stems from low measurements from the GPCP and Cramer datasets. While the exact magnitude can be debated, the global data does seem to have underestimated precipitation in the Sacramento/San Joaquin basin.

We also have 2 additional sources of runoff data. One of these estimates, at 181 mm/yr, is equal to the estimate we used based on USGS gage data. The other is somewhat higher, at 240 mm/yr. However, the 3 estimates of runoff are in fairly good agreement.

Unfortunately, we have no additional ET data with which to compare our selective average. However, based on the large discrepancy in precipitation estimates and on observations showing small actual groundwater depletion, the proper interpretation for the large estimate of groundwater depletion seems to be poor quality input data. In fact, over large basins with mixed land use, large storage changes estimates are unlikely to be real and may cast suspicion on the quality of the input data.

Water balance with a surrogate storage change measurement

Having concluded that some of our input data is poor, we can use the water balance estimator to improve our estimates of each element of the water balance. It allows us not only to use multiple measurements (as in the previous analysis), but also provides a systematic approach to adjust our final estimates of each element of the water balance. The adjustments are based on the uncertainty in each individual measurement, and can yield improved estimates and reduced uncertainty in not only $\Delta\hat{S}$, but also $\hat{P}$, $\hat{E}$, and $\hat{R}$. The reductions in uncertainty in each variable which result from application of the water balance estimator with a surrogate measurement of $\Delta S = 0$ are shown in Figure 5-3. The largest gains can be found when the initial uncertainty is high. The water balance estimator is able to reduce uncertainty by incorporating data from other elements of the water balance when making an estimate for a single water balance component. If the standard deviation of other variables are lower, then the standard deviation of the resulting estimate can be reduced considerably. However, as seen for runoff, if the original measurement already has a low standard deviation relative to the other variables, then the standard deviation of the estimate will not be significantly altered.

Estimation with a surrogate measurement of ΔS nudges the precipitation and storage change up closer to their actual values, without significantly altering runoff. It does this at the cost of the evapotranspiration estimate, which is nudged downwards below its probable value.

As shown in Figure 5-4b, the new estimate of ΔS is well within the acceptance region for the null hypothesis. Based on the available data, we again cannot show that the storage change is different from zero at the 5% significance level.

Discussion

The Sacramento/San Joaquin case study shows that while multiple estimates can be useful in reducing uncertainty, poor data quality can still limit our ability to estimate groundwater

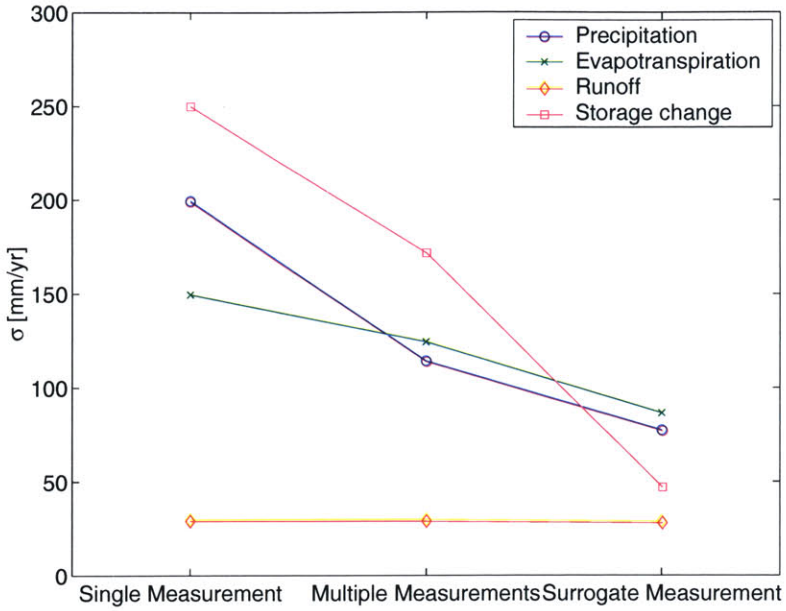

Figure 5-3: The use of multiple estimates and the water balance estimator can significantly reduce the standard deviation of our estimates, particularly when the original measurements have high uncertainty, as shown here for the Sacramento/San Joaquin watershed.

depletion. In fact, very large estimates of storage change can be indicative of shortcomings in the input data and not large groundwater overdrafts. However, application of the water balance estimator can improve our estimates of not only the storage change, but other elements of the water balance as well.

While the water balance estimator is able to give us some indication of whether or not groundwater depletion is likely to be a problem in a watershed, further reductions in the uncertainty would clearly be beneficial. The detectability of groundwater storage changes would be improved in basins with higher rates of storage change. The dilution of the signal when averaging over large basins is one source of difficulty in detecting groundwater storage change. When averaged over the entire watershed, groundwater depletion is relatively small in the Sacramento/San Joaquin watershed. However, locally, the actual groundwater depletion rates can be much higher. For example, average groundwater depletion in the Tulare Lake hydrologic region of the Central Valley is 30-40 mm/yr. When the surrounding (non-agricultural) mountains are excluded from the average, the local groundwater depletion is even higher at 50-60 mm/yr. Unfortunately, accounting for all lateral flows into regions defined by land use rather than hydrologic divides is difficult and introduces considerable uncertainty into the water balance.

Results can also be sensitive to the standard deviation assigned to the inputs. As we discussed in Chapter 2, using a surrogate measurement of zero storage change introduces some bias into the estimation, with a tradeoff between higher bias and lower estimation error. In addition, the standard deviation of the storage change estimate is largely determined by the standard deviation assigned to the surrogate measurement if the standard deviation assigned to the surrogate measurement is substantially lower than the standard deviation of the measurements of the other variables. Storage change estimates need to be considered

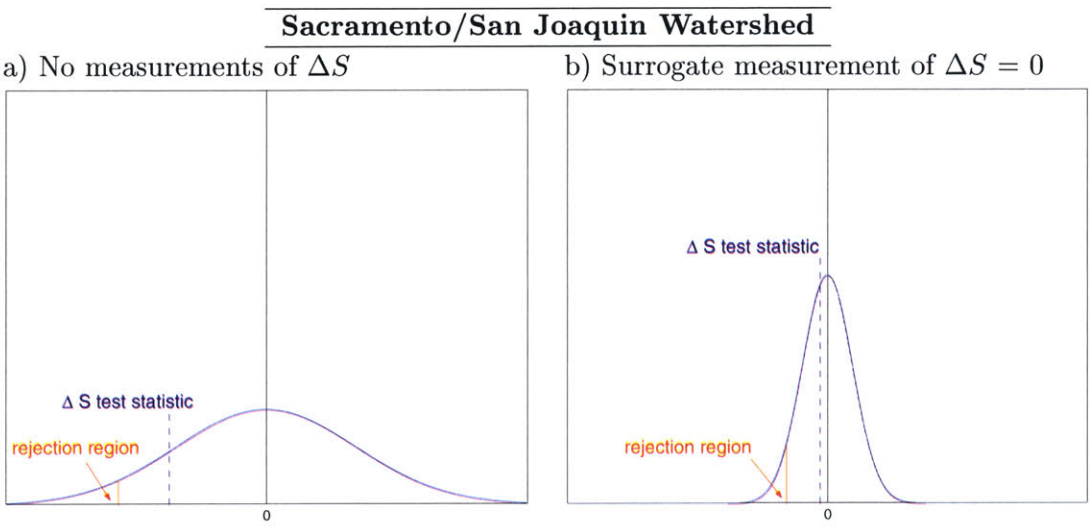

$\hat{P}$ = 454 mm/yr	$\sigma_{\hat{P}}$ = 115 mm/yr	$\hat{P}$ = 531 mm/yr	$\sigma_{\hat{P}}$ = 78 mm/yr
$\hat{E}$ = 445 mm/yr	$\sigma_{\hat{E}}$ = 125 mm/yr	$\hat{E}$ = 355 mm/yr	$\sigma_{\hat{E}}$ = 87 mm/yr
$\hat{R}$ = 181 mm/yr	$\sigma_{\hat{R}}$ = 30 mm/yr	$\hat{R}$ = 176 mm/yr	$\sigma_{\hat{R}}$ = 29 mm/yr
$\Delta\hat{S}$ = -186 mm/yr	$\sigma_{\Delta\hat{S}}$ = 173 mm/yr	$\Delta\hat{S}$ = -14 mm/yr	$\sigma_{\Delta\hat{S}}$ = 48 mm/yr

Figure 5-4: Sacramento/San Joaquin Watershed. Estimation results for a) no storage change measurements and b) a surrogate storage change measurement of zero. The estimated values of $\hat{P}$, $\hat{E}$, $\hat{R}$, and $\Delta\hat{S}$ are shown along with the pdf for $\Delta\hat{S}$. (The quantity $\hat{P} - \hat{E} - \hat{R} - \Delta\hat{S}$ does not equal zero because of imports and exports to the watershed, which constitute a net loss of an additional 14 mm/yr.)

in light of this effect and also the bias introduced by introduction of a surrogate measurement of zero. Use of the surrogate measurement is most appropriate for reducing uncertainty in $\hat{P}, \hat{E}$, and $\hat{R}$, rather than $\Delta\hat{S}$ The standard deviation assigned to measurements of each of the other variables also affects the outcome of the estimation by determining which measurements are weighted most heavily.

5.2 Salinas River Basin

The Salinas River basin is located near the Central Coast of California, as shown in Figure 5-1. The watershed has an area of about 11,000 km^2 and includes some irrigated agricultural areas. Figure 5-5 summarizes the information used for the estimation in the Salinas basin. The data are discussed in greater detail in the sections below.

As can be seen in Figure 5-5, there is some contradiction between the land use specified by the croplands dataset and the irrigated area dataset. Whereas the cropland dataset only indicates small pockets of cropped area, the irrigated area dataset shows a somewhat more extensive agricultural area, albeit at low irrigation intensity. Irrigation appears in the upper watershed, where little irrigation actually takes place. It is likely due to the large grid resolution relative to the watershed size, and includes irrigated lands from the San Joaquin basin across the watershed divide. When 1km GLCC data is considered, we do see a band of irrigation in the valley area of the lower watershed. Other publications also cite the prevalence of irrigation in the lower watershed. This mismatch was also seen to some degree in the Sacramento/San Joaquin watersheds and highlights the difficulty in using global scale datasets for smaller watersheds.

5.2.1 Interbasin Transfer

Interbasin transfers are at most about 3 mm/year (DWR 1998). This figure assumes that all water transfers into DWR's central coast hydrologic region are used in the Salinas basin. The central coast region includes the Salinas River basin as well as some metropolitan areas outside of the basin. It is likely that some of the imports to the central coast region are actually used by metropolitan areas outside of the Salinas River basin. The USGS groundwater atlas for the region reports zero imports into the Salinas basin. In any case, interbasin transfers are small.

5.2.2 Precipitation

Precipitation data were taken from the global sources identified in Chapter 3: GPCP (304 mm/yr), Willmott et al. climatology (446 mm/yr), and Cramer climatology (359 mm/yr). The GPCP reported error is on the order of 110 mm/year, while the Willmott et al. cross validation error is on the order of 150 mm/year for the watershed. Based on these figures, we assigned each precipitation measurement a standard deviation of 125 mm/yr.

We have one additional measurement of precipitation, based on NCDC surface gage data as distributed by EarthInfo. Our own interpolation of this data gave a mean annual precipitation of 394 mm/yr for the Salinas River basin.

5.2.3 Evapotranspiration

Evapotranspiration was estimated using the selective average described in Chapter 4. Mean annual AET is estimated at approximately 357 mm/yr. The standard deviation of the individual measurements was estimated at approximately 125 mm/yr and the selective average was assigned a standard deviation of 100 mm/yr.

5.2.4 Runoff

Streamflow data for the Salinas River near Spreckels, CA were used to calculate runoff for the watershed. This station has a reported area of 10,800 km^2, with data available for water years 1930-1999. Runoff was calculated as the mean annual streamflow divided by the basin area, to give 32 mm/year.

Based on Hydro1K topography, we delineated the basin boundaries using ArcInfo, yielding a basin area of 12,400 km^2. This basin area is approximately 15% higher than the reported value.

5.2.5 Groundwater

According to the USGS (Groundwater Atlas of the U.S.), groundwater declines were prevalent in the lower basin in the 1950's. Since then, construction of 2 dams has helped to ease the burden on groundwater resources. However, large withdrawals from groundwater continue near Monterey Bay and groundwater levels have continued to decline in that region.

Preliminary data from the DWR suggests that groundwater overdrafts in the Salinas basin as a whole are small, at about 6 mm/yr (DWR 1995). Monterey County officials, based on their own detailed analysis, believe that 3 mm/year is a reasonable estimate of groundwater overdraft in the basin (Franklin 2001, personal communication).

5.2.6 Application of the water balance estimator

Using multiple measurements from global data sources only and no measurement of storage change, the water balance estimator gives $\Delta\hat{S}$ = -16 mm/yr. The standard deviation of the error in that estimate is 110 mm/yr. As shown in Figure 5-6a, we must accept the null hypothesis at the 5% significance level. The standard deviation of the estimate is too large relative to the magnitude of the estimate to bring our test statistic close to the rejection region. However, the relatively small magnitude of the storage change estimate suggests that there are no large errors in the data for this watershed.

When a surrogate measurement of $\Delta S = 0$ is utilized, the water balance estimator gives $\Delta\hat{S}$ = -3 mm/yr with standard deviation in the error of 46 mm/yr. Again, the small magnitude of $\Delta\hat{S}$ when compared to the standard deviation of the error forces us to accept the null hypothesis, that groundwater depletion is zero (see Figure 5-6). However, as shown in Figure 5-7, application of the water balance estimator does result in a substantial reduction in uncertainty in the precipitation and evapotranspiration estimates.

Unlike the Sacramento/San Joaquin basin, there is not a large difference between estimation results with and without the use of a surrogate measurement of storage change. This also suggests that there are no major discrepancies in the data. In the Salinas watershed, the precipitation data obtained from global data are consistent with our own estimate from local precipitation stations. The estimated storage change is small, also consistent with the

small rates of groundwater depletion reported by DWR and Monterey County. Additional sources of runoff and evapotranspiration were unavailable for comparison. However, the results are consistent with the idea that large errors in the data will be manifested in a large storage change, if such errors exist.

5.3 Conclusions from California test basins

Results from the Sacramento/San Joaquin and Salinas River watersheds suggest that the water balance estimator can be a useful tool for reducing uncertainty in all elements of the water balance. However, they also suggest that the uncertainty in global datasets is probably too large to detect the rates of groundwater depletion we can reasonably expect to be present in other basins. The water balance retains utility for identifying basins where there are large inconsistencies in the data, and can be used as a screening tool for basins where the data quality is poor. In addition, the water balance estimator can be used to improve estimates of all elements of the water balance and to reduce the uncertainty in those estimates.

Salinas River Watershed
Basin area: 10,700 km^2

a) Cropping Intensity
(Ramankutty and Foley, 1998)

b) Irrigation Intensity
(Döll and Siebert, 1999)

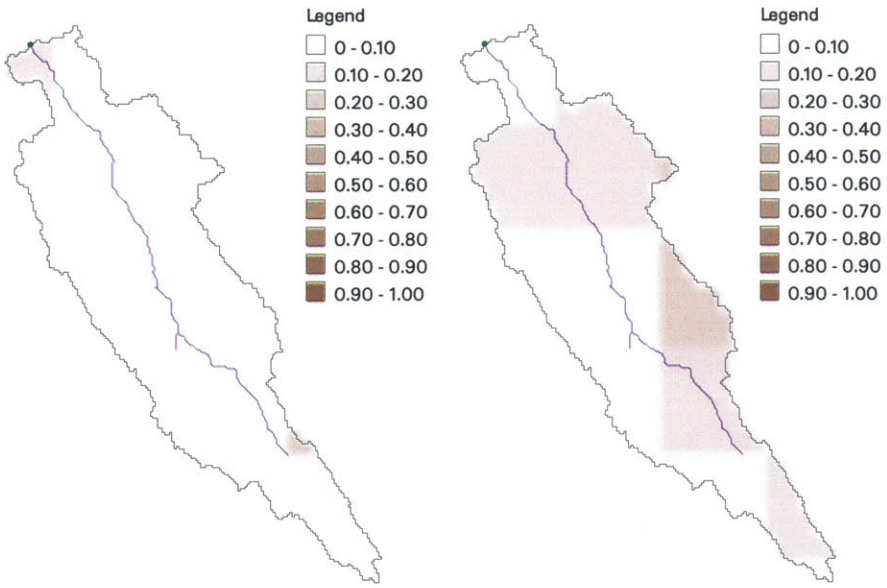

	Value [mm/yr]	Std Dev [mm/yr]
PRECIPITATION		
GPCP	304	125
Willmott et al.	446	125
Cramer and Leemans	359	125
EVAPOTRANSPIRATON		
Selective Average	357	100
RUNOFF		
Streamflow gage	32	15
GROUNDWATER		
DWR Bulletin	-24	-
Monterey County	-3	-
INTERBASIN TRANSFERS		
Imports	3	-
Exports	0	-

Figure 5-5: Salinas River Watershed. Fraction of each 0.5 degree grid cell a) used for agriculture and b) equipped for irrigation.

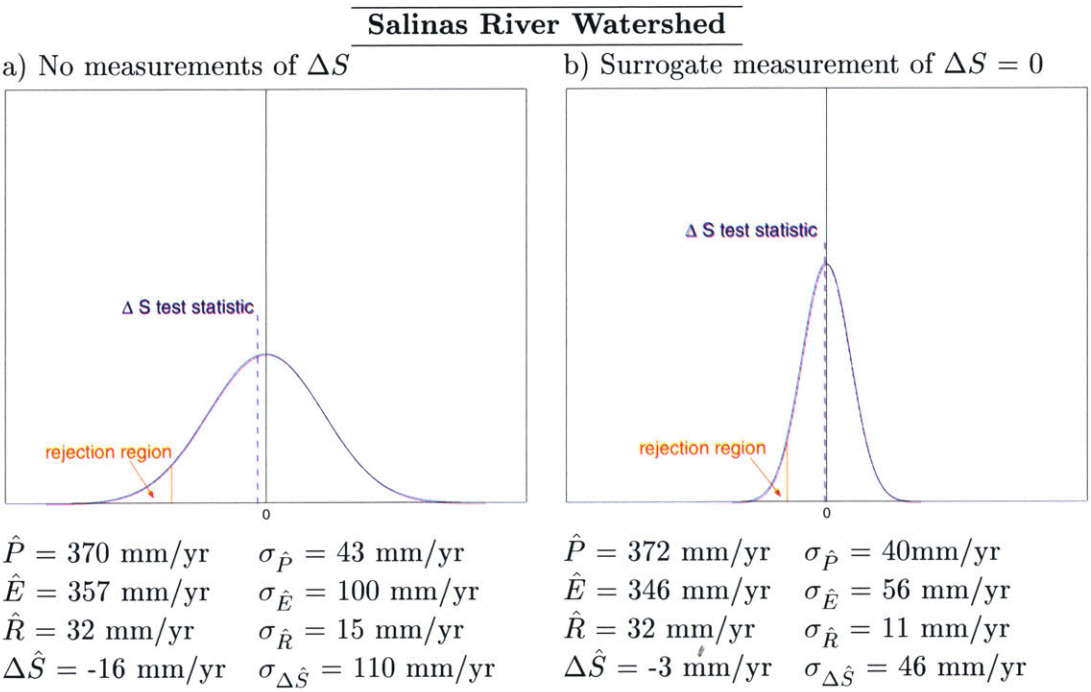

Figure 5-6: Salinas River Watershed. Estimation results for a) no storage change measurements and b) an surrogate storage change measurement of zero. The estimated values of $\hat{P}$, $\hat{E}$, $\hat{R}$, and $\Delta\hat{S}$ are shown along with the pdf for $\Delta\hat{S}$. (The quantity $\hat{P} - \hat{E} - \hat{R} - \Delta\hat{S}$ does not equal zero because of imports and exports to the watershed, which constitute a net loss of an additional 14 mm/yr.)

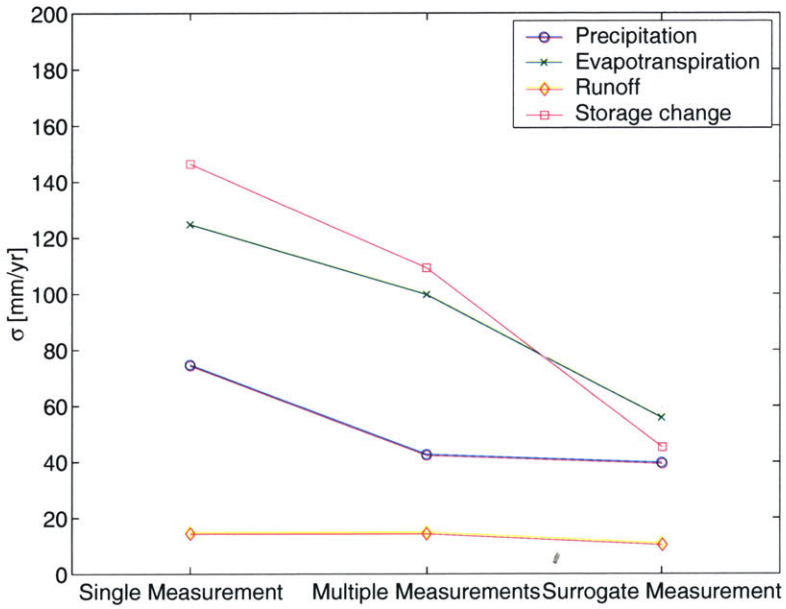

Figure 5-7: The use of multiple estimates and the water balance estimator can significantly reduce the standard deviation of our estimates, particularly when the original measurements have high uncertainty, as shown here for the Salinas River basin.

Chapter 6

Asia

Our study region in Asia was shown in Figure 1-2 of Chapter 1. It includes basins that drain into the Pacific and Indian Oceans, but not those that drain northwards into the Arctic Ocean. It also includes some of the inland basins of central Asia.

This study region was selected to include heavily irrigated areas and areas where groundwater depletion has already begun to manifest as a problem. Water withdrawals in Asia account for 70% of the global consumptive use of freshwater (Shiklomanov 1998) and the bulk of this water is used for irrigation. Postel (2001) lists the 10 nations with the largest irrigated acreage worldwide. Our study area includes 5 of those nations: India, China, Pakistan, Thailand, and Uzbekistan. In fact, India, China, and Pakistan together contain 45% of the world's irrigated acreage (WBGU 1999). As much as 70% of China's total food production may depend on irrigation (deVilliers 2000). Similarly, as much as 70% - 80% of India's agricultural output and 90% of Pakistan's food production in the Indus River basin may be dependent on groundwater irrigation (Burke and Moench 1998).

Figure 6-1 shows the fraction of each 0.5 degree grid cell within our study domain that is used as permanent cropland and the percentage of each 0.5 degree grid cell that is equipped for irrigation. As can be seen, the dominant landuse in many parts of India, China, and southeast Asia is cropland. Widespread irrigation is also observed in some of these areas.

Where groundwater is used extensively, groundwater depletion has the potential to become a problem. It has already been cited as a problem in parts of India and Pakistan and in the North China Plain, an area drained by the Huang He (Yellow), Huai He, Hai He, and Luan He Rivers (Postel 1999, WBGU 1999). In additionl, more localized depletion near large metropolitan areas which rely on groundwater has also been reported. For example, land subsidence has become a problem in Bangkok due to large groundwater overdrafts in the metropolitan area (Postel, Daily and Ehrlich 1996).

While groundwater monitoring networks exist in many of these regions and farmers are certainly aware if groundwater levels in their wells is declining, to our knowledge, there has been no systematic colection of groundwater data worldwide or throughout Asia. Historically, some nations have been reluctant to share groundwater data, as water is sometimes considered a strategic resource. Further, many of the groundwater monitoring networks are relatively new, and long term data are not always available (Moench 2001). To effectively monitor groundwater, the monitoring network must also be fairly dense, so that localized conditions are not misinterpreted as representative of large areas. Care must also be taken in obtaining measurements when groundwater levels have had a chance to equilibrate after pumping. The lack of a global database of groundwater levels means that large scale

monitoring of the sustainability of groundwater use has thus far been impossible.

As was shown in our case studies of California basins, global datasets have limitations and despite our efforts to reduce uncertainty we cannot generally say anything definitive about groundwater depletion with the currently available data. However, water balance techniques can still be used to inform us about the quality of data over large areas. In this chapter, using multiple measurements of the water balance variables, the water balance equation will be used as a screening tool for basins where data quality is poor. The water balance estimator will be used to reduce the uncertainty in our estimates of all components of the water balance.

6.1 Basins

The basins included in our analysis were chosen based on size and the availability of streamflow records. They are listed in Table 6.1. A few important basins which were not included bear mentioning. The Indus River basin in Pakistan is an important agricultural region, in which extensive irrigation is practiced. Streamflow records were only available for 4 years and the basin was excluded for this reason. A number of other basins were not studied because of a lack of streamflow data. In other cases, streamflow stations were located upstream of areas with significant irrigated agriculture. Additional runoff information from modeling and our regression analysis may be useful in extending the analysis to these regions, but were not tested in this study. We have also excluded the Aral Sea basin from this analysis primarily because the Hydro1K topography did not capture the drainage patterns in this region well. In addition, shrinking storage in the Aral Sea prevents distinction between groundwater changes and surface storage changes.

6.2 Water balance estimator with multiple measurements

By using multple estimates of each water balance component and application of the water balance equation, we have estimated the storage change of each basin. As seen in Figure 6-2, very large storage change was calculated for a number of basins. Because storage changes can generally be expected to be small, particularly when averaged over a large basin, a large storage change estimate can be indicative of poor input data quality. We have identified several basins where the quality of global data is poor. These basins are highlighted in Figure 6-3. The ChangJiang, XiJiang, Brahmaputra, Irawaddy, Chao Phrya, and Krishna rivers all had storage changes with an absolute value greater than 100 mm/yr. In these basins, it is very likely that there are problems with the input data. In fact, runoff exceeded all available measurements of precipitation in the Irawaddy basin, a clearly suspect scenario. The absolute value of storage change in the Godavari, Mahi, Penner, and Tapti river basins was between 50 mm and 100 mm, a relatively large amount which may also indicate inconsistencies in the input data. The absolute value of storage change was less than 50 mm in the remainder of the basins studied.

The water balance estimator with a surrogate measurement of ΔS can help to reduce the uncertainty in estimates of each element of the water balance.

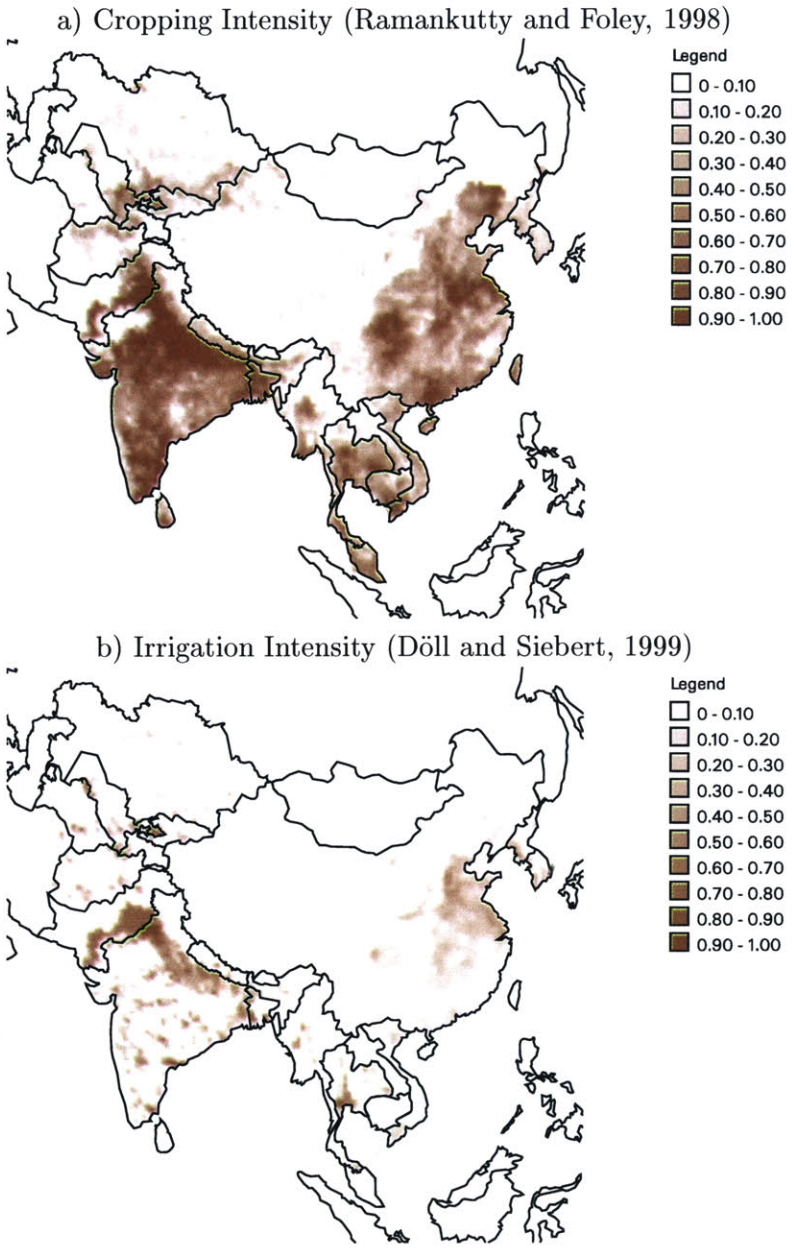

Figure 6-1: Fraction of each 0.5 degree grid cell a) used for agriculture and b) equipped for irrigation.

Table 6.1: Basins with adequate streamflow records in our study region in Asia.

Basin	Gage Location	Drainage Area [km^2]
Huang He (Yellow River)	Hua Yuan Kou	730,000
Huai He	Bengbu	121,000
Luan He	Luanxian	44,000
Hai He	at mouth	214,000
Chang Jiang (Yangzi River)	Datong	1,705,000
XiJiang (Pearl River)	WuZhou3	329,700
Mekong	Pakse	545,000
Chao Phrya	Nakhon Sawan	111,000
Irawaddy	Sagaing	118,000
Brahmaputra	Bahadurabad	636,000
Ganges	Farakka	935,000
Godavari	Polavaram	309,000
Krishna	Vijayawada	255,900
Mahi	Sevalia	34,000
Narmada	Garudeshwar	89,000
Tapti	Kathore	62,000
Penner	Nellore	53,000

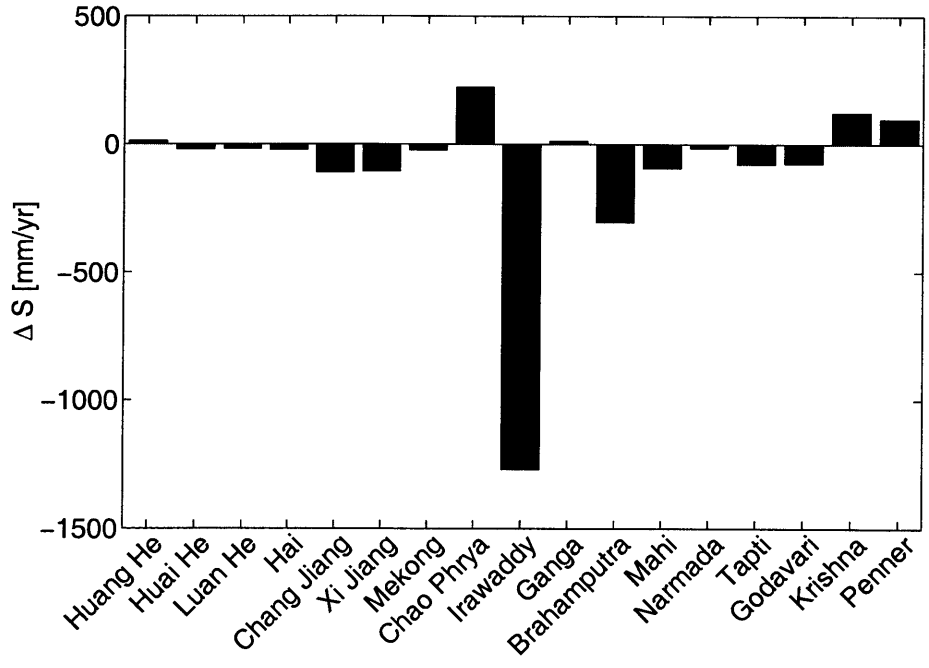

Figure 6-2: $\Delta\hat{S}$ estimated for Asian basins, using multiple measurements of precipitation and evapotranspiration.

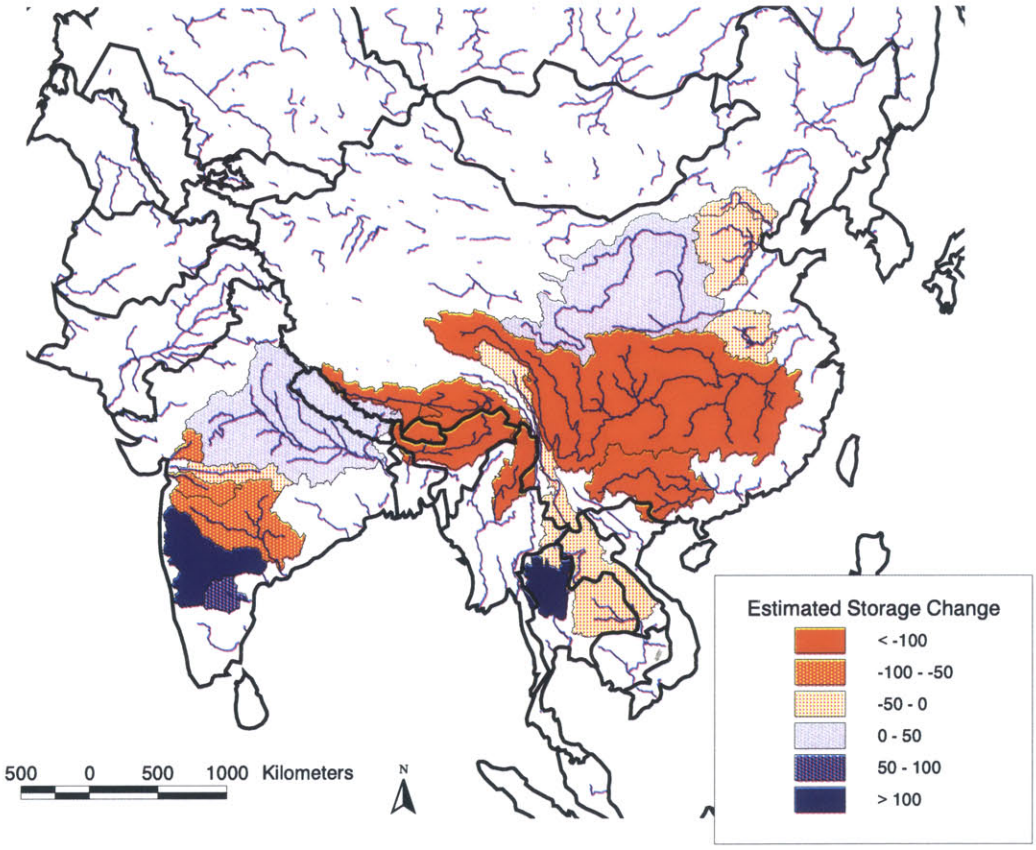

Figure 6-3: Basins with large $\Delta\hat{S}$ are highlighted. A large $\Delta\hat{S}$ estimate can be indicative of poor quality input data.

6.3 Discussion

The poor data quality has implications not only for estimating groundwater depletion with the water balance method, but also for other studies which make use of the same global data sources. Poor measurements can create problems in validating models designed to consider river flow, evapotranspiration, or precipitation at climatological timescales. Further, when poor data is used as an input to models, the results from those models become less dependable. Fekete et al. (2000), for example, cite inaccurate precipitation data as a possible hindrance to their ability to accurately predict global runoff with a simple soil moisture accounting model.

Our work suggests the need for more data, of improved accuracy, and at higher spatial resolution. In contrast, the availability of data collected using traditional methods seems to be on the decline, as reported by Vorosmarty et al. (2001) and Shiklomanov (1998) for streamflow stations. The authors suggest that this decline is impeding efforts to validate models and newer data products. Our work suggests that it may also be limiting our ability to monitor the sustainability of our water and agricultural systems.

High uncertainty in other types of global data relevant to agricultural systems has also been pointed out by Rojstaczer et al. (2001). They estimate the human appropriation of photosynthesis products, with estimates of uncertainty based on Monte Carlo simulation with uncertain parameters. They conclude that despite incorporation of recent data, any estimate of this quantity is subject to very large uncertainty. As Rojstaczer et al. point out, the large uncertainty makes it impossible for us to know the true human impact on natural systems. As our analysis has shown, the impact of human activity on groundwater resources is also difficult to determine with existing data.

While we have incorporated some remote sensing products into our analysis, the availability of data from remote sensing is expanding rapidly. Remote sensing measurements have the potential to provide high quality data with good spatial and temporal resolution. In the next chapter, we highlight some of the forthcoming datasets which may be of particular value for application of the least squares water balance estimator.

Chapter 7

Information needs for improved estimation

In the previous chapters, we have noted that the contrained water balance estimator is able to reduce uncertainty in our estimates of each element of the water balance, including the storage change. However, results cannot generally be used to make a definitive statement about groundwater depletion in a basin. This chapter discusses possible improvements.

7.1 Detectability of groundwater depletion in different climates

In all of the basins analyzed in this study, the uncertainty in our estimates of groundwater depletion remains high. The water balance estimator cannot completely circumvent the pitfalls of differencing large numbers to calculate a smaller one. As a result, the overall rate of groundwater depletion must be quite high to be detected using this method. The use of more detailed local data can help to decrease the uncertainty in the estimates and increase the usefulness of this estimation method. However, data limitations continue to restrict the usefulness of this estimation technique.

Under different climatic settings, the water balance technique may have varying effectiveness for estimating the change in groundwater storage. In particular, the water balance method may be easier to apply in more arid areas, where surface fluxes, especially precipitation and runoff, are relatively small. Groundwater overdrafts causing storage change would make up a larger percentage of the overall budget and thus be easier to detect.

We tested this hypothesis by solving the estimation problem analytically. First we identified a "true" climate. The first test climate was similar to that found in the Sacramento/San Joaquin basin of California (P = 600mm/yr, E = 425mm/yr, R = 200mm/yr, ΔS = -25mm/yr). The standard deviation of the $\Delta\hat{S}$ estimate was derived by assuming that 3 measurements of precipitation, 3 measurements of evapotranspiration, 1 measurement of runoff, and no measurements of ΔS were available. Based on the standard deviation of the storage change estimate, we can calculate the pdf for the null hypothesis and define a rejection region. The null hypothesis, that the storage change is equal to zero is only rejected when there is strong evidence favoring the alternate hypothesis, that the storage change is less than zero. The significance level is the probability of rejecting the null hypothesis when it is actually true. Rejection regions are typically chosen to give significance levels in the range 0.01 to 0.10.

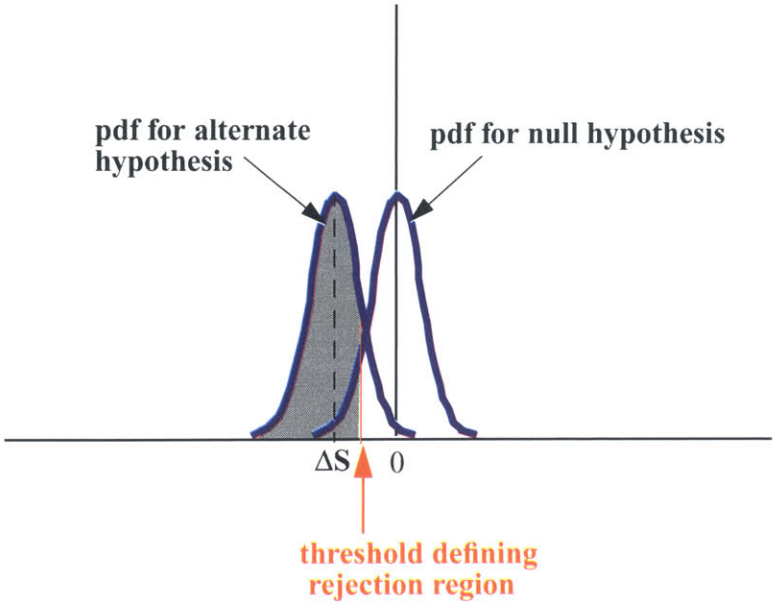

Figure 7-1: The superposition of the pdf for the null hypothesis and the alternate hypothesis allows us to calculate the percent of the time the null hypothesis is correctly rejected in favor of the alternate hypothesis, indicated by the shaded region.

As shown in Figure 7-1, we can also define a pdf based on the true ΔS = -25 mm/yr, in essense a reprensentation of a particular alternate hypothesis. From the superposition of the two probability density functions, we can then calculate the probability that the null hypothesis is correctly rejected in favor of the alternate hypothesis. This is often called the power of the hypothesis test.

Figure 7-2 shows the standard deviation of the $\Delta\hat{S}$ estimate in mm/year and the test power when the significance level is 5%. The x-axis shows the measurement error, defined as the standard deviation of the measurements expressed in terms of of percent of the true mean. For example, a measurement error of 25% implies that the standard deviation of each measurement was 25% of the true value of each measurement. With 25% measurement error, the standard deviation for precipitation would be 150 mm/yr, for ET would be 106 mm/yr, and for runoff would be 50 mm/yr. The analytical solution to the estimation problem indicates that we must measure precipitation, evapotranspiration, and runoff to within about 3% to correctly reject the null hypothesis more than 50% of the time (a power of 0.50). Even greater accuracy is required to obtain higher test powers. This level of accuracy is quite difficult to achieve given the current measuring techniques and the spatial and temporal variability in the measured quantities, especially precipitation and ET.

Figure 7-2 also shows the same plot for hypothetical dry (P = 200 mm/yr, ET = 225 mm/year, R = 0 mm/year, ΔS = -25 mm/yr) and very dry climates (P = 100 mm/yr, ET = 125 mm/yr, R = 0 mm/yr, ΔS = -25 mm/yr). The standard deviation of the measurements were calculated in the same manner, except that the standard deviation of the runoff estimate was held constant at 5 mm/yr. As Figure 7-2 shows, it becomes relatively easier to detect the same change in groundwater storage change in these drier climates. In the dry climate, we can detect a groundwater storage change of -25 mm/yr

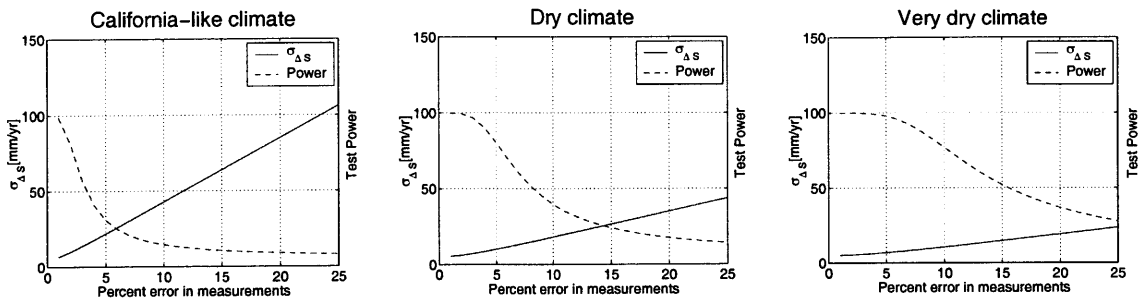

Figure 7-2: The solid line shows the standard deviation of the $\Delta\hat{S}$ estimate as a function of the percent measurement error for a) a climate similar to that found in California, b) a hypothetical dry climate, c) a hypothetical very dry climate with 25 mm/yr of groundwater depletion. The dashed line shows the test power (probability that the null hypothesis will be correctly rejected) when the significance level is 0.05.

50% of the time when our measurement error approaches 8%, still a smaller error than expected in most of the currently available data. In a very dry climate, the allowable measurement error increases to about 15%, and this level of error may be feasible in well-monitored regions. Thus, detection of groundwater depletion may be easier in arid regions such as the Middle East, North Africa, and Arabian peninsula. Significant groundwater pumping is also taking place in parts of these regions. Throughout this discussion we have adhered to a relatively stringent criteria, using a significance level of 0.05. If we are willing to accept a higher significance level, the feasibility of detecting groundwater depletion in arid regions will increase.

7.2 Possible improvements with forthcoming data

A number of data sources which are becoming available may help to reduce uncertainty in our water balance estimates significantly. Data which can help to improve our measurements of each component of the water balance are discussed in the following sections.

7.2.1 Improved precipitation

The Tropical Rainfall Measuring Mission (TRMM) is a joint project between NASA and the National Aeronautics and Space Development Agency of Japan (NASDA, Japan). The project was designed to give information on both the vertical and the horizontal structure of precipitation in the tropics. The TRMM satelllite was launched on November 27, 1997 and provides measurements for the zonal swath between approximately 40N and 40S. The satellite carries three instruments for measuring rainfall, the TRMM Microwave Imager (TMI), the Visible Infrared Scanner (VIRS), and the Precipitation Radar (PR). The satellite's orbit allows all locations to be covered every day, but at a different local time each day. The satellite data are validated by ground radar at a number of sites scattered throughout the measurment domain. (NASA 2000)

While data have been collected for almost 4 years, TRMM data were not included in

our analysis because of the relatively short period of record. The satellite is expected to remain in orbit until approximately March 2004, yielding a total of 6-7 years of data. Even with the entire length of record, however, conversion of the sporadic daily measurements to long term mean precipitation will be difficult.

Another reason TRMM data were not used in this study was the geographic limits of the dataset. Because data are available only for the tropics and subtropics, data for many of our mid-latitude watersheds were not available. The Global Precipitation Measurement (GPM) mission should address this geographical limitation. The GPM is a joint mission between NASA, NASDA in Japan, and the European Space Agency (ESA) and is scheduled to launch in the year 2007 or 2008. A constellation of 9 satellites will be used to provide global precipitation coverage with more frequent temporal sampling than TRMM. It is expected to sample at all locations at least once every 3 hours (Smith 2001).

In addition to satellite missions, ground-based radar has been used to enhance spatial coverage of precipitation measurements. The Next Generation Weather Radar (NEXRAD) system uses approximately 160 Weather Surveillance Radar-1988 Doppler (WSR-88D) sites throughout the United States and selected overseas locations to collect information which can be used to estimate spatially distributed precipitation. Data are available throughout the U.S.on a 4km x 4km grid at an hourly timescale. Expansion of such radar systems to additional global locations can provide additional high quality precipitation data.

7.2.2 Improved Evapotranspiration Estimation

Actual evapotranspiration is limited by the availability of water to values less than or equal to potential evapotranspiration. It follows that if we have information on the availability of water, we can make better estimates of evapotranspiration. Soil moisture measurements thus have the potential to significantly improve our estimates of actual evapotranspiration. Only scattered point measurements of soil moisture are currently available. However, global soil moisture measurements should become available in the near future through application of remote sensing technology.

Soil moisture measurements can be made using microwave radiometry. Previous research has indicated that brightness temperatures measured by L-band microwave radiometers have the best potential for monitoring surface soil moisture, being able to reliably estimate soil moisture in the upper 5 cm of the soil column to within about 3 percent (Jackson et al. 1995, Jackson et al. 1999). A recent study using data collected from remote sensing instruments mounted on aircraft have demonstrated improvement in evapotranspiration estimation with the assimilation of remote sensing data. (Margulis et al. 2001) Data assimilation is an important component of evapotranspiration estimation using soil moisture measurements because remote sensing measurements of soil moisture only give information for the uppermost layers of the soil, while plants are able to extract water from deeper layers as well.

The HYDROS (Hydrosphere States) Mission is a proposed satellite mission, still in the planning phase (NASA 2002). It is being designed to measure soil moisture using an L-band radar/radiometer. Current project specifications include global soil moisture measurements at 10 km and 40 km resolution, at approximately a 3-day temporal resolution. However, data will not be available for at least several years.

In the meantime, NASA's Aqua satellite is due to launch in 2002 and is also designed to measure soil moisture around the globe (NASA 2001b). It is intended to cover all locations on the globe every 16 days, and provide soil moisture data at 25 km x 25 km horizontal

resolution. The mission is designed to operate for about 6 years. Soil moisture will be measured using a C-band radiometer, which is more limited than L-band in its ability to penetrate cloud cover and vegetative cover. When available, data from L-band radiometers should provide superior penetration of cloud cover and vegetation so that more accurate soil moisture measurements can be obtained.

Even using L-band radiometers, satellite remote sensing of soil moisture is unlikely to be effective for heavily vegetated forest locations, as dense vegetative cover masks the signal from underlying soils.

7.2.3 Extended runoff

Runoff measurements are limited mainly by the temporal length of the record, and by the existence of numerous ungaged streams, including some major rivers. Runoff modeling can help to fill in the gaps. Models have improved in recent years, by using more detailed spatially distributed information on land surface characteristics and precipitation. Soil moisture measurements can also be used to improve runoff modeling, as runoff production is influenced by soil moisture. It is important to note that the accuracy of runoff models depends not only on the realism of the algorithms and parameters employed, but also on the accuracy of inputs like precipitation.

An alternative means of monitoring remote locations is through the use of remote sensing. Koblinsky et al. (1993) and Birkett (1998) have examined the feasibility of using satellite altimetry data to monitor river flow in remote locations. Koblinsky et al. showed that the U.S. Navy's GEOSAT radar was able to measure river level at locations on the Amazon River with an RMS accuracy of about 0.7m. In a more recent study, Birkett showed that NASA's TOPEX/POSEIDON satellite can successfully measure water levels in rivers of 1 km or greater width. Birkett showed an RMS error of just 11 cm for select major rivers. The use of satellite altimetry to monitor river discharge depends on the accuracy of the stage-discharge curve calculated for a given river location.

7.2.4 Measurements of storage change

Advances in remote sensing may soon provide a means of directly monitoring changes in water storage. NASA's Gravity Recovery and Climate Experiment (GRACE) is a satellite mission intended to measure the Earth's gravity field at 2-4 week intervals at high accuracy (NASA 2001a). The mission is scheduled to launch in February 2002 and will provide detailed spatial as well as temporal information on the gravity field. Perturbations in the gravity field can be attributed to the redistribution of mass within the Earth or on its surface. Movement of water resulting in changes in water storage is a primary source of that redistribution of mass. At scales of a few hundred kilometers, GRACE may be able to detect storage changes of as little as 2 mm (Wahr et al. 1998). Rodell and Famiglietti (1999) analysed the detectability of changes in water storage using the GRACE measurements. The accuracy for any particular watershed will depend on its size, the temporal period, and atmospheric conditions. The authors chose 20 continental-scale watersheds scattered around the world for further study. They used 10 modeled datasets of soil moisture and snow water content to characterize the seasonal and annual variability of water storage over a period of 2 years. Their results indicated that seasonal and annual variability is detectable in many basins. The total uncertainty in annual storage change expected from GRACE-derived estimates depends on the watershed size and range from as little as 2 mm up to

almost 40mm. The estimated uncertainty for 80% of the watersheds was less than 10mm. As the authors also note, their analysis of detectability relied on models which considered changes in storage only in the unsaturated zone and in snow cover. Long term changes in groundwater storage were not considered, but could also conceivably be monitored, as changes in groundwater storage would also affect the GRACE measurements. An annual storage change estimate with an uncertainty on the order of 10mm has far less uncertainty than most of our other measurements of the elements of the water balance. In fact, that degree of accuracy could turn our estimation on its head, and be useful in developing better estimates of precipitation, evapotranspiration, and runoff.

The biggest limitation in the usefulness of the GRACE data in our water balance estimation may be the length of the mission. The GRACE satellite is currently scheduled for a 5-year mission, which may not be long enough to justify some of our assumptions. For example, going from a wet period to a dry period during those five years could create differences in soil moisture which are not accounted for in our estimation technique. But if used in conjunction with additional snow and ice data and soil moisture data, the water balance would not necessarily have to be conducted at the mean annual timescale. With sufficient data on other storage changes, interannual and even monthly changes in groundwater storage could be resolved. As already noted, global soil moisture measurements should become available in the future. In addition, data on snow and ice extent has been collected for some time.

If measurements from GRACE are able to provide good estimates of storage change, then the ability of the water balance estimator to make improved estimates of the other elements of the water balance will be enhanced. By eliminating storage change as a significant source of uncertainty, estimates of precipitation, evapotranspiration, and runoff will also benefit.

Although satellite based data can undoubtedly enhance our understanding of hydrological processes on the earth's surface, they cannot replace more traditional surface-based measurements. These surface measurements are still needed for calibration and validation of satellite measurements and can provide a consistent record dating back many years. Unfortunately, the availability of some types of data seems to be on the decline. Vorosmarty et al. (2001) report a significant reduction in streamflow discharge measurements in recent years. They suggest that this decline is impeding efforts to validate models and newer data products. Our work suggests that it may also be limiting our ability to monitor the sustainability of our water and agricultural systems.

It is also important to note that while promising, many of these data are not yet available and a long term record will take many years to accumulate. In the meantime, poor quality data has implications not only in our ability to estimate groundwater depletion using the water balance estimator, but also in our ability to validate and use the results of other large scale modeling studies.

Chapter 8

Conclusions

8.1 Contributions of this work

- **A new AET estimate was developed based on NDVI measurements and land use information.** The algorithm can be applied globally, without calibration. Results are presented for the continental U.S. and for our study region in Asia. This AET estimate is particularly useful for irrigated areas as the growing season is defined by observed changes in vegetation and not natural rainfall. It is included in a selective average AET estimate, which is used to reduce uncertainty and to capitalize on the strengths of the individual AET estimates used.

- **Multiple regression of runoff against basin characteristics was shown to provide additional information on runoff in ungaged areas.** Runoff estimates for 39 Asian basins based on the regression are as good as or better than estimates based on the water balance equation and estimates from a gridded runoff dataset developed by spatial interpolation from gaged areas. However, the regression was not used as an additional source of runoff data in subsequent water balance analyses of Asian basins.

- **The water balance estimator was shown to be a useful tool for enhancing water balance analyses.** It is able to reduce uncertainty in estimates of not only ΔS, but also P, ET, and R. In addition, it can be used to flag basins in which data quality is poor. A number of basins in Asia where the water balance implies poor quality data were identified.

- **Applications to Californian and Asian basins showed that currently available data is inadequate for estimation of groundwater depletion using the water balance approach.** Thus, the sustainability sustainability of irrigated agriculture in areas which rely on groundwater remains an open question. Forthcoming sources of data which may improve our ability to estimate groundwater depletion were identified. The water balance estimator may also be more effective in drier climates.

8.2 Implications for the water scarcity debate

A number of recent publications diagnose water scarcity problems through the use of indicators such as the percent of renewable water resources utilized or the per capita availability

of fresh water. We have proposed that the rate of groundwater depletion is a more appropriate measure of the sustainability of water resources use. However, our analysis shows that groundwater depletion over large areas is extremely difficult to monitor effectively, given the current data. Because of large uncertainty in the data used in the water balance, our estimates of groundwater depletion are inconclusive. Some of the same sources of data are used to estimate total renewable water resources and indicators of water scarcity that rely on such estimates should also be considered in light of that uncertainty. Placing error bounds on estimates of these water scarcity indices can help to give a clearer picture of the true state of our knowledge about global water scarcity.

8.3 Implications for other areas of research

This study has highlighted the large uncertainty in currently available global data for the different components of the water balance. This uncertainty has implications beyond the scope of the current study, impacting many other global modeling efforts which rely on data similar to that used in this study. Many models developed to study climate change issues use precipitation and runoff data for calibration and validation. If the measurements used to calibrate or validate a model are themselves highly uncertain, the dependability of model results becomes suspect. In addition, many models use precipitation as an input. Again, results become less reliable when the inputs themselves are uncertain. Finally, uncertain measurements used for input, calibration, or validation can make it difficult to evaluate whether unexpected modeling results are real or are the result of problems with the model algorithm, the by-product of poor input data, or problems with the data used for validation. If our goal is to understand the natural system, our impacts on it, and the sustainability of our actions, additional energy devoted to improving global monitoring of basic hydrologic variables may reap more rewards than the development of ever more complicated models.

8.4 Future work

We focused only on Asian basins in this study. Future work can expand the analysis to other continents to identify additional areas where data quality may be poor. In addition, current data may be sufficient to identify rapid groundwater depletion in very arid areas of North Africa or the Middle East. Application of the water balance for estimation of groundwater depletion in Asian basins can be revisited when additional data becomes available.

Our AET work can also be expanded to encompass the entire globe. Data are available which allow application of the NDVI-based AET algorithm worldwide. In addition, enhancements to the NDVI-based AET algorithm are possible. In particular, inclusion of information from microwave radiometer polarization differences may yield improvements to the AET estimates.

Our work has also suggested that estimates of runoff in ungaged areas may be obtained through multiple regression techniques. This analysis can also be expanded to other regions worldwide. It would be interesting to assess whether a single regression function could be applied worldwide, or if there are significant differences in the importance of specific watershed characteristics in different regions.

Appendix A

Proof that the water balance estimator is unbiased

Proof That Constrained Least-Squares Estimate Is Unbiased
DMcL. 21 Aug. 2001

Governing equations for mass balance are:

Measurement equation: $z = Mx + v$
Mass balance constraint: $Ax = b$

Where (dimensions shown in parentheses):

x = unknown fluxes to be estimated (N_x, 1)
z = measured fluxes (N_z, 1)
v = measurement error (N_z, 1)
M = measurement matrix (N_z, N_x)
A = constraint matrix (N_b, N_x)
b = constraint vector (N_b, 1)

For our problem M is composed of ones and zeros, $N_b = 1$, A is composed of ones and minus ones, and $b = 0$.

Least-squares estimate of x is obtained by minimizing:

$$J = [z - Mx]^T C_v^{-1} [z - Mx]$$

with respect to x subject to constraint:

$Ax=b$

There are really only N_x - N_b degrees of freedom (free unknowns) in the problem. To account for this define a "dummy" variable w (N_x - N_b, 1) and a (non-unique) matrix D (N_x , N_x - N_b) such that:

$x=Dw$

The constraint holds so long as D is chosen to insure that $Ax=ADw=b$ Then least-squares objective, with constraint included, can be written as:

$$J = [z - MDw]^T C_v^{-1} [z - MDw]$$

Value of w which minimizes this is:

$$\hat{w} = [D^T M^T C_v^{-1} MD]^{-1} D^T M^T C_v^{-1} z$$

Note that matrix in brackets is invertible since it has rank N_x - N_b (so long as $N_z > N_x$ - N_b). Therefore constrained least-squares estimate of x is:

$$\hat{x} = D\hat{w} = D[D^T M^T C_v^{-1} MD]^{-1} D^T M^T C_v^{-1} z$$

To check bias, take expectation of this expression:

$$E[x] = DE[w] = D[D^T M^T C_v^{-1} MD]^{-1} D^T M^T C_v^{-1} E[z]$$
$$= D[D^T M^T C_v^{-1} MD]^{-1} D^T M^T C_v^{-1} Mx$$
$$= D[D^T M^T C_v^{-1} MD]^{-1} D^T M^T C_v^{-1} MDw$$
$$= Dw$$
$$= x$$

So constrained least-squares estimate of x is unbiased.

References

Allan, J. A. (1999). Water stress and global mitigation: Water, food and trade, *Aridlands Newletter* (45).

Allen, R. G. et al. (1998). Crop evapotranspiration - guidelines for computing crop water requirements, *FAO Irrigation and Drainage Paper 56*, Food and Agriculture Organization of the United Nations, Rome. www.fao.org/docrep/X0490E/x0490e00.htm.

Asante, K. et al. (1999). Digital atlas of the world water balance, version 3.0, june 1999, CD-ROM. Center for Research in Water Resources at the University of Texas at Austin.

Baumgartner, A. and Reichel, E. (1975). *The World Water Balance*, Elsevier, New York. translated by Richard Lee.

Birkett, C. M. (1998). Contribution of topex nasa radar altimeter to the global monitoring of large rivers and wetlands, *Water Resources Research* **34**(5): 1223–1239.

Bras, R. L. (1990). *Hydrology: An Introduction to Hydrologic Science*, Addison Wesley Publishing Co., New York.

Brown, L. R. et al. (1999). *State of the World 1999 - Millennial Edition*, Worldwatch Institute, Washington, D.C.

Brown, L. R. et al. (2000). *State of the World 2000*, Worldwatch Institute, Washington, D.C.

Burke, J. J. and Moench, M. H. (1998). *Groundwater and Society: Tesources, Tensions and Opportunities*, U.N. Department of Economic and Social Affairs and Institute for Social and Environmental Transition.

Burt, C. M., Howes, D. J. and Mutziger, A. (2001). Evaporation estimates for irrigated agriculture in california, *Irrigation Association Conference - San Antonio, Texas - November 3-6,2001*, The Irrigation Association. ITRC Paper No. P 01-002.

Choudhury, B. J. (1989). Relating Nimbus-7 GHz data to land surface evaporation, *in* A. Rango (ed.), *Remote sensing and large-scale global processes*, IAHS Publication No. 186, IAHS, pp. 59–66.

Choudhury, B. J. (1997). Global pattern of potential evaporation calculated from the penman-monteith equation using satellite and assimilated data, *Remote Sensing of Environment* **61**: 64–81.

Choudhury, B. J. and DiGirolamo, N. E. (1998). A biophysical process-based estimate of global land surface evaporation using satellite and ancillary data: I. Model description and comparison with observations, *Journal of Hydrology* **205**: 164–185.

Choudhury, B. J. et al. (1994). Relations between evaporation coefficients and vegetation indices studied by model simulations, *Remote Sensing of Environment* **50**: 1–17.

Choudhury, B. J. et al. (1998). A biophysical process-based estimate of global land surface evaporation using staellite and ancillary data: Ii. regional and global patterns of seasonal and annual variations, *Journal of Hydrology* **205**: 186–204.

Cihlar, J., St.-Laurent, L. and Dyer, J. A. (1991). Relation between the normalized difference vegetaion index and ecological variables, *Remote Sensing of Environment* **35**: 279–298.

Deichmann, U. and Eklundh, L. (1991). *Global digital data sets for land degradation studies: a GIS approach*, number 4 in *GRID Case Study Series*, UNEP/GEMS and GRID, Nairobi, Kenya. 103 pp.

den Hartog, G. and Ferguson, H. L. (1978). *Hydrological Atlas of Canada*, Canadian National Committee for the International Hydrological Decade, chapter Plate 25. Water Balance Derived Precipitation and Evapotranspiration.

deVilliers, M. (2000). *Water: The Fate of our Most Precious Resource*, Houghton Mifflin Company, Boston. 352 pp.

Döll, P. and Siebert, S. (1999). A digital global map of irrigated areas, *Technical Report Report Number A9901*, Center for Environmental Systems Research, University of Kassel, Germany.

Doorenbos, J. and Pruitt, W. (1977). Guideline for predicting crop water requirements, *FAO Irrigation and Drainage Paper 24*, Food and Agriculture Organization of the United Nations, Rome. Revised version.

DWR (1993). California Water Plan Update Bulletin 160-93, *Technical report*, California Department of Water Resources, Sacramento, CA.

DWR (1995). Bulletin 118, *Technical report*, California Department of Water Resources. http://wwwdpla.water.ca.gov/sjd/groundwater/118salin.html.

DWR (1998). California Water Plan Update Bulletin 160-98, *Technical report*, California Department of Water Resources, Sacramento, CA.

FAO (2000). Crops and drops: Making the best use of land and water, http://www.fao.org. Food and Agriculture Organization of the United Nations.

Fekete, B. M. et al. (2000). Global, composite runoff fields based on observed river discharge and simulated water balances, unh website.

Galloway, D. et al. (2000). Land subsidence in the united states, USGS Fact Sheet 087-00. http://water.usgs.gov/ogw/pubs/fs00087.

Garatuza-Payan, J. et al. (1998). Measurement and modelling evaporation for irrigated crops in north-west mexico, *Hydrological Processes* **12**(9): 1397–1418.

Gleick, P. (ed.) (1993). *Water in Crisis: A Guide to the World's Fresh Water Resources*, Oxford University Press, New York.

Gutman, G. and Rukhovetz, L. (1996). Towards satellite-derived global estimation of monthly evapotranspiration over land surfaces, *Advances in Space Research* **18**(7): 67–71.

Hall, M. et al. (1999). Dealing with water scarcity, *Physics and Chemistry of the Earth. B: Hydrology, Oceans and Atmosphere* **24**(4): 359.

Huffman, G. et al. (1997). The Global Precipitation Climatology Project (GPCP) Combined Precipitation Data Set, *Bulletin of the American Meteorological Society* **78**: 5–20.

Jackson, I. (1989). *Climate, Water and Agriculture in the Tropics*, 2nd edn, Longman Scientific and Technical, Essex, England.

Jackson, T. J. et al. (1995). Large Area Mapping of Soil Moisture Using the ESTAR Passive Microwave Radiometer in Washita'92, *Remote Sensing of Environment* **53**: 27–37.

Jackson, T. K. et al. (1999). Soil Moisture Mapping at Regional Scales Using Microwave Radiometry: The Southern Great Plains Hydrology Experiment, *IEEE Transactions on Geoscience and Remote Sensing* **37**(5): 2136–2151.

Kerr, Y. H. et al. (1989). Noaa avhrr and its used for rainfall and evapotranspiration monitoring, *International Journal of Remote Sensing* **10**(4-5): 847–854.

Koblinsky, C. et al. (1993). Measurement of river level variations with satellit altimetry, *Water Resources Research* **29**(6): 1839–1848.

Korzoun, V. (ed.) (1974). *Atlas of World Water Balance*, U.S.S.R. National Committee for the International Hydrological Decade, The Unesco Press. English translation.

Leemans, R. and Cramer, W. (1991). The IIASA database for mean monthly values of temperature, precipitation and cloudiness of a global terrestrial grid, *Technical report*, International Institute for Applied Systems Analysis.

Legates, D. and Willmott, C. (1990). Mean seasonal and spatial variability in gauge-corrected, global precipitation, *International Journal of Climatology* **10**: 111–127.

Margulis, S. et al. (2001). Land data assimilation and estimation of soil moisture using measurements from the southern great plains 1997 field experiment, *submitted to Water Resources Research* .

Miller, D. W., Geraghty, J. J. and Collins, R. S. (1962). *Water Atlas of the United States*, Water Information Center, Inc., Port Washington, NY.

Mintz, Y. and Walker, G. (1993). Global fields of soil moisture and land surface evapotranspiration derived from observed precipitation and surface air temperature, *Journal of Applied Meteorology* **32**: 1305 – 1334.

Moench, M. (1992). Drawing Down the Buffer: Science and Politics of Ground Water Management in India, *Economic and Political Weekly* **27**: A7–A14.

Moench, M. (2000). Global groundwater: The underlying resource, http://www.i-s-e-t.org/globalground.html. Executive Summary.

Moench, M. (2001). Groundwater: Potential and constraints, *in* R. S. Meinzen-Dick and M. W. Rosengrant (eds), *Overcoming Water Scarcity and Quality Constraints*, Vol. 2020 Focus 9, Brief 8, International Food Policy Reserarch Institute.

NASA (2000). Tropical rainfall data, http://daac.gsfc.nasa.gov/CAMPAIGN_DOCS/ hydrology/hd_trmm_intro.html. Goddard DAAC.

NASA (2001a). ESSP Missions: GRACE, http://essp.gsfc.nasa.gov/grace. National Aeronautical and Space Administration.

NASA (2001b). Watching soil moisture from space, http://liftoff.msfc.nasa.gov/news/2001/news-soil.asp. National Aeronautical and Space Administration.

NASA (2002). HYDROS, http://hydros.gsfc.nasa.gov/. National Aeronautical and Space Administration.

Nations, U. (1997). Sustainable development of water resources in asia and the pacific: An overview, *Technical report*, Economic and Social Commission for Asia and the Pacific.

Oki, T., Musiake, K., Masuda, K. and Matsuyama, H. (1993). Global runoff estimation by atmospheric water balance using ecmwf data set, *in* B. Wilkinson (ed.), *Macroscale Modeling of the Hydrosphere*, number 24 in *IAHS Publication*, International Association Hydrologic Sciences, Wallingford, UK, pp. 163–171.

Oki, T. et al. (1995). Global atmospheric water balance and runoff from large river basins, *Hydrological Processes* **9**: 655–678.

Pike, J. (1964). The estimation of annual runoff from meteorological data in a tropical climate, *Journal of Hydrology* **2**: 116–123.

Postel, S. (1996). *Dividing the Waters: Food Security, Ecosystem Health, and the New Politics of Scarcity*, number 132 in *Worldwatch Paper*, Worldwatch Institute, Washington, D.C. 76 pp.

Postel, S. (1999). *Pillar of Sand: Can the Irrigation Miracle Last?*, W.W. Norton, New York.

Postel, S. (2001). Something about water and ag..., *Scientific American* .

Postel, S. L., Daily, G. C. and Ehrlich, P. R. (1996). Human appropriation of renewable fresh water, *Science* **271**: 785–787.

Ramankutty, N. and Foley, J. A. (1998). Characterizing patterns of global land use: An analysis of global croplands data, *Global Biogeochemical Cycles* **12**(4): 667–685.

Rockstrom, J. (1999). On-farm green water estimates as a tool for increased food production in water scarce regions, *Physics and Chemistry of the Earth B: Hydrology, Oceans, and Atmosphere* **24**(4): 375–383.

Rodell, M. and Famiglietti, J. (1999). Detectability of variations in continental water storage from satellite observations of the time dependent gravity field, *Water Resources Research* **35**(9): 2705–2723.

Rojstaczer, S. et al. (2001). Human appropriation of photosynthesis products, *Science* **294**: 2549–2552.

Savenije, H. (2000). Water scarcity indicators; the deception of the numbers, *Physics and Chemistry of the Earth (B)* **25**(3): 199–204.

Seevers, P. and Ottmann, R. (1994). Evapotranspiration estimation using a normalized difference vegetation index transformation of satellite data, *Hydrological Sciences Journal* **39**(4): 333–345.

Shah, T. et al. (2000). The global groundwater situation: Overview of opportunities and challenges, Notes prepared for the Second World Water Forum. International Water Management Institute.

Shiklomanov, I. A. (1993). World fresh water resources, *in* P. H. Gleick (ed.), *Water in Crisis: A Guide to the World's Fresh Water Resources*, Oxford University Press, New York, chapter 2, pp. 13–24.

Shiklomanov, I. A. (1998). World water resources: A new appraisal and assessment for the 21st century, a summary of the monograph world water resources, *Technical report*, UNESCO, Internaitonal Hydrological Programme, St. Petersburg, Russia.

Shuttleworth, W. J. (1993). Evaporation, *in* D. R. Maidment (ed.), *Handbook of Hydrology*, McGraw-Hill, Inc., New York, pp. 4.1 – 4.53.

Shuval, H. (2001). A Reevaluation of Conventional Wisdom on Water Security, Food Security and Water Stress in Arid Countries in the Middle East, http://www.gci.ch/GreenCrossPrograms/waterres/middleeast/shuval.html. The Hebrew Univesity of Jerusalem.

Singh, V. P. (1992). *Elementary Hydrology*, Prentice Hall, Englewood Cliffs.

Smith, E. (2001). Overview and scientific agenda of global precipitation mission, *Proceedings of the European Geophysical Meeting, Nice 2001*, European Geophysical Society. http://www.copernicus.org/EGS/egsga/nice01/programme/abstracts/aac7083.pdf.

Smith, M., Allen, R. and Pereira, L. (2000). Revised FAO Methodlogy for Crop Water Requirements, ftp://ftp.fao.org/AGL/AGLW/ET0-REV/ASAE-PAP.ZIP.

Smith, R. and Choudhury, B. (1990). Relationshi pof multispectral satellite data to land surface evaporation from the Australian continent, *International Journal of Remote Sensing* **11**(11): 2069–2088.

Szilagyi, J. (2000). Can a vegetation index derived from remote sensing be indicative of areal transpiration?, *Ecological Modelling* **127**: 65–79.

Szilagyi, J. and Parlange, M. B. (1999). Defining watershed-scale evaporation using a normalized difference vegetation index, *Journal of the American Water Resources Association* **35**(5): 1245–1255.

Szilagyi, J. et al. (1998). NDVI relationship to monthly evaporation, *Geophysical Research Letters* **25**(10): 1753–1756.

Thornthwaite, C. (1944). Report of the committee on transpiration and evaporation, *Transactions of the American Geophysical Union* **26**(5): 683–693.

Turc, L. (1954). Le bilan d'eau des sols. relation entre les precipitation, l'evaporation et l'ecoulement, *Annales Agronomique* **5**: 491–595. (in French).

UNEP (1999). *Global Environment Outlook 2000*, United Nations Environment Program. http://www.unep.org/Geo2000.

UNEP/GRID (n.d.). Mean annual potential evapotranspiration from UNEP/GRID and UEA/CRU, GNV177 documentation.

USGS (2001a). GTOPO30 Documentation, http://edcdaac.usgs.gov/gtopo30. EROS Data Center.

USGS (2001b). HYDRO1K Documentation, http://edcdaac.usgs.gov/gtopo30/hydro. EROS Data Center.

van der Leeden, F. (1975). *Water Resources of the World: Selected Statistics*, Water Information Center, Inc., Port Washington, New York.

Vogel, R. M. et al. (1999). Regional regression models of annual streamflow for the United States, *Journal of Irrigation and Drainage Engineering* **125**(3): 148–157.

Vorosmarty, C., Federer, C. and Schloss, A. (1998). Potential evaporation functions compared on US watersheds: Possible implications for global-scale water balance and terrestrial ecosystem modeling, *Journal of Hydrology* **207**: 147–169.

Vorosmarty, C. et al. (2001). Global water data: A newly endangered species, *EOS* **82**(5): 54,56,58. Transactions, American Geophysical Union.

Wahr, J. et al. (1998). Time variability of the Earth's gravity field: hydrological and oceanic effects and their possible detection using GRACE, *Journal of Geophysical Research* **103**(B12): 30204–30229.

WBGU (1999). World in transition: Ways towards sustainable management of freshwater resources, *Technical report*, German Advisory Council on Global Change.

Willmott, C. J. and Matsuura, K. (2001). Terrestrial water budget data archive: Monthly time series (1950-1999), http://climate.geog.udel.edu/ climate/html_pages/README.wb_ts2.html.

Willmott, C. J., Matsuura, K. and Legates, D. R. (1998). Global air temperature and precipitation: Regridded monthly and annual climatologies, http://www.scd.ucar.edu/dss/datasets/ds236.0.html. Version 2.01.

Willmott, C. et al. (1985). Climatology of the terrestrial seasonal water cycle, *Journal of Climatology* **5**: 589–606.

WRI (1996). *World Resources 1996-1997 A Guide to the Global Environment, The Urban Environment*, Oxford University Press. World Resources Institute, UNEP, UNDP and World Bank, 400 pages.

WWC (2000). A water secure world: Vision for water, life, and the environment, World Commission for Water in the 21st Century, World Water Vision Commission Report, World Water Council.

Yeh, P. J.-F., Irizarry, M. and Eltahir, E. A. (1998). Hydroclimatology of Illinois: A comparison of monthly evaporation estimates based on atmospheric water balance and soil water balance, *Journal of Geophysical Research* **103**(D16): 19,823–19837.

Zeng, X. et al. (2000). Derivation and evaluation of global 1-km fractional vegetation cover data for land modeling, *Journal of Applied Meteorology* **39**: 826–839.